THE UNIVERSITY OF CHICAGO

MULTI-LEVEL ENCODING OF INFLAMMATORY MEMORY IN THE NF-κB NETWORK

A DISSERTATION SUBMITTED TO
THE FACULTY OF THE DIVISION OF THE BIOLOGICAL SCIENCES
AND THE PRITZKER SCHOOL OF MEDICINE
IN CANDIDACY FOR THE DEGREE OF
DOCTOR OF PHILOSOPHY

INDERDISCIPLINARY SCIENTIST TRAINING PROGRAM:
BIOCHEMISTRY AND MOLECULAR BIOPHYSICS

BY

ANDREW G. WANG

CHICAGO, ILLINOIS

AUGUST 2023

To my 姥爷, who set me on the path to science
starting with some turtles,
and my 姥姥, the first educator in my life

"Faith" is a fine invention
For Gentlemen who *see!*
But Microscopes are prudent
In an Emergency!

– Emily Dickinson

TABLE OF CONTENTS

LIST OF FIGURES

LIST OF TABLES

ACKNOWLEDGEMENTS

As is usual with a project spanning nearly 20% of my life, there are plenty of people to thank along the way, so I should get started. Scientifically, of course, my Ph.D. advisor Savaş Tay is the whole reason this work exists. From early on as a rotation student, Savaş encouraged me to take ownership of the literature, of our tools, and of my work to really find questions that were worth pursuing. Savaş supported my fledgling attempts to push the boundaries of the lab and find interesting questions, whether my trial work with *Shigella* infection on chip (which will probably never see the light of day) or setting up our very first animal protocol and delving into epigenetics (which have become cornerstones of my thesis work). I can think of several key instances when I felt stuck and directionless, whether in experimentation or in writing, where Savaş was able to reframe my slightly myopic gaze, remind me of the big questions that were actually interesting, and find experiments and narrative throughlines which tied projects together. Savaş is the reason for my interest in cell signaling, immunology, and systems biology (most of which I actively avoided as a student). We still have work to finish up, but I will forever be proud of what we have put forth in the lab.

In the Tay lab, I have to extend a broad thank you to lab members past and present. Luke, Van, Jing, Fatih, Adil, Nir, Parthiv, Brooke, Navid, Nicky, Liv, Abinash, Gabriel, Suhail, Huili, Junjie, Susan, and Bianca, thank you for lending ears and introducing me to all the diverse work that you are passionate about. Countless times, you all have helped me with my questions and taught me to ask new ones. The greatest thing about our lab is the people, and you all have made me the scientist I am today. I have to extend a special thanks to Minjun Son, who has been a mentor from the very beginning of my time in the lab. Everything I know about microfluidics,

image analysis, single cell biology, mathematical modeling, information theory, and a good portion of coding is thanks to Minjun. It is no exaggeration to say that every idea in this thesis was once argued in the space between our desks at one point or another. I had the unique opportunity to mentor Nick Thom, a former undergrad, and Emma Kenna, a research assistant, over the latter part of my Ph.D. Thanks for putting up with my somewhat scattered mentorship style and hope you still got something out of it. Thanks especially to Emma, who became an invaluable part of our work with primary macrophages and who can do some of the mouse work better than I can at this point. Emma and her commitment made the challenging work that we did with primary cell cultures in microfluidic devices possible.

Thank you to my committee for being with me on this process. Each of them has added something unique to my thesis work and I am honored that they took the time to advise me on the weird little nook in biology I inhabit. Thank you to Juan, who is my chair, Marcus, who has been a role model and a valuable source of advice on what academic medicine might look like, and Nicolas, who, along with his lab, has been a gracious resource as I have stumbled my way into more immunologically relevant systems and questions. On that front, thank you to Kat, Surya, Michihiro, and Adil for being the people I went to first when entirely confused about working with mice.

Thank you to my collaborators, especially Alexander Hoffmann and Aleksander Gorin at UCLA. Many of the ideas and experiments (and our mouse!) came from discussions with Alex as well as some of the experimental work in this thesis came from his group.

Thank you to the Medical Scientist Training Program (MSTP), which has been the framework in which all my studies have taken place. Thank you again to Marcus, to Alison,

Kristin, Marisa, Hafsa, Lucia and all the others who have put their time and energy into making the MSTP the supportive and enriching program it is.

Although I have far too many people to thank on the research side of things, I would be remiss not to mention the communities and love ones who have made this possible. Having been in Chicago 10 years, there have been so many people who have opened up their homes to me and made Chicago my home. Thank you to my old college friends who have stuck around just as long as I have and have seen our lives change just as much as it hasn't. Thank you to my small group, which has continued to overthink the Bible with me through five years of semi-chaos. And thank you so much to my church, which has provided me with role models, grounded in faith, and constantly reminded of the need to serve and build community beyond the ivory tower.

Of course, thank you to my family and my fiancée Maggie. Maggie has supported me through the weird hours and late nights and although she wasn't there at the beginning of this journey, I am so excited for her to be there for everything that comes after (And thank you to Maggie for finding the epigraph). Thank you to my 姥爷, who couldn't see me graduate but set me up to get to this point. Thank you to my sister Angela, who takes her job of keeping me humble very seriously (but all in love). And thank you to my parents, who have been there from the very beginning, have tolerated my incessant questions, provided for me in so many ways beyond listing, raised me in my faith, and taught me to seek what is right and good.

Soli Deo Gloria.

ABSTRACT

Despite the need for sentinel cells to respond to temporally evolving pathogenic and host signals, it is still unclear whether memory of previous signals shapes the response of sentinel cells to new stimulus. Many of the inflammatory stimuli which sentinel cells respond to converge on information bottlenecks during signal transduction. How individual cells extract information about fluctuating signals from these limited networks is unknown. Is memory predictable and determined by initial cell state or random and due to inherent biological stochasticity? Characterization of signaling memory in individual sentinel cells would enable new approaches to targeting pathogenic and programming desired memory states in disease. Here, we systematically profile stimulus memory in individual cells using automated microfluidics, live cell imaging, mathematical cells, and gene expression and chromatin profiling. We show that memory in single cells is encoded in NFκB activation dynamics, and that this memory is deterministic and predictable by prior stimulus response. In fibroblasts, this memory is dependent on overlap between inflammatory signaling pathways, whereas in macrophages, memory is broadly encoded for all stimuli. Combining stimulus-dependent remodeling of NFκB activation dynamics and chromatin accessibility explains the transcriptomic landscape of memory-conditioned macrophages. These results demonstrate that single sentinel cells can encode memory in signaling dynamics which play a key role in shaping the functional state of the cell.

INTRODUCTION

The progression of acute inflammation

The process of acute inflammation can be triggered by infection or injury and follows a defined series of temporal phases (Figure 1a). Molecules from pathogenic microbes (pathogen associated molecular patterns or PAMPs) and self-molecules released in the process of tissue injury (damage associated molecular patterns or DAMPs) can both be sensed by cells at the site of infection or injury[1]. This initial sensing is done by local non-specialized epithelial and mesenchymal cells, as well as tissue resident cells of the innate immune system such as macrophages, dendritic cells, and innate lymphoid cells[2]. In response, these cells undergo a number of cellular responses, including apoptosis, phagocytosis of the foreign or damaged material, production of anti-microbial compounds, repair, and recruitment of systemic immune responses[1]. These local cells make decisions to contain small inflammatory triggers or to recruit additional systemic cells to the site of inflammation if the trigger is too great to resolve[3,4].

In order to recruit a broader immune response, local cells produce a number of secreted factors to recruit systemic leukocytes and provide information about the state of the inflammatory insult. Numerous chemokines recruit circulating monocytes, neutrophils, and T-cells, including CXCL1 and 2, CCL5, IL-8, and CXCL10[5]. Pro-inflammatory cytokines like TNFα, IL-1β, and IL-6 program both neighboring cells and newly-recruited circulating cells to amplify the clearance of pathogens and/or damaged tissue[1,5]. Newly recruited monocytes can be programmed into macrophages or dendritic cells, which phagocytose foreign and damaged material for killing and presentation to lymphoid cells[6]. Neutrophils both phagocytose and produce toxic local environments through release of free radicals and production of neutrophil

extracellular traps[1]. Recruited antigen-specific T-cells can kill infected cells and tune the local inflammatory response through release of pro-inflammatory IFN-γ, IL-17, and additional TNFα[7]. Properly regulation inflammation is limited so that after clearance of the infection or damaged tissue, a different class of anti-inflammatory signals and cell types are recruited. Secretion of anti-inflammatory lipoxins, IL-10, and TGFβ by macrophages prevent the continued infiltration of neutrophils and program local monocytes, fibroblasts, and T-cells to resolve their inflammatory programs and initiate wound healing programs and secretion of growth factors[1,5].

Local inflammatory processes also change organismal health systemically. Inflamed tissue increases the permeability of neighboring capillaries to ease the extravasation of leukocytes while also producing edema and increased blood flow via vasodilators like nitric oxide and histamines[1]. Pro-inflammatory cytokines like TNFα, IL-6, and IFN-γ not only exert local effects but also enter the systemic circulation and trigger fever, fatigue, anorexia and other global physiological changes[1,8]. Ultimately, if the infection or the inflammatory response become uncontrolled, inflammation can become life-threatening as in sepsis, autoimmunity, severe viral infection, and others conditions[9–12].

Convergent signaling networks involved in inflammation

Despite the vast number of environmental triggers for inflammation, the proteins which make up the intracellular signal transduction networks for these triggers are often highly shared (Figure 1b). At the receptor level, a diverse set of proteins from different families sense pathogenic peptides, nucleotides, and polysaccharides, including the toll-like receptors (TLRs), RIG-I like receptors (RLRs), cyclic GMP–AMP synthase (cGAS), NOD-like receptors (NLRs), and C-type lectin receptors (CLRs)[13]. However, even with the diversity of receptors involved in

pathogen sensing, many of these receptors simultaneously act as the primary sensors of DAMPs and tissue injury. For example, TLR4, a classical receptor for lipopolysaccharide (LPS) from Gram-negative bacteria, also responds to a wide array of DAMPs including fragments of the extracellular matrix like biglycan and heparan sulfate, extracellular histones, and serum amyloid A[14]. In addition to these markers of infection or injury, cytokines and chemokines secreted by local and systemic cells also are sensed cell-surface receptors, although, interestingly, there are several known examples where multiple signals bind the same receptor and where multiple receptors exist for the same signal[15]. The importance of cellular usage of the same receptors to bind multiple signals and its potential for therapeutics is still an active area of research[16,17].

Although redundancy begins at the receptor level, intracellular signaling networks in innate immunity collapse rapidly down to an information bottleneck. A limited number of central nodes regulate signaling from receptors. Convergence can occur at receptor-recruited adaptors. For example, MyD88 and downstream IRAK proteins regulate signaling through many TLRs and the IL-1β receptor (Figure 1b)[18]. Central kinases also are the regulatory target of many receptors. For example, TAK1 integrates signaling through TLRs, cytokine receptors, and NLRs, and TBK1 integrates signaling through other TLRs and cytokine receptors, RLRs, and the cGAS-STING pathway[19,20]. Thus, the dozens of receptors which respond to inflammatory signals in the environment ultimately converge on only a small set of intracellular nodes which transmit these signals onto the transcription factors which ultimately initiate the inflammatory response in individual cells. How these intracellular nodes integrate signals from multiple receptors and pathways to produce a distinct response is still unclear.

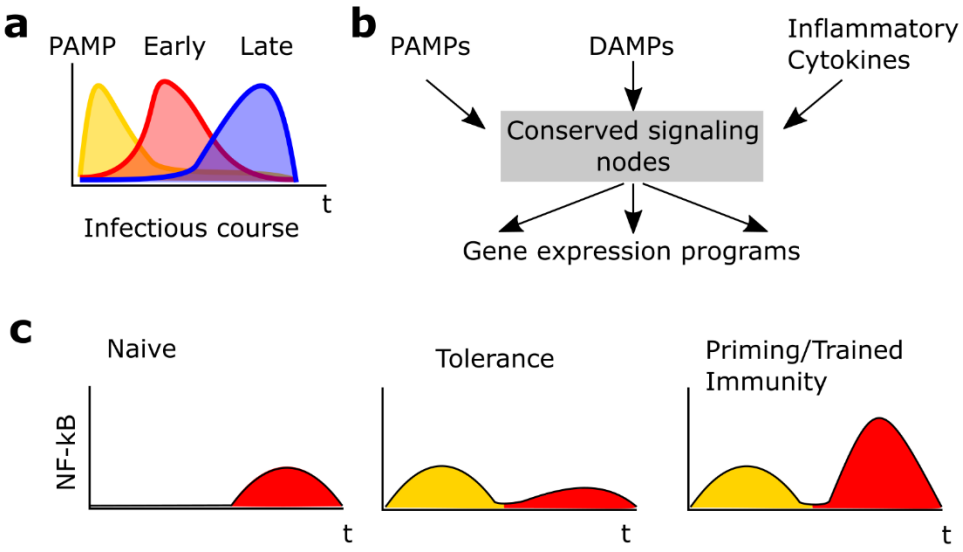

Figure 1. Inflammatory signaling operates under complex dynamics but utilizes limited intracellular nodes and different memory models.

a) Dynamics of an acute infectious challenge sensed by sentinel cells in tissue. Initial exposure to PAMP signals produces rise in early, pro-inflammatory signals, and when infection is controlled, a late rise in anti-inflammatory and repair signals takes place. These dynamics are different under sterile inflammation, uncontrolled infection, or systemic disease. b) Diverse signals and outputs pass through a signaling bottleneck. Despite the number of different receptors for PAMPs, DAMPs, and cytokines, the networks interpreting these signals are highly limited. However, these limited networks interpret these diverse extracellular signals and produce largely distinct gene expression programs. c) Models of innate immune memory. Memory induced by a prior ligand (yellow) can induce attenuation of a subsequent response (red), *i.e.*, tolerance, or potentiation of the subsequent response (red), *i.e.*, priming or trained immunity, depending on the timescale.

At the level of transcription, further convergence is evident, with many receptors ultimately activating the same families of transcription factors, including the canonical NFκB, AP-1, IRF, STAT, and SMAD families of transcription factors[21]. For example, TAK1 activates NFκB and AP-1 through IKK and the MAPKs, respectively[20]. The NFκB family of transcription factors, however, includes five different proteins which can homo- and heterodimerize[22], and the AP-1 family includes heterodimers of more than a dozen proteins[23]. Although particular family members are strongly associated with signaling (e.g. RelA-p50 for the canonical NFκB family and RelB-p52 for the noncanonical NFκB family), other family members are also activated simultaneously[22]. How central signaling nodes "select" for and activate particular transcription family members and different roles of these family members once activated are often not clear. Thus, many inflammatory signaling networks integrate a large number of potential signals through a highly limited set of intracellular signaling nodes which regulate families of transcription factors to execute appropriate genetic programs.

Stimulus dynamics as a means of distinguishing convergent inflammatory signals

A possible approach that sentinel cells use to overcome this signaling bottleneck is to process and respond to the temporal dynamics of inflammatory signals. Depending on location and severity, sentinel cells can be exposed to PAMPs, inflammatory cytokines, and DAMPs in varying orders and magnitudes[24–26]. These different sequentially occurring stimuli provide sentinel cells with information about the context of a particular inflammatory insult. Similarly, systemic dynamics of cytokine levels encode critical information about severity and progression in a number of infectious processes, including bacterial sepsis and viral respiratory infections[27–29]. Taken together, decoding the sequence and dynamics of inflammatory signals can provide

context to sentinel cells about disease state and overcome some of the limitations which come from bottlenecked signaling.

In order for sentinel cells to accurately extract information from sequential stimuli, however, they must encode memory of prior inflammatory stimuli. In this sense, memory refers to the biochemical changes which happen in the signal transduction networks and DNA organization in a cell following an inflammatory stimulus which then alter or "contextualize" the cell's response to subsequent inflammatory stimuli. Over the past several decades, this sort of memory has increasingly been recognized in traditionally "memory-less" innate immune cells which comprise the majority of sentinel cells, leading to concepts of innate immune tolerance, priming, and trained immunity (Figure 1c)[30].

Tolerance was recognized early on a a model of context-dependent changes in innate immune responses. Sublethal treatment of mice with bacterial endotoxin resulted in an attenuated response or "tolerance" to a lethal dose of endotoxin days to weeks later[31]. Tolerance has since been recognized to occur on a cellular level in macrophages, monocytes, and dendritic cells[32]. This state is induced by production of intracellular negative feedback proteins and miRNAs which limit inflammatory signaling transduction and remodeling of the genome to limit the induction of inflammatory gene programs by activated transcription factors[33]. Attenuated signaling thus leads to decreased production of proinflammatory cytokines and other markers of inflammation. Importantly, however, tolerance is targeted, as certain antimicrobial programs are left unaffected or enhanced, suggesting that tolerance can be adaptive in contexts of uncontrolled inflammation[34].

In contrast, priming and trained immunity are models of enhanced innate immune response following prior inflammatory exposure. Priming describes the enhanced innate immune response in invertebrates and plants, which both lack adaptive immunity, following challenge with a pathogenic stimulus and which lasts beyond the duration of the initial challenge[35]. Trained immunity, has been primarily recognized mammals as the ability of individuals challenged by pathogenic molecules to induce non-specifically enhanced immune responses to subsequent stimuli[36–38]. This concept originates in studies showing enhanced clearance of other pathogens in individuals previously exposed to the pathogenic yeast *Candida albicans* or the fungal cell wall component β-glucan[36,37]. Human studies have also recognized that the Bacillus Calmette–Guerin (BCG) vaccine which is designed to vaccinate against tuberculosis also improves survival against other infectious causes of mortality largely due to enhancement in non-specific enhancement of innate immune responses to infection[39,40]. Studies of priming and trained immunity have largely pointed to lasting changes to histone modifications in long-lived cell populations as drivers of enhanced innate immune response[41].

In these examples of innate immune memory, molecular and biochemical changes take place at the level of the signal transduction network, chromatin modifications and organization, and even at the level of RNA translation and degradation. Due to the oftentimes long-term and heritable nature of memory, changes at the chromatin level have been the focus of most research. Endotoxin tolerance is associated with histone modifications which silence and recruit inhibitory factors to inflammatory gene promoters[34,42], while enhancer-specific histone modifications are associated with hyperresponsiveness in trained immunity[37,43]. Furthermore, alternative splicing and miRNA-based regulation of RNA degradation act post-transcriptionally to induce memory.

Alternative splicing into dominant-negative forms of key signaling proteins attenuates signaling in tolerance[44], and miRNA mediates degradation of inflammatory cytokine transcripts, histone modifying enzymes, and signaling intermediaries[33,45,46]. Similarly, in trained immunity, miRNAs and lncRNAs mediate reduced phosphatase activity and stabilize transcription, respectively[47,48]. Changes at the level of the signal transduction network also can play a key role in encoding inflammatory memory. The aforementioned translation of dominant negative splice variants of key signaling proteins, in addition to other negative feedback proteins and downregulation of PAMP and pro-inflammatory cytokine receptors are involved in tolerance[49]. While significantly less studied, network level changes may also play a role in trained immunity.

Importantly, the majority of research on innate immune memory has focused on timescales longer than the temporal dynamics involved in acute inflammation. Models for both tolerance and priming have involved restimulus after days, weeks, or months, simulating multiple acute infectious challenges[32,38]. While the concepts and conclusions drawn from these studies are still relevant, it is important to consider how dynamic fluctuations relevant in acute inflammation, which primarily take place on the timescale of minutes to hours, might be differently recorded. For example, changes in signaling networks due to inactivation, degradation, or translation of feedback proteins, while relatively understudied, may play an outsized role at these timescales due to the speed of these changes compared to more graduale changes in chromatin rearrangement and silencing[50].

Finally, innate immune memory can be both adaptive and pathological depending on context. Endotoxin tolerance is largely thought to take place during clinical sepsis as a check on uncontrolled inflammation and tissue injury[32], but can leave sepsis survivors at elevated risk of

death from uncleared or secondary infections[51]. While innate immune hyperresponsiveness following training results in superior infection clearance[36], it may also play a role in autoimmune disease and overreaction to DAMPs during sterile inflammation[52,53]. Further study of how memory aids sentinel cells in decoding complex environmental stimuli may be important in disentangling the adaptive and pathological potential for memory.

The NFκB network as a convergent sensor of diverse inflammatory signals

A central regulator of inflammatory sensing is the NFκB family of transcription factors. The five main family members are RelA, c-Rel, RelB, p50, and p52, which exist in the cell as homo- or heterodimers[22]. RelA-p50 is typically considered the most abundant dimer of the NFκB family, though RelA/RelA, RelA/c-Rel, RelA/p52, c-Rel/c-Rel, p52/c-Rel, p50/c-Rel, p50/p50, RelB/p50, and RelB/p52 have also been reported[54]. RelA, c-Rel, and p50 are described as canonical NFκB transcription factors and are associated with integrating pro-inflammatory responses after exposure to pathogenic signals or inflammatory cytokines[22]. In contrast, RelB and p52 are more associated with the non-canonical NFκB pathway, which is involved in B cell development and mediating anti-inflammatory responses to inflammatory stimuli[55,56]. Due to the focus of this work on the early temporal phases of acute inflammation, attention will primarily be devoted to the canonical NFκB pathway (Figure 2a).

Canonical NFκB transcription factors are activated downstream of signal transduction through a number of membrane-bound and cytosolic receptors. The combination of these pathways involved in signal transduction to NFκB will be referred to as the "NFκB network". Importantly, however, these receptors also mediate signaling through different transcriptional outputs, including the AP-1 family of transcription factors, activated by JNK and p38 signaling[20],

and several IRF family transcription factors[21]. Receptors in the NFκB network sense a diverse range of molecular signatures. The TLRs, C-type lectins, RLRs, cGAS/STING, and NLRs all activate canonical NFκB signaling following sensing of pathogenic protein, lipid, polysaccharide, and nucleic acid signals in extracellular, endosomal, or cytosolic contexts[13]. A number of cytokine receptors also converge on activation of canonical NFκB signaling, including TNFR1, which senses the ubiquitous inflammatory cytokine TNFα[57], type 1 IL-1R, which senses IL-1β released by pyroptotic macrophages[58], and IL-17R, which senses IL-17 released by Th17 T cells and other activated lymphocytes[59]. Thus, immune signaling uses NFκB activation as a convergent node controlling the cellular response to numerous signals from different contexts.

Despite the diversity of receptors and sensing mechanisms for NFκB-activating ligands, the NFκB network shares a highly conserved set of central nodes which integrate signaling. Many TLRs and type 1 IL-1R all require the receptor adaptor protein MyD88 for signal transduction, with the entire subsequent signaling pathway sharing recruitment of IRAK1/4 and TRAF6[58]. Other TLRs signal through the receptor adaptor protein TRIF, which activates TBK1[19]. cGAS/STING and RLR signaling also converge on TBK1 activation[19]. TNFR1 and NLRs both signal through RIPK1, although other intermediaries differ[60]. Both IL-17R and C-type dectins can activate the CARD9-BCL-10-MALT1 complex as part of the signal transduction pathway leading to NFκB activation[61]. Although the details are complex and still being worked out in many cases, the overall principle of the intracellular NFκB signaling network is that diverse receptors converge on activation of 4-5 key cytosolic signaling complexes.

From this point, signal transduction in the NFκB network is highly conserved. Although alternative activation pathways can occur, the central shared node in activation of NFκB is the trimeric IκB kinase (IKK) complex. Composed of two kinase domains, IKKα and IKKβ, and a regulatory domain, NEMO/IKKγ, IKK integrates signals from upstream pathways and acts directly on the inactive NFκB complex[62]. IKK cycles between poised, active, and inactive states regulated by activating phosphorylation (poised to active), inactivating phosphorylation (active to inactive), and dephosphorylation by intrinsic phosphatase activity (inactive to neutral)[63]. For canonical NFκB transcription factors, activation is primarily regulated through nuclear localization. Inactive NFκB is sequestered in the cytosol by the IκB family of proteins, which obscure the nuclear localization signal of the NFκB dimers. In the case of RelA/p65, which is primarily regulated by IκBα, IκBα is phosphorylated by IKK upon activation, which marks IκBα for addition of K48-linked ubiquitin chains by ubiquitin ligases and ultimately degradation by the proteome[64]. Upon degradation of IκBα, the nuclear localization signals on the canonical NFκB dimer are freed and the NFκB dimer is translocated into the nucleus, becoming transcriptionally active.

In the nucleus, NFκB transcription factors regulate a number of different cellular functions, including increasing transcription of genes involved in proliferative, apoptotic, pro-inflammatory, anti-inflammatory, anti-microbial, and developmental programs[65]. How NFκB acts within individual cells to balance transcription and favor a subset of these oftentimes contradictory gene expression programs is still largely unknown and a focus of study. Each NFκB dimer recognizes very similar motifs in promoter and enhancer regions, including the consensus κB motif GGRRNNYYCC[66,67], though individual dimers have their own specific

binding motifs and affitinities as well[68,69]. Although regulation of NFκB activation primarily takes place through control of nuclear translocation, NFκB dimers can also be post-translationally modified by phosphorylation and acetylation[22]. While many of these modifications are still poorly understood, they appear to play roles in tuning magnitude and specificity of transcriptional induction. Ser276 phosphorylation and acetylation at Lys221 and Lys310 are better characterized post-translational modifications on RelA and increase transcriptional activity[70,71]. Altogether, the NFκB network is a critical mediator of inflammation and integrates diverse molecular inputs through a limited and highly conserved IKK node before inducing transcription of numerous gene expression programs.

NF-κB activation dynamics as a model for memory encoding

Traditional models of signaling largely ignore the dynamic component of signal transduction and treat it as a single square pulse. In this model, an input produces an instantaneous and temporally invariant level of signal transduction, which then, through transcription and translation, produces a gradually increasing phenotypic output to the input. Time-resolved tracking of TNFα-induced activation of NFκB, however, produced one of the earliest challenges to this model of signaling. NFκB nuclear translocation revealed oscillatory dynamics, where a constant pulse of TNFα induced multiple rounds of NFκB nuclear localization and exit[72,73]. This observation led to the hypothesis that the temporal pattern of activation in response to a stimulus - the activation dynamics of a stimulus – can be important to regulate a stimulus response. For example, oscillatory activation dynamics may produce oscillatory or stepped increases in output from constant input, and elongated activation dynamics may induce genes which require extended transcription factor nuclear occupancy for

activation[50,74]. Although first observed in NFκB signaling, oscillatory activation dynamics have now been observed in p53[75], MAPK[76], Notch[77], and other pathways. Different parameters of dynamic activation, including duration, oscillation, time to activation, and amplitude have been linked to phenotypic outcomes of signaling[78].

In the NFκB network, activation dynamics are largely dictated by interplay between signal transduction and subsequent positive and negative feedback responses. Depending on the receptor and associated signaling molecules involved in activation of NFκB, the initial activation features, including time to activation and magnitude, can differ greatly. For example, MyD88 or RIPK1-mediated NFκB activation is rapid, occurring within an hour of stimulus exposure, oftentimes within 30 minutes for RIPK1[78], while TRIF-mediated activation is significantly slower and takes longer to reach maximal activation[79]. Similarly, ligands which require endocytosis prior to activation can display a longer delay between stimulation and activation[80]. Termination of receptor and intermediary level signaling typically takes place through receptor internalization and degradation[81], de-ubiquitination of ubiquitin assemblies necessary to recruit IKK to activated protein scaffolds[82,83], inhibitory phosphorylation of active intermediaries[84], or dephosphorylation of activating phosphorylation sites[85]. The dynamics of different termination mechanisms are not well characterized however, and likely take place on different timescales. The later phases of NFκB activation dynamics, including both duration and oscillation, are controlled by interplay between residual activation signals from the receptor and induction of negative and positive feedback. Oscillation in the NFκB network is due to this interplay, as IκBα is a strongly induced early NFκB target gene, resulting in a strong pulse of IκBα production while NFκB is active which then binds NFκB and sequesters it from the nucleus to terminate

signaling. However, if IKK is still active, it continues to phosphorylate IκBα and mark it for degradation, which then frees NFκB for another round of nuclear translocation and IκBα production[86]. Thus, activation-dependent feedback plays a major role in modulating and terminating the NFκB response. Interestingly, NFκB activation dynamics appear to differ between cell types and depend on ligand, which raises the possibility of cell-type specific regulation of NFκB dynamics[78].

While IκBα is the most well studied of the NFκB-induced negative feedback molecules acting on the NFκB network, a number of others also play major roles in terminating the NFκB response (Figure 2a). Some negative feedback molecules act as activity-inert mimics of key signal transduction proteins to prevent downstream transduction. In this category are MyD88-S, a truncated splice variant of MyD88[44], and IRAK-M, a myeloid specific kinase-inactive member of IRAK family of key signaling proteins[87]. Other negative feedbacks act on the ubiquitin chains which form the scaffold for recruitment of IKK to TRAF complexes, including the A20/TAX1BP1/ITCH complex, which may act through both deubiquitination and steric exclusion[83,88], and CYLD, which acts as a deubiquitinase[82]. The IκB family of proteins acts as a third class of negative feedback. In addition to IκBα, IκBβ and IκBε are NFκB sequestering proteins[89,90]. Both are insensitive to IKK mediated degradation and induced at a much lower rate than IκBα, however, which produces a gradual damping effect to NFκB activation instead of the distinctive rapid sequestration and oscillation associated with IκBα. The precursor protein to p52, p100, also known as IκBδ, is also induced by NFκB activation and can act like IκB family members by binding an NFκB dimer and sequestering it in the cytosol[91]. Secreted anti-inflammatory cytokines like IL-10 can inhibit on NFκB activation, though typically much more

slowly than the direct NFκB negative feedback proteins[92]. These different NFκB-induced negative feedback regulators act at different places in the network, with variable overlap with other pathways and magnitude of inhibition.

Positive feedback in the NFκB network is far less characterized. While NFκB can cross-talk with other pathways and act to amplify signaling in other contexts like MAPK signaling[93], direct action of NFκB transcriptional targets on the NFκB network is not well recognized. The primary recognized mechanism for positive feedback is through NFκB-dependent production and secretion of pro-inflammatory cytokines, particularly TNFα, which then bind to receptors on the same or neighboring cells to continue passing NFκB-activating signals into the cell[94,95]. This time-delayed positive feedback loop has been described to play a role in late-phase NFκB activation dynamics and sustained oscillatory behavior to stimuli other than TNFα[78]. NFκB-dependent production of NFκB proteins has also been described in some cases, particularly for RelA, and may provide a way for positive feedback mechanisms to overcome the many forms of negative feedback present in the NFκB network[96]. Finally, cross-talk between NFκB in the nucleus and other transcription factors which amplify the NFκB response may provide a way for NFκB transcripts to be regulated by positive feedback even without increased nuclear NFκB levels. For example, the transcription factors Ikaros and c/EBPδ play roles in amplifying and sustaining NFκB-dependent transcription[97,98]. However, no mechanisms for NFκB-dependent regulation of the intracellular signal transduction network have yet been identified.

Due to the role of feedback in regulation of NFκB and the overlapping pathways converging on NFκB, it is possible that feedback can encode memory in the NFκB response (Figure 2b). IκBδ controls induction of attenuated NFκB activation, i.e. tolerance, in fibroblasts

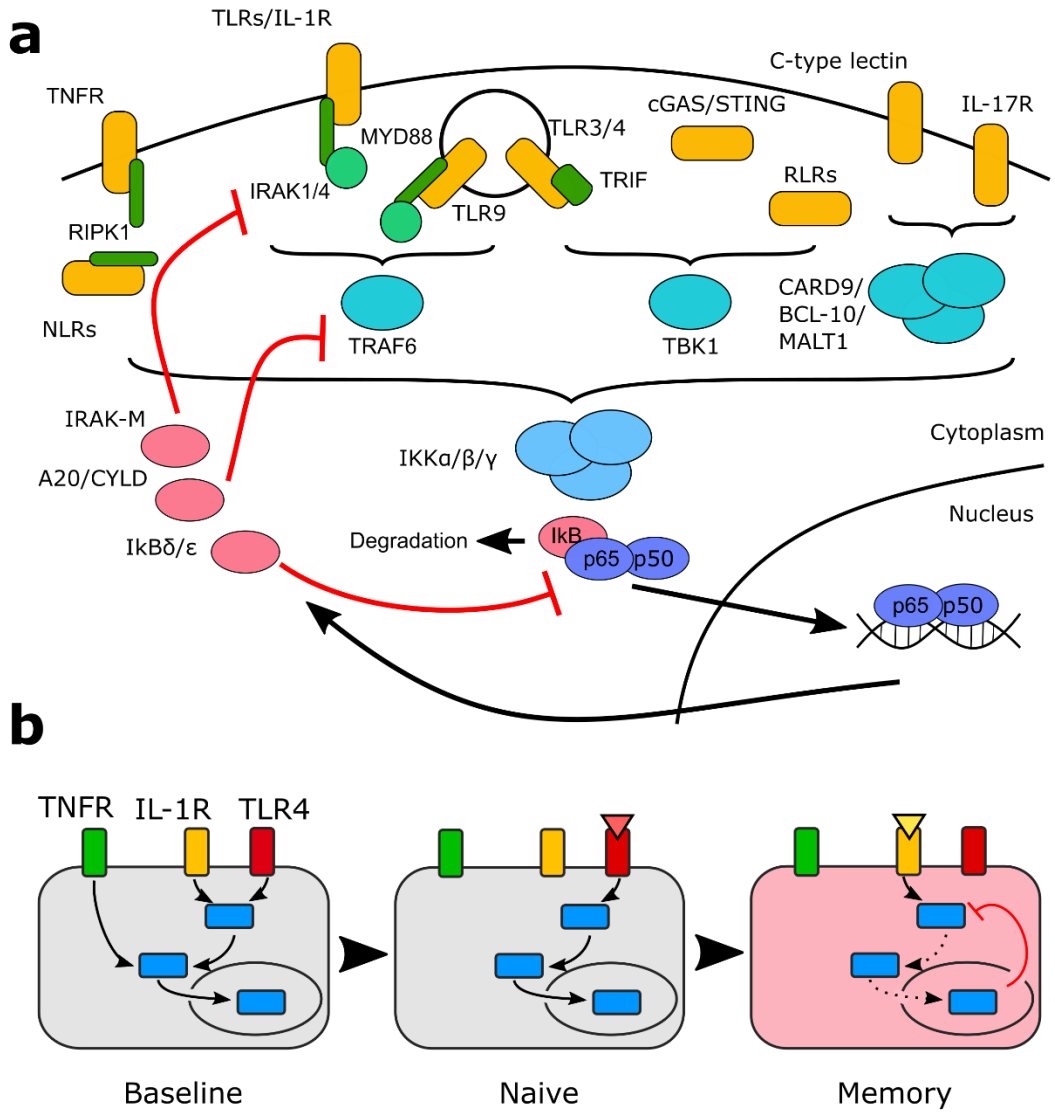

Figure 2. Signal transduction and feedback in the NFκB network potentially produces memory through network remodeling.

a) Network map of signaling convergent on canonical NFκB activation. Many classes of receptor (yellow) activate different types of intracellular signaling adaptors (dark green), which then recruit conserved signaling intermediaries (teal), before ultimately converging on IKK mediated degradation of IκB and nuclear translocation of canonical NFκB dimers (blue). NFκB dependent feedback (red) is then produced and acts on the NFκB network to attenuate signaling at different nodes. b) NFκB feedback can produce memory. NFκB response through a ligand (TLR4, red) induced negative feedback acting on a shared node with signaling through another ligand (IL-1R, yellow), which attenuates signal transduction by the other ligand.

following 24 hour exposure to any of LPS, TNFα, or IL-1β due to NFκB-dependent production[91]. Within only hours of stimulus, high dose IL-1β and LPS stimulus can render fibroblasts tolerogenic to re-stimulus with either IL-1β or LPS due to autoinhibitory phosphorylation of IRAK1, a key node in the upstream network, though TNF-α stimulus does not rely on that node and is unaffected prior stimulation with IL-1β or LPS[84]. A transient refractory period was also observed in neuroblastoma cell lines where TNFα stimulation rendered cells tolerant to subsequent TNFα but not subsequent IL-1β restimulus within an hour, but the tolerant state is gone by three hours[99]. Over an extended period, IκBβ and IκBε act to dampen NFκB oscillations in fibroblasts as well, limiting the effects of oscillatory IκBα production and degradation by competing for free NFκB dimers[89]. These mechanisms of regulation in the NFκB network at different timescales suggest that feedback is finely tuned as an approach to control not only the dynamics and termination of NFκB signaling to a ligand, but also in a memory response which controls cellular responses to restimulus.

Mathematical modeling in the NFκB network

One particularly fruitful approach to understanding signaling dynamics and emergent behavior in NFκB activation has been the use of mathematical modeling with ordinary differential equations (ODEs)[72,100–102]. First used to describe the role of transcription factors in promoting gene expression, ODEs, and in particular systems of ODEs, have proved to be valuable in modeling current understandings of signal transduction networks and identifying necessary areas of expansion.

Models of the NFκB network have primarily described protein-protein relationships assuming the law of mass action[103]. Briefly, to consider a simple case involving the association of unbound IκBα and NFκB, the second order equation can be written as follows:

$$\mathrm{NF\kappa B} + \mathrm{I\kappa B\alpha} \rightleftharpoons \mathrm{NF\kappa B|\, I\kappa B\alpha} \quad (1)$$

This equation can be expressed as a differential equation focusing on the rate of change of NFκB|IκBα dependent on the binding of unbound species and the unbinding of the bound complex:

$$\frac{\mathrm{dNF\kappa B|\, I\kappa B\alpha}}{\mathrm{dt}} = \mathrm{k_{binding}\, NF\kappa B} * \mathrm{I\kappa B\alpha} - \mathrm{k_{unbinding} NF\kappa B|\, I\kappa B\alpha} \quad (2)$$

Expressing key species in a signaling network in terms of the other species produces a system of ODEs which can be solved numerically at different timesteps. This gives a solution for the behavior of each species of the system given particular initial conditions and the mathematical parameters constructed.

In biologically relevant systems of equations, relevant features of ODEs typically take the form of several "modules". Constant rate growth/decay is oftentimes a simplification of "constitutive" production/decay rates:

$$\frac{\mathrm{dmRNA}}{\mathrm{dt}} = \mathrm{k_{const.\ transc.}} \quad (3)$$

Abundance dependent increase and decrease generally models processes described by first or second order mass action relationships:

$$\frac{\mathrm{dmRNA}}{\mathrm{dt}} = \mathrm{k_{const.\ transc.}} - \mathrm{k_{degradation}} * \mathrm{mRNA} \quad (4)$$

Finally, Hill functions describe cooperative reactions dependent on assembly of macromolecular complexes where the Hill coefficient describes the "steepness" of the relationship between input and output. A derivation of the Hill function from the law of mass action can be found elsewhere[103].

$$\frac{\mathrm{dmRNA}}{\mathrm{dt}} = \mathrm{k_{const.\ transc.}} - \mathrm{k_{degradation}} * \mathrm{mRNA} + \beta_{\max} \frac{\mathrm{NF\kappa B^4}}{\mathrm{K^4_{activation}} + \mathrm{NF\kappa B^4}} \quad (5)$$

As shown in this example, the rate terms for a particular species oftentimes combine multiple different modules depending on the nature of the interaction.

In the case of the NFκB network, modeling studies seeking to reproduce oscillation activation dynamics following TNFα stimulus have been generated since the early 2000s and the beginnings of the field of systems biology. Early models of the NFκB network focused on the interaction between NFκB and IκBα. These models included transcription, translation, and induced degradation of IκBα, IκBβ, IκBγ and nuclear transport of NFκB and IκBα and were calibrated to knockouts of key species[72,86,89]. These models were further refined as experimental evidence and increased insight into the system revealed high constitutive production and degradation of IκBα when unbound to NFκB and a role for IκBδ in the system[91,104]. Later developments included additions of the negative feedback protein A20[105], incorporation of stochasticity to model the variability in single-cell behavior[101], and adding positive feedback through production of TNFα[106]. The most recent models have incorporated complex network topologies which move beyond the core IKK- IκB- NFκB circuit to include the upstream receptors and intermediaries which govern signal transduction between different ligands[78,107].

Another movement in the development of mathematical models of NFκB signaling has been towards simplified minimal models which seek to reduce the number of parameters and equations[100,108]. These approaches, which have gone so far as to produce a three-equation model of NFκB activation which reproduces key features of NFκB activation[100], seek to identify simplified modules and motifs explaining activation behavior without capturing the complexity latent in the true biology. The underlying motivation for this approach is to reduce the expensive and time-consuming computational time necessary for highly complex models and to reduce the risk of generating overfit models which match experimental data at the expense of losing generalizability and true insight into the biological system.

Through these different approaches to computational modeling of the NFκB network, advances have been made in understanding the dynamic features of NFκB signaling and exploring features of NFκB activation. Key advances introduced by mathematical modeling have included the identification of different roles for the different IκB proteins, introducing IKK cycling as a feature of NFκB signaling[63], showing a role for positive feedback in sustained activation[96], and providing insight into single cell heterogeneity in NFκB activation[101,109]. Modeling thus stands to be a major means of revealing new insights into features of NFκB signaling and gaining understanding of how to perturb this key pathway.

Inflammation and inflammatory memory at a single cell level

Recently, it has become clear that individual cells can vary greatly in response to identical infectious or inflammatory stimulus (Figure 3a-b). Stochastic events early in the infection cycle of individual epithelial cells or macrophages can give rise to multiple log-order differences in viral progeny or intracellular bacterial replication[110–112]. Single cell variability in

macrophage response can be due to induction of distinct cell states, including differentiation, inflammation, and antimicrobial activity[113]. Single cell studies have revealed the presence of bystander and abortively infected cells in a variety of disease contexts, raising the possibility of therapeutic avenues that amplify cellular processes associated with these infection outcomes[110,111]. Heterogenous infection states have been associated with activation dynamics in different pathways, including interplay between activation of the NFκB and MAPK families[114]. Single cell study of infection in innate immune cells has revealed unappreciated aspects of how individual cellular decisions and subpopulation outcomes give rise to population level behaviors.

Similarly, generalized inflammatory signaling without infectious pathogens has also been shown to depend in large part on single cell behaviors. Bimodality in the LPS response in dendritic cells is tied to heterogeneous induction of an interferon feedback motif[115], while population level responses to LPS signaling in macrophages is due to a small subpopulation of early and strong activators which produce TNFα and coordinate responses in other cells[95]. In co-culture between macrophage-like cells and fibroblasts, single cell heterogeneity in the macrophage response to LPS can greatly alter the magnitude and range of signaling in the fibroblast population[116,117]. *In vivo*, macrophage heterogeneity in the tumor environment results in diverse subpopulations with different programs, including pro- and anti-inflammatory, angiogenic, and proliferative programs[118,119]. Thus, single cell variability in the response of innate immune cells to inflammatory stimuli also plays a role in determining physiological responses to inflammation.

Despite the increasing evidence for single cell heterogeneity in response to infectious and inflammatory signals, it is still unclear how this heterogeneity arises in the first place. Study of

single cell behavior has emphasized the importance of noise in producing heterogeneity between cells. An entirely deterministic system, given identical input and initial conditions, would produce identical output. Some level of stochasticity is apparent in single cells, which can push cells into bifurcating subpopulations reinforced by feedback or produce broad heterogeneity in response[120,121]. How this stochasticity manifests in single cells, however, distinguishes what mechanisms are possible for manipulating or targeting heterogeneous subpopulations. Heterogeneity can be due to intrinsic noise and stochastic events at low probability or between low copy number species reinforced by positive feedback[122], e.g. low probability of initialization of a productive viral infection and high production of viral progeny following initialization[110]. In these cases, largely identical cell populations can have bifurcating outcomes due to probabilistic interactions in individual cells, and subpopulations cannot be predicted prior to stimulation (Figure 3a). In contrast, heterogeneity can also be due to extrinsic noise and distinct cell states from cell cycle, prior stimulus exposure, or chromatin state, e.g. poised NFκB and IκBα levels determining which cells respond to low-dose TNFα[123]. In these cases, subtle differences in initial state are revealed through magnified differences in subsequent response and subpopulations can be identified prior to stimulation (Figure 3b). Innate immune memory is an example of a system where extrinsic noise in single cell state (*i.e.* single cell differences in memory) could contribute to different biologically relevant outcomes, though as of yet, no extrinsically variable factors of innate immune memory have been identified.

Focusing on single cell memory in innate immune signaling opens a new opportunity to identify key cell states which drive immune and infectious pathology. While innate immune memory has primarily been studied at the level of bulk cytokine secretion or transcriptomic state,

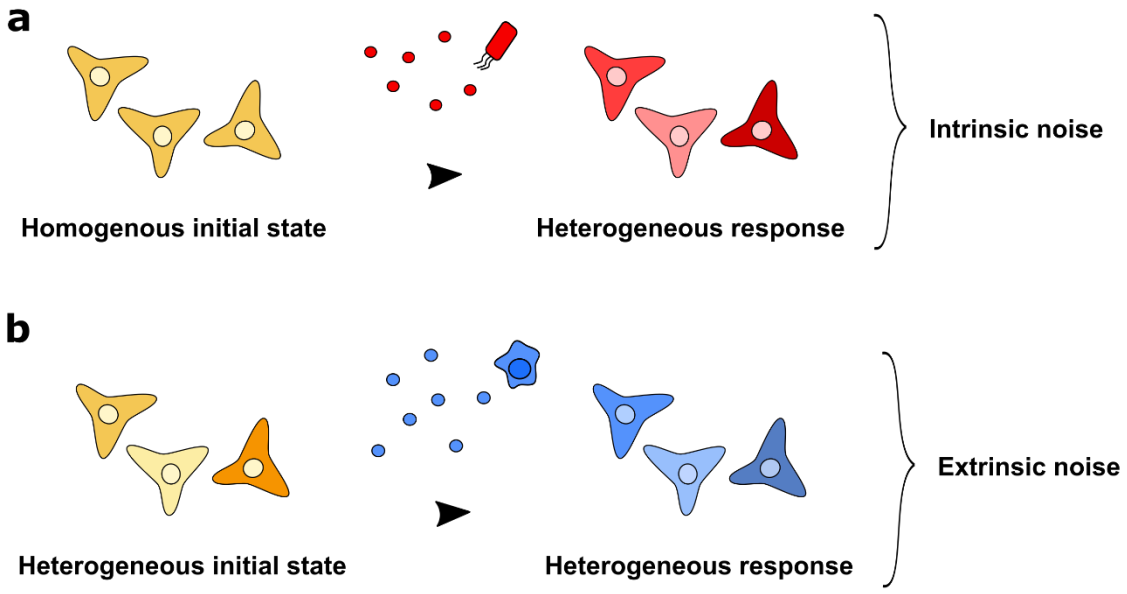

Figure 3. Intrinsic and extrinsic noise mediate single-cell heterogeneity in innate immune response.

a) Intrinsic noise produces heterogeneity in a homogenous cell population. Stochastic processes like low probability transitions or random collision between low copy number molecules produce varying responses to a homogenous stimulus within a homogenous population. b) Extrinsic noise results in population heterogeneity and subsequent heterogenous response. Cellular variability due to environmental factors like prior history, cell cycle, produce heterogeneity in cell population which alters how subpopulations respond to identical stimulus.

identifying single cell heterogeneity in memory and subsequent heterogeneity in memory-informed inflammatory response can identify key driver populations which can be targeted therapeutically. In addition, the rise of cell-based therapeutics, *e.g.*, chimeric antigen receptor T-cell therapy, increases the importance of profiling different states of cellular programming for improved programming and enrichment of therapeutically active cells.

Aims of this Thesis

Innate immune signaling takes place on multiple timescales, yet most research has focused on signaling over days to weeks. Innate immune memory at the timescale of hours is important to shape epithelial and myeloid responses to initial infectious and inflammatory insult. Furthermore, many inflammatory stimuli which appear on this timescale converge on activation of a few key transcription factor families, yet the effects of this convergence on memory encoding in the signaling network has been lacking. This thesis focuses on systematic profiling of memory responses in the NFκB network as an example of a highly convergent node of inflammatory signaling on the timescale of one to eight hours. Through a combination of high-throughput microfluidics, chemical inhibition, cytokine blockade, transcriptomic profiling, and epigenetic profiling, this thesis will address memory on the timescale of hours and ask whether memory encoded in feedback at the level of signal transduction alters NFκB dynamics to restimulus. This thesis will also link network level and chromatin-accessibility level changes in cell state as a result of memory and ask whether memory-dependent changes in transcriptional output upon restimulus correspond to a combination of these forms of memory encoding.

Additionally, innate immune memory has not been well characterized in single cells. This thesis combines non-perturbative stimulus, tracking of single cells through multiple stimuli, and mathematical modeling to show how baseline cell state shapes response to an initial stimulus and subsequent memory state. Cells will be tracked through restimulus to show how memory states are encoded in subsequent response to restimulus. This thesis will use information theoretic approaches to study whether these memory-informed responses are differentiable and encode meaningful information about prior stimulus exposure. Ultimately, this thesis seeks to build a model of memory encoding in the NFκB network on a single cell level and characterize the ability of activation dynamics to distinguish convergent inflammatory signals.

MATERIALS AND METHODS[a]

Mouse models and cell lines

Endogenously-tagged mVenus-RelA ($RelA^{V/V}$) C57BL/6J mice [78] were housed and bred in specific pathogen free conditions at the University of Chicago or the University of California Los Angeles. All experiments were performed in accordance with the NIH Guide for the Care and Use of Laboratory Animals and approved by the University of Chicago or UCLA Institutional Animal Care and Use Committees.

6-8 week old male and female $RelA^{V/V}$ mice were injected intraperitoneally with PBS, LPS, or polyI:C at the indicated doses diluted in PBS. Immediately prior to injection and 4, 8, 24, and 48 hours post-injection, weight and core body temperature were recorded. For extraction of peritoneal macrophages, mice were euthanized by CO_2 asphyxiation 4 hours post-injection.

Bone-marrow derived macrophages (BMDMs) were differentiated and cultured in RPMI with 10% heat-inactivated FBS (Omega), 1% penicillin/streptomycin (Lonza, Corning), 1% NEAA (Corning), 1% HEPES (Gibco, Corning), 1% sodium pyruvate (Corning), 1% L-glutamine (Fisher, Corning), 0.1% β-mercaptoethanol (Gibco) (complete media) supplemented with 20 ng/mL recombinant murine m-CSF (Peprotech).

Peritoneal macrophages (PMPs) were cultured in complete media. Isolation described in method details.

[a] Parts of this section are adapted from Wang AG, Son M, Kenna E, Thom S, and Tay S. NF-κB memory coordinates transcriptional responses to dynamic inflammatory stimuli. *Cell Reports* 40(7):111159. (2022)

RelA-/- NIH3T3 immortalized mouse embryonic fibroblasts (3T3s) stably expressing RelA-DsRed, JNK-kinase translocation reporter-mCerulean3 (JNK-KTR)(Regot et al., 2014), and histone 2B-green fluorescent protein (H2B-GFP) were cultured with Dulbecco's Modified Eagle Medium – High Glucose (DMEM; Gibco) supplemented with 10% fetal bovine serum (Omega Scientific), 1% GlutaMAX (Gibco), and 100 u/mL penicillin-streptomycin (Gibco) in tissue-culture treated flasks.

Bone-marrow derived macrophages (BMDMs) were prepared by culturing bone marrow cells isolated from the femurs and tibias of 6-12 week old male and female $RelA^{V/V}$ mice in complete media supplemented with 20 ng/mL m-CSF. BMDMs were fed on days 2, 4, and 6 with additional complete media supplemented with m-CSF. On day 7-9, adherent BMDMs were washed with PBS and lifted from culture dish with 10 mM EDTA (Fisher) in PBS (Gibco) and either replated in well plates or loaded onto microfluidic devices depending on use.

Peritoneal macrophages (PMPs) were isolated from the peritoneal cavities of 6-8 week old male and female $RelA^{V/V}$ mice by peritoneal lavage with ice cold PBS containing 1% FBS and 2 mM EDTA. PMPs were isolated from the resultant peritoneal cells by negative selection using a Macrophage Isolation Kit (Peritoneum) (Milyenyi) in the MACS MS system (Milyenyi). Peritoneal macrophages were cultured in complete media for subsequent uses.

3T3s were cultured in a tissue culture incubator maintained at 37°C and 5% CO2. Cells were passed prior to reaching 100% confluency and maintained for no more than 15 passages.

To knock out Myd88, a Myd88-targeting guide RNA (5'-TCGCGCTTAACGTGGGAGTG-3') was cloned into the pX330 plasmid backbone (Addgene Plasmid #42230) and transfected using

electroporation (Lonza) into 3T3s. 48 hours post-transfection, single cells were sorted into a 96-well plate and allowed to grow into clonal populations. Screening by Sanger sequencing identified three clones with frameshift mutations in one or both copies of the gene. Successful knockout was confirmed with western blot probing for MyD88 (1° rabbit anti-MyD88 1:1000, Cell Signaling Technologies. 2° goat anti-rabbit DyLight 800 1:25000), following which the blot was stripped and reprobed for β-actin as a loading control (mouse anti-β-Actin DyLight 680, 1:1000). Blots were imaged on a LICOR scanner on the 700 and 800 nm channels.

Reagents

Ultrapure lipopolysaccharide from E. coli O111:B4 (LPS) (Invivogen), PAM2CSK4 (PAM) (Invivogen), ODN 1668 (CpG) (Invivogen), HMW polyinosinic-polycytidylic acid (polyI:C) (Invivogen), murine tumor necrosis factor alpha (TNFα) (R&D Systems), murine interleukin 1 beta (IL-1β) (R&D Systems), and murine m-CSF (Peprotech) were reconstituted in ultrapure water, aliquoted, and stored at -80C until individual aliquots were used. For cytokine blocking experiments, murine TNFRSF1A (R&D Systems) and IL10R alpha (R&D Systems) were treated in the same manner. For IKK inhibition experiments, PS1145 (Tocris, 4569) was diluted in complete media to 40 μM.

Microfluidics enabled live-cell imaging and stimulation

A previously designed and published cell culture device was utilized for automated cell culture and ligand stimulus (Son et al., 2021a). The design contains 14 unique stimulus inputs and 64 independently controlled cell culture chambers measuring 3.5 x 0.8 x 0.035 mm, where each can load more than 500 cells. Master molds for this chip were fabricated by patterning photoresist

deposited on silicon wafers through multilayer soft lithography (Gómez-Sjöberg et al., 2007). Microfluidic devices were fabricated by pouring polydimethylsiloxane (PDMS; Momentive, RTV-615) on the control and flow master molds and bonding these two layers. Control layer wafers were poured with 66 g PDMS (10:1 monomer to catalyst), air bubbles removed under vacuum, and cured at 80°C overnight to make a ~2 cm thick PDM slab with the control pattern grooved on the bottom. Flow layer wafers were poured with 15 g PDMS (10:1 monomer to catalyst) and spun at 2200 rpm to achieve a thickness of ~50 μm and cured at 80°C for at least 1 hour. After curing, holes intended for control pins were punched in the control layer, both PDM layers were treated with oxygen plasma (Harrick, PDC-001), aligned using a custom stereomicroscope, and the aligned chip were baked at 80°C overnight. After bonding, holes intended for fluid input and output were punched; then the chip was bonded to a glass slide through plasma treatment and baking. A detailed fabrication protocol can be found in our previous publications[102,124].

Device control valves were connected to electronically actuated pneumatic solenoid valves which can be controlled using a custom graphical interface or pre-written scripts (MATLAB). By actuating different sets of valves, flow pathways in the microfluidic device can be directed from a particular input to a particular chamber. The device was mounted on an epifluorescence microscope (Nikon) and cell chambers were filled with a 0.2-0.4 mg/mL fibronectin solution (Thermo Fisher, R&D Systems) in PBS overnight. All paths on the microfluidic device were then flushed with complete medium to remove the fibronectin and the live imaging apparatus (Life Imaging Services) was set to 37°C, 5% CO_2, 98% humidity to optimize cell growth conditions. As previously described, BMMPs or PMPs were isolated in suspension, pelleted (5

min, 400 xg), and resuspended at a concentration of 10^7/mL in complete media with phenol red-free RPMI (Gibco) to minimize background fluorescence. Cells were loaded into the microfluidic device and allowed to attach. To stain nuclei for cell tracking 1 hour prior to the start of the experiment, cells were treated with 1 μM Hoechst 33342 in complete media for 5 minutes before washing with complete media. No Hoechst induced cell-death or morphological changes were observed over the 12-16 hours of imaging using the conditions described below.

3T3s were harvested with trypsin from flasks, washed with complete medium, and resuspended at ~$5*10^6$ cells/mL in FluoroBrite DMEM (Gibco) with the same supplements to reduce background fluorescence. Cells were loaded at approximately 50% confluency to optimize tracking efficiency, and cells were allowed to settle and equilibrate for 5 hours prior to start of stimulation and imaging.

Epifluorescence images were acquired using a Nikon Ti2 microscope enclosed within a temperature-controlled incubator (Life Imaging Services). Images were captured at 20X magnification through a complementary metal-oxide semiconductor camera (Hamamatsu, ORCA-Flash4.0 V2) every 6 minutes. Each position was imaged for mVenus-RelA (508-nm, 1 s) and Hoechst (395-nm, 50 ms) (BMMPs, PMPs). Alternatively, each chamber position was imaged for p65-DsRed (555-nm excitation, 0.5-1 s exposure time), H2B-GFP (485-nm, 50-100 ms), and/or KTR-JNK-mCerulean3 (440-nm, 100 ms) (3T3s). No photobleaching or phototoxicity was observed over the course of the imaging process. For the time resolved experiments with 3T3s switching from LPS to IL-1β, imaging was conducted every 3 minutes instead in order to increase the temporal resolution of the trace.

Previously described reagents were diluted from stock solutions in complete media (supplemented with 20 ng/mL m-CSF for BMMP). Each microfluidic experiment for the BMMPs included at least two positive controls (complete media to 10 ng/mL TNFα, 1 ng/mL LPS) and one negative control (complete media only) to ensure comparability and no cross contamination. Ligand doses were chosen to capture 1-1.5 log variation in reagent concentration over a dynamic range of BMMP responsiveness. Ligand were diluted immediately prior to use, stored on ice over the duration of the experiment, and delivered to the device using polyetheretherketone tubing (VICI).

For experiments with 3T3s, based on experimental quantification of NF-κB translocation following titration of each ligand, we selected high, mid, and low doses of each ligand with comparable activation (TNF-α: 90, 30, 3 ng/mL; IL-1β: 3, 0.2, 0.05 ng/mL; LPS: 400, 100, 12.5 ng/mL; PAM: 1, 0.1, 0.01 ng/mL). For each set of high, middle, and low dose ligands, all non-repeating combinations of the four ligands were supplied at 2-hour intervals, producing 24 conditions per dose over 8 hours. One condition was maintained as a positive control (mid dose TNF-α, IL-1β, LPs, PAM) and one condition maintained as a negative control (4 feedings of complete media). For other experimental conditions, ligands were provided and switched at the indicated dose at the indicated time.

Input pressure was maintained at 4 psi to minimize cell shearing during feeding. For cytokine blocking experiments, stimulus A was provided with excess receptor in complete media, followed by stimulus B in complete media without receptor. For IKK inhibition experiments, PS1145 (Tocris, 4569) was diluted in complete media to 40 μM. Cells were pretreated with PS1145 for 90 minutes, then exposed to media containing PS1145 and LPS for 4 hours, washed

for 30 minutes in complete media, and stimulated with IL-1β (3 ng/mL). Other details can be found in our previous published methods [124]. All BMMP and PMP experiments were done in at least biological duplicate with two independent preparations of cells from different mice on different days.

Measurement of surface and intracellular protein and secreted cytokine levels

Flow cytometry for CD11b (APC-Cy7, 1:100) (BioLegend) and F4/80 (PerCP-Cy5.5, 1:20) (BioLegend) was performed on live BMDMs or PMPs preblocked with TruStain FcX mouse (BioLegend) on an LSR Fortessa 4-15. Compensation was performed using UltraComp eBeads (Invitrogen) and gates set using fluorescent minus one (FMO) controls.

For intracellular flow cytometry of IκBα, anti-IκBα (Abcam) was DBCO-functionalized (Sigma) [125], and reacted with azide-functionalized Cy5 (Sigma) overnight at 4°C. BMDMs were fixed with 4% PFA and permeabilized with 0.1% Triton-X100. BMDMs were then stained with 17 nM conjugated antibodies in Probe Binding Buffer (PBS, 0.1% BSA (Thermo Scientific), 0.1 mg/ml sonicated salmon sperm DNA (Invitrogen), 250 nM of isotype control) for 60 min at 37°C. Flow was performed on an LSR Fortessa 4-15.

Secreted cytokines TNFα and IL-10 were detected using sandwich ELISA kits (Invitrogen) based on manufacturer protocol. Briefly, supernatant from 200k cells seeded in a 24 well plate was used for each test condition and the end point absorbance of each microwell was read on a spectro-photometer (Biotek Synergy H1). Concentrations were calculated from calibration curves generated using TNF-alpha and IL-10 standards.

Measurement of bulk RNA-seq expression

To facilitate retrieval of cells, the corner of the microfluidic device with the outlet was cut to expose the outlet channel. At the indicated time following stimulation, cells in the target chamber were treated with TrypLE Express (Gibco) for ~ 1 min to detach them from the treated surface, then sent to the outlet channel by washing with PBS. Detached cells accumulated at the outlet channel, were removed in a ~2 uL droplet by manual pipetting and deposited in 10 uL ice-cold lysis buffer containing 0.1% Triton-X 100 and RNase inhibitor (Takara) and stored at -80°C until further processing. Approximately 1500 cells were retrieved per replicate per condition.

BMMP were replated in 24-well plates at 150,000 cells/well in complete media supplemented with 20 ng/mL m-CSF and allowed to rest overnight. Media was aspirated and Stimulus A in complete media and m-CSF added. After 4 hours, Stimulus A was aspirated and Stimulus B in complete media and m-CSF added. After another 4 hours, stimulus B was aspirated and cells lysed using RLT buffer (Qiagen) + 1% β-mercaptoethanol. RNA was extracted using Dynabeads (Invitrogen), reverse transcription was performed using Maxima HMinus RT (Thermo Fisher) with a poly-dT oligo and a template switching oligo (5’ -AAGCAGTGGTATCAACGCAGAGTGAATrGrGrG -3’) followed by one cycle of second strand synthesis using KAPA HiFi (Roche, primer: 5’-AAGCAGTGGTATCAACGCAGAGT-3’) and purification with Ampure XP beads (Beckman Coulter). Library prep was performed following the Nextera XT procedure. Mean fragment length was between 400-600 bp for each sample. Libraries were sequenced on the NextSeq550 platform (Illumina) using the NextSeq 500/550 high output kit v2.

For 3T3s, samples for both qPCR and next generation sequencing were taken from microfluidic device directly (see "Cell retrieval from microfluidic device"). Sample prep for RNA-sequencing followed the SMART-Seq2 pipeline for single cells[126]. Briefly, cell lysate was incubated at 72 °C with oligo-dT_{30}VN to anneal, followed by the rest of the SMART-Seq2 reverse transcriptase mix and incubated at 42C for 90 minutes followed by 10 cycles between 50°C and 42°C to unfold secondary structure. Template switching using the same modified TSO oligo as above provided a PCR handle on the 3' end of the newly synthesized cDNA strand. 6 cycles of single primer preamplification with KAPA HiFi, and purification with Ampure XP beads (1:1 ratio, Beckman Coulter) produced a purified cDNA library. Library prep was performed by the University of Chicago Genomics Facility using the Nextera XT procedure. Samples were then single end sequenced in the same facility on an Illumina HiSEQ4000 with a read length of 50 bp. For qPCR, Targeted reverse transcription and preamplification were done using a CellDirect One-Step RT-qPCR kit (Themo Fisher). qPCR was performed with custom primer/probe sets (Tnfaip3, FWD: GCAGCTGGAATCTCTGAAATCT, REV: AGTTGTCCCATTCGTCATTCC, PRB: /56-FAM/AAACAGGAC/ZEN/TTTGCTACGACACTCGG/3IABkFQ/), predesigned IDT PrimeTime probe assays (Csf2: Mm.PT.58.10456839, Csf3: Mm.PT.58.43222334.g, Cxcl2: Mm.PT.58.7603454.g, Cxcl3: Mm.PT.58.45877295.g, Il23a: Mm.PT.58.10594618.g, Gapdh: Mm.PT.39a.1), or predesigned TaqMan probe assays (Nfkbia: Mm00477798_m1, Nfkbie: Mm01269649_m1).

Measurement of chromatin accessibility using ATAC-seq

BMMP were replated in 6 well plates at 600,000 cells/well in complete media supplemented with 20 ng/mL m-CSF and allowed to rest overnight. Media was aspirated and Stimulus A in

complete media with m-CSF added. After 4 hours, Stimulus A was aspirated, and Stimulus B added. After another 4 hours, BMDMs were detached with Accutase (Thermo Scientific) and lysed using cold lysis buffer (10mM Tris-HCl pH7.5, 46 3mM MgCl2, 10mM NaCl and 0.1% IGEPAL CA-630). Nuclei were pelleted and resuspended in transposase mixture () at 37°C for 30 minutes. Fragmented DNA was purified and libraries were purified using the Illumina DNA prep kit (Illumina) and sequenced at a depth of ~15 million reads/sample on a Novaseq 6000 (Illumina).

Image analysis and trace processing

Images were exported to MATLAB 2021a for processing and single cell analysis using custom code. Flat field and dark frame corrections were applied to images. Individual cell nuclei were segmented using Hoechst or H2B-GFP images and tracked over successive frames. Background fluorescence was quantified from mean intensity of regions of each image without cells and subtracted from the respective frame. Nuclear segmentation was used to identify median nuclear fluorescence in each frame and normalized to median cytoplasmic fluorescence evaluated from a ring of cytoplasm surrounding the segmented nuclear region[127]. The resulting traces were processed to remove cells which undergo death, division, or other sources of error during the experimental images. Only traces which were complete over the time interval of interest for each condition were included in subsequent analysis. Cells were accurately tracked with >99% accuracy over up to 8-hour intervals.

Each trace was normalized to the mean nuclear/cytoplasmic ratio from the two frames prior to the interval of interest. Key features were identified using MATLAB. For BMMPs, AUC was calculated by trapezoidal approximation, and early and late AUC were defined by AUC in the

first and last 20 frames (120 minutes). Maximum amplitude was identified by finding the index of maximum amplitude from a smoothed trace (loess method, 3 frame interval, minimum prominence 0.1) to reduce noise, then identifying the nuclear/cytoplasmic ratio for that index in the unsmoothed trace. Peak timing was identified by finding the frame at which a trace first reaches its half-maximal amplitude. For all BMMP experiments, stimulus B (TNF or LPS) AUC and amplitude were normalized to the naïve response to the same stimulus. For PMPs, traces were first smoothed (loess method, 5 frame interval) to reduce the noise due to the small size and movement of PMPs. AUC was calculated by trapezoidal approximation from the smoothed trace and the upper and lower 5% of cells were discarded.

For 3T3s, to account for the possibility of oscillations in nuclear translocation, multiple local maxima were allowed with a minimum distance between maxima of 5 frames (30 minutes). To distinguish true maxima from noise due to frame-by-frame fluctuation in nuclear fluorescence, we set the 95th percentile of maxima identified from unstimulated cells as the cutoff and set all stimulus maxima below that cutoff to be zero. Area under the curve (AUC) for each stimulus interval was calculated by taking the trapezoidal approximate of the integral for each trace in the defined time interval. No other processing was done unless otherwise noted.

Information theory analysis

Two different approaches were used for mutual information analysis. For macrophages, we used the methods for mutual information calculation developed by Jetka et al.[128]. Every other point from the dynamic trace obtained from microscopy were extracted and used as an input for calculation of mutual information. The mutual information *I* between the responses *R* from a pair

of samples *S* can be calculated as the difference between the entropy *H* of the entire response (non-conditional entropy) and the sum of entropies from the responses specific to each sample:

$$I(R; S) = H(R) - H(R|S)$$

I describes the reduction in entropy, or uncertainty, in identifying the sample which a response belongs to due to observing the response. Thus the mutual information can be thought of as representing the "distinguishability" between two sample responses. This calculation of mutual information assumes the probability of a response coming from each sample is 0.5 and can vary from 0 (indistinguishable) to 1 bit (entirely distinguishable). Additional information about the calculation of mutual information can be found in the original publication [128].

For 3T3s, we employed the method and codes developed by Selimkhanov et al.[129]. After obtaining the dynamic of NF-κB translocation in each cell, the nuclear NF-κB level at multiple time points were extracted and used as response (variable R) to evaluate the mutual information (variable I). However, in this setup, each sample may have different probability of happening. Cells may be exposed a particular ligand sequence more frequently than other sequences. The conditional entropy can fluctuate depending on the probability of each sample (or ligand sequence). However, it is still possible to evaluate the theoretical maximum information transfer possible through the given system. This is defined as channel capacity, C, and can be evaluated by finding a set of probabilities that would maximize the mutual information:

$$C(R;S) = \max_{Q} I(R;S) \begin{cases} \sum_i q_i = 1 \\ q_i \geq 0 \end{cases}$$

, where C indicates the channel capacity, Q is a set of probabilities for m samples, [q1, q2,... qm]. Further details about the calculating entropies and how the mutual information was maximized can be found in the previous publication[129]. In this study, the NF-κB levels at multiple time points during each ligand interval in each sample were used as input (variable R) to calculate the channel capacity of the NFκB network in distinguishing a particular ligand at each step (S1-4) or prior history of ligand.

NFκB network simulation: Model 1 structure, fitting, and parameters

Two models were built in this thesis to capture the experimental features of NFκB memory in BMMP ("Model 1") and 3T3s ("Model 2"). The entire model structure and parameter table for Model 1 is given first, followed by the model structure and parameter table for Model 2.

Previous mathematical models have been developed and parametrized which describe NFκB translocation due to a variety of stimuli [90,100,101]. These models vary in complexity from minimal three equation models [100] to models which strive to capture many of the pathways and processes involved in NFκB signaling [78]. In this work, we based our model off a previously published reduced ordinary differential equation model [102] to identify simple network motifs which could explain our memory phenotypes. This model simplifies interactions between signaling intermediaries upstream of IKK and reduces the number of intermediate protein states, but still accurately complex signaling behaviors following dynamic ligand input.

In our final model, we include two equations governing nuclear and cytoplasmic free NFκB (eq. 1-2), free IκBα (eq. 3-4), and NFκB bound to IκBα (eq. 5-6). Based on previous studies reporting high constitutive translation and degradation of free IκBα [104,131], we modeled constitutive

transcription and degradation of IκBα mRNA and constitutive translation and degradation of free IκBα protein (eq. 7). Induced mRNA is also produced in an NFκB-dependent manner and subject to intrinsic degradation (eq. 8). To simplify the model, the same mRNA species is used for induced transcription of IκBα, negative feedback, and positive feedback. IKK becomes activated by CpG, polyI:C, and ligand B (which can represent either TNFα or LPS as the network topology is identical), and activation is inhibited by the negative feedback species (eq. 8). The same rate of activation and feedback inhibition is assumed for all three ligands. We chose to simulate negative feedback acting on activation of IKK as several known negative feedback proteins act at this point (A20, CYLD, IRAKM) [82,87,132], however the negative feedback could also act at other points (e.g. IκBδ and IκBε acting as non-degradable analogs of IκBα) [89,91]. Active IKK becomes inhibited by phosphorylation (eq. 9). The negative feedback module and the additional receptor B are translated from the mRNA and subject to intrinsic degradation, but to represent our experimental finding that positive feedback is only upregulated following polyI:C stimulus, we only allowed translation of receptor level positive feedback during stimulus with polyI:C (eq. 10-11). We assume the rate of translation for the negative feedback and the receptor level positive feedback are linearly related. CpG, polyI:C, and ligand B undergo degradation at the same constant rate (eq. 12-14). The system of equations for our model is:

$$\frac{dNFkB_n}{dt} = r_{NFc\rightarrow NFn} * NFkB_c - r_{NFn\rightarrow NFc} * NFkB_n - r_{NF+IkB\rightarrow NF|IkBa} * {V_{ratio}}^2 * NFkB_n * IkB_n \quad (1)$$

$$\frac{dNFkB_c}{dt} = -r_{NFc\rightarrow NFn} * NFkB_c + r_{NFn\rightarrow NFc} * NFkB_n - r_{NF+IkB\rightarrow NF|IkBa} * NFkB_c * IkB_c + r_{IkBa\ deg} * IKK_a * NFkB|IkB_c \quad (2)$$

$$\frac{dIkB_n}{dt} = r_{IkBc\rightarrow IkBn} * IkB_c - r_{IkBn\rightarrow IkBc} * IkB_n - r_{NF+IkB\rightarrow NF|IkB} * {V_{ratio}}^2 * NFkB_n * IkB_n \quad (3)$$

$$\frac{dIkB_c}{dt} = -r_{IkBc\rightarrow IkBn} * IkB_c + r_{IkBn\rightarrow IkBc} * IkB_n - r_{NF+IkB\rightarrow NF|IkB} * NFkB_n * IkB_n - r_{IkB\ const.\ deg} * IkB_c + r_{transl\ IkB} * (mRNA_{ind.} + mRNA_{const.}) \quad (4)$$

$$\frac{dNFkB|IkB_n}{dt} = r_{NF|IkBc\rightarrow NF|IkBn} * NFkB|IkB_c - r_{NF|IkBn\rightarrow NF|IkBc} * NFkB|IkB_n + r_{NF+IkB\rightarrow NF|IkB} * {V_{ratio}}^2 * NFkB_n * IkB_n \quad (5)$$

$$\frac{dNFkB|IkB_c}{dt} = -r_{NF|IkBc\rightarrow NF|IkBn} * NFkB|IkB_c + r_{NF|IkBn\rightarrow NF|IkBc} * NFkB|IkB_n + r_{NF+IkB\rightarrow NF|IkB} * NFkB_c * IkB_c - r_{IkB\ ind.\ deg} * IKK_a * NFkB|IkB_c \quad (6)$$

$$\frac{dmRNA_{const.}}{dt} = r_{transc\ const.} - r_{mRNA\ deg} * mRNA_{const.} \quad (7)$$

$$\frac{dmRNA_{ind.}}{dt} = r_{transc\ ind.} * \frac{{NFkB_n}^{n1}}{{K_{mRNA}}^{n1} + {NFkB_n}^{n1}} - r_{mRNA\ deg} * mRNA_{ind.} \quad (8)$$

$$\frac{dIKKa}{dt} = r_{IKKn\rightarrow IKKa} * CpG * (IKK_{tot} - IKK_a - IKK_i) * \frac{{K_{FB}}^{n2}}{{K_{FB}}^{n2} + {FB}^{n2}} + r_{IKKn\rightarrow IKKa} * polyI{:}C * (IKK_{tot} - IKK_a - IKK_i) * \frac{{K_{FB}}^{n2}}{{K_{FB}}^{n2} + {FB}^{n2}} + r_{IKKn\rightarrow IKKa} * LB * (1 + S_{RB} * RB) * (IKK_{tot} - IKK_a - IKK_i) * \frac{{K_{FB}}^{n2}}{{K_{FB}}^{n2} + {FB}^{n2}} \quad (9)$$

$$\frac{dIKK_i}{dt} = r_{IKKa\rightarrow IKKi} * IKK_a - r_{IKKi\rightarrow IKKn} * IKK_n \quad (10)$$

$$\frac{dNFB}{dt} = r_{ind.\ transl} * mRNA - r_{deg} * NFB \quad (11)$$

$$\frac{dPFB}{dt} = r_{ind.\ trans} * \delta_{polyI:C} * mRNA - r_{deg} * PFB \quad (12)$$

$$\frac{dCpG}{dt} = r_{lig\ deg} * CpG \quad (13)$$

$$\frac{dpolyI{:}C}{dt} = r_{lig\ deg} * polyI{:}C \quad (14)$$

$$\frac{dLB}{dt} = r_{lig\ deg} * LB \quad (15)$$

The 15 equations above include 27 parameters. 8 of these are based on previous measured values, 7 are based on the original model (values within ~50% of previously published values), and 12 are new or refitted in this work [102]. Parameters were fitted to produce a model which matched mean peak amplitude from experimental data for polyI:C to TNFα and CpG to LPS. We optimized the model to fit amplitudes due to its importance as a marker of maximum NFκB signal transduction and because the reduced model simplifies several nodes which contribute to more complex signaling dynamics (important for AUC). Parameter sensitivity calculations were accomplished by varying each parameter +/- 10 fold from the global minimum.

Parameter	Value	Description (reference)
V_{ratio}	4	Ratio of cytoplasmic to nuclear volume [133]
$n1$	4	Cooperativity for mRNA transcription by nuclear NFκB [134]
$n2$	2	Cooperativity for negative feedback [102]
$NFkB_{total}$	$3.5*10^4$	Total molecules of NFκB [135]
$IkB_{initial}$	$5.24*10^3$	Initial molecules of excess IκBα [131]
IKK_{total}	$6.0*10^3$	Total molecules of IKK [135]
$r_{IKKn \rightarrow IKKa}$	0.0262 min^{-1}	Max activation rate of IKKn (fitted)
$r_{IKKa \rightarrow IKKi}$	0.276 min^{-1}	Inactivation rate of IKKa (fitted)
$r_{IKKi \rightarrow IKKn}$	$1.2*10^{-3}$ min^{-1}	Rate of transition from IKKi to IKKn (fitted)
$r_{NFc \rightarrow NFn}$	9.32 min^{-1}	Import rate for free cytosolic NFκB (fitted)
$r_{NFn \rightarrow NFc}$	$2.5*10^{-3}$ min^{-1}	Export rate for free nuclear NFκB (fitted)
$r_{IkBc \rightarrow IkBn}$	$5.1*10^{-3}$ min^{-1}	Import rate for free cytosolic IκB (fitted)
$r_{IkBn \rightarrow IkBc}$	0.244 min^{-1}	Export rate for free nuclear IκB [102]
$r_{NF\|IkBc \rightarrow NF\|IkBn}$	$1.0*10^{-5}$ min^{-1}	Import rate for cytosolic NFκB|IκB [102]
$r_{NF\|IkBn \rightarrow NF\|IkBc}$	0.77 min^{-1}	Export rate for nuclear NFκB|IκB [102]
$r_{NF+IkB \rightarrow NF\|IkB}$	$4.0*10^{-6}$ min^{-1}	Association rate for NFκB|IκB (fitted)
K_{mRNA}	14000 molecules	Dissociation constant for nuclear NFκB inducing mRNA (fitted)
$r_{transc\ const.}$	0.713 min^{-1}	Constitutive transcription rate for IκB mRNA (fitted)
$r_{transc\ ind.}$	7.70 min^{-1}	NFκB induced maximum transcription rate [102]
$r_{mRNA\ deg}$	0.045 min^{-1}	mRNA degradation rate [102]
$r_{ind.\ transl}$	22.8 min^{-1}	Induced translation rate [102]
$r_{IkB\ transl}$	50 min^{-1}	Constitutive translation rate for IkB (fitted)
$r_{IkB\ ind.\ deg}$	$5.0*10^{-5}$ min^{-1}	Induced IκB degradation [104]
$r_{IkB\ const.\ deg}$	0.1 min^{-1}	Constitutive IκB degradation [104]
$r_{lig\ deg}$	0.053 min^{-1}	Ligand degradation rate (fitted)
r_{deg}	0.0014 min^{-1}	Feedback degradation rate (fitted)
S_{RB}	$2.92*10^{-4}$	Scaling factor for additional receptor B (fitted)
K_{FB}	$1.83*10^4$	Dissociation constant for negative feedback [102]

Table 1. Parameters used for model 1
All parameters associated with Model 1 and source for parameter values.

NFκB network simulation: Model 2 structure, fitting, and parameters

To investigate if the two negative feedback model is sufficient for the ligand history effect in 3T3s, we built a simplified network simulation. We extended the previous minimal NFκB model[100], which comprises three coupled differential equations each describing the dynamics of nuclear NFκB (Eq. 1), mRNA of IκBα (Eq. 2), and cytoplasmic IκBα (Eq. 3). Previous study reports that nuclear NFκB activates the transcription of downstream gene in a sigmoidal fashion with sharp threshold [109,134]. Thus, we adapted the Hill function to describe mRNA transcription and applied a Hill coefficient of four to accurately describe the dynamics (Eq. 2). Our study involved various ligand stimuli, where each corresponds to different receptor and involves various cytoplasmic kinases for NFκB activation. However, all signaling pathways converge on an essential mediator, IKK, prior to NFκB translocation[136]. Upon activation, neutral IKK becomes active IKK and degrades IκBα initiating NFκB translocation. Active IKK gradually becomes inactive IKK, which then cycles back to the neutral state over time[63]. We added two differential equations to describe this cycling of IKK (Eq. 10 and 11). Then, we incorporated the two negative feedbacks discussed in our study. Upstream of IKK, MyD88-dependent ligands (LPS or IL-1β) converge on another common kinase, IRAK1/4, which was shown to have auto-inhibitory negative feedback function reliant on aggregation[84]. To integrate this important upstream negative feedback, we added IRAK1/4 activation and inactivation dynamics for each MyD88 dependent receptor (Eq. 6 ─ 9). To minimize variables, we assumed that the activation and inactivation rates by different receptors are same, and thus that IRAK1 kinetics depend only on the amount of each receptor in the active state. Since the inactivation rate varied by the amount of active IRAK, we made the inactivation term non-linear, where the inactivation rate is proportional to the squared concentration of active

IRAK. Another important negative feedback originates downstream of NFκB. Other than IκBα, previous works report many downstream genes, which inhibit nuclear NFκB in various ways[49]. Among them, several inhibitors target upstream of IKK, where many negative feedbacks including A20, SOCS-1/3, and Trim30α, repress the receptor activity and thereby hinder the activation of IKK. Hence, we added the expression of the downstream negative inhibitor (Eq. 4 and 5) and adjusted the IKK activation term in Eq. 10 to incorporate this effect. The Hill coefficient of 3 in this inhibition term includes the high cooperativity that arises in the complex interactions between upstream molecules. For example, for A20 to be fully active, it not only needs to be dimerized but also needs other adaptor proteins to inhibit the phosphorylation of IKK[83]. Additionally, IKK has multiple phosphorylation sites, which may require multiple inhibitor complexes to successfully repress the IKK activation[62]. Lastly, for the amount of activate ligand receptors, we normalized the dose range of ligand such that similar dose would activate similar number or ratio of receptors. For simplicity, we applied fast equilibrium approximation for the receptor dynamics, *i.e.*, at any given time the activity of receptor simply corresponds to the dose of ligand (Eq. 12 ─ 14). All receptors investigated in our study require multimerization to be active [57,137]; hence, we used non-linear relationship between the dose and the active receptor. The system of equations for our model is listed below:

$$\frac{dN_n}{dt} = r_{Nim} * \frac{1-N_n}{K_{Ic}+I} - r_{Iim} * \frac{I*N_n}{K_{In}+N_n} \quad \text{(Eq. 1)}$$

$$\frac{dI_m}{dt} = tr_I * \frac{N_n^4}{(K_N^4+N_n^4)} - d_{Im} * I_m \quad \text{(Eq. 2)}$$

$$\frac{dI}{dt} = tl_I * I_m - a_{IKK} * IKK_a * (1 - N_n) * \frac{I}{K_{Ic}+I} \quad \text{(Eq. 3)}$$

$$\frac{dA_m}{dt} = tr_A * \frac{N_n^4}{K_N^4 + N_n^4} - d_{Am} * A_m \quad \text{(Eq. 4)}$$

$$\frac{dA}{dt} = tl_A * A_m - d_A * A \quad \text{(Eq. 5)}$$

$$\frac{dIRAK_{LPS}}{dt} = a_{IRAK} * R_{LPS} * (1 - IRAK_{LPS} - IRAKi_{LPS} - IRAK_{IL1} - IRAKi_{IL1}) - d_{IRAK} * IRAK_{LPS}^2 \quad \text{(Eq. 6)}$$

$$\frac{dIRAKi_{LPS}}{dt} = d_{IRAK} * IRAK_{LPS}^2 - d_{IRAKi} * IRAKi_{LPS} \quad \text{(Eq. 7)}$$

$$\frac{dIRAK_{IL1}}{dt} = a_{IRAK} * R_{IL1} * (1 - IRAK_{LPS} - IRAKi_{LPS} - IRAK_{IL1} - IRAKi_{IL1}) - d_{IRAK} * IRAK_{IL1}^2 \quad \text{(Eq. 8)}$$

$$\frac{dIRAKi_{IL1}}{dt} = d_{IRAK} * IRAK_{IL1}^2 - d_{IRAKi} * IRAKi_{IL1} \quad \text{(Eq. 9)}$$

$$\frac{dIKK_a}{dt} = (1 - IKK_a - IKK_i) * a_R * \left(R_{TNF} * \frac{C^3}{C^3 + A^3} + IRAK_{LPS} * \frac{C^3}{C^3 + A^3} + IRAK_{IL1} * \frac{C^3}{C^3 + A^3}\right) - \mu * IKK_a^2 \quad \text{(Eq. 10)}$$

$$\frac{dIKK_i}{dt} = \mu * IKK_a^2 - \beta * IKK_i \quad \text{(Eq. 11)}$$

$$R_{TNF} = \frac{TNF^3}{TNF^3 + 1} \quad \text{(Eq. 12)}$$

$$R_{LPS} = \frac{LPS^3}{LPS^3 + 1} \quad \text{(Eq. 13)}$$

$$R_{IL1} = \frac{IL1^3}{IL1^3 + 1} \quad \text{(Eq. 14)}$$

Even though our model consists of the two negative feedbacks and multiple receptors, we managed to reduce the number of parameters to twenty. Roughly half of these are related to NFκB and IκBα dynamics. The other half describes the newly added mechanisms, which involve dynamics of IKK cycling and negative feedback regulations. Since our model is based on the minimal model from the previous publications, we adapted parameters from them to where applicable. For the newly added components, we assumed or fitted the parameters to the period of NFκB oscillation (~ 2h). The list of parameters and their values are described in the table [72,100–102].

Computer simulations were performed using Python. The differential equations were integrated using *odeint* from *scipy.integrate* solver. To determine the basal stationary state of the network prior to stimulation, a short pulse of TNFα was introduced at the beginning, then the dynamic of each component in the network was monitored up to 48 h after the pulse. After confirming the dynamics of all components became stationary, we stimulated the network with one of the first ligands (TNFα, IL-1β, or LPS), then replaced it with another ligand after 2 h. Simulated dynamics of different components were plotted using Bokeh visualization library.

Description	Parameter	Value	Unit	Reference
Importation rate of cytosolic NFκB into nucleus	r_{Nim}	11.3	$\mu M \cdot h^{-1}$	Hoffmann et al., 2002
Dissociation constant for IκBα binding to NFκB in cytosol	K_{Ic}	$3.5 \cdot 10^{-2}$	μM	Krishna et al., 2006
Importation rate of cytosolic IκBα into nucleus	r_{Iim}	1.09	h^{-1}	Hoffmann et al., 2002
Dissociation constant for IκBα binding to NFκB in nucleus	K_{In}	$2.90 \cdot 10^{-2}$	μM	Krishna et al., 2006
Transcription rate of IκBα mRNA	tr_I	59.5	$\mu M \cdot h^{-1}$	Hoffmann et al., 2002
Dissociation constant for nuclear NFκB inducing downstream transcription	K_N	0.6	μM	Fitted
Degradation rate of IκBα mRNA	d_{Im}	2.00	h^{-1}	Krishna et al., 2006
Translation rate of IκBα	tl_I	14.4	h^{-1}	Hoffmann et al., 2002
Degradation rate of IκBα by active IKK	a_{IKK}	126	$\mu M^{-1} \cdot h^{-1}$	Hoffmann et al., 2002
Transcription rate of downstream feedback mRNA	tr_A	5.0	$\mu M \cdot h^{-1}$	Fitted
Degradation rate of downstream feedback mRNA	d_{Am}	1.0	h^{-1}	Tay et al., 2010 and Son et al., 2021
Translation rate of downstream feedback proteins	tl_A	15.0	h^{-1}	Fitted
Degradation rate of downstream feedback proteins	d_A	0.25	h^{-1}	Fitted
IRAK activation rate by active MyD88-dependent receptor	a_{IRAK}	252	h^{-1}	Fitted
IRAK inactivation rate	d_{IRAK}	200	$\mu M^{-1} \cdot h^{-1}$	Fitted
Rate for inactive IRAK to go back to neutral state	d_{IRAKi}	0.005	h^{-1}	Fitted
Rate for either active TNFR or IRAK activating neutral IKK	a_R	4.00	h^{-1}	Assumed
Dissociation constant for downstream feedback inhibiting IKK activation	C	8.0	$\mu M^{-1} \cdot h^{-1}$	Fitted
Inactivation rate of active IKK	μ	28.3	$\mu M^{-1} \cdot h^{-1}$	Fitted
Rate for inactive IKK going back to neutral state	β	0.2	h^{-1}	Fitted

Table 2. Parameters used for model 2
All parameters associated with Model 2 and source for parameter values.

To simulate the difference in the expression level of the downstream negative feedback, we adjusted the dissociation constant for the inhibition of IKK activation (parameter *C*). If we added the different downstream expression parameters for each ligand, it would dramatically increase the number of parameters necessary to describe the dynamics of downstream negative feedback. To simply model differential strength of IKK inhibition, we adjusted the dissociation constant for IKK inhibition. For LPS stimulation, the dissociation constant was reduced by four-fold, meaning the threshold for negative feedback molecules to inhibit the IKK activation is reduced by four-fold. This way we could still monitor the effect from the different downstream negative feedback strength, while minimizing the number of parameters.

RNA sequencing analysis

Adapter trimming and read mapping to the reference genome (GRCm38) was done using STAR with default parameters [138]. Transcript abundance was quantified using the R package featureCounts [139]. Raw counts were normalized and differential gene expression identified using the R packages edgeR and limma [140,141]. For BMDMs differential genes (DEGs) were identified compared to naïve BMDMs using the cutoffs of Benjamini-Hochberg false discovery rate (FDR) < 0.01 and fold change > 1.

For 3T3s, differential genes were identified between IL-1β and untreated, PAM and untreated, LPS and untreated, and IL-1β and LPS using cutoffs of Benjamini-Hochberg false discovery rate (FDR) < 0.01 and log fold change > 1.

Visualization of DEGs in the NFκB pathway (KEGG: mmu04064) between polyI:C and CpG treatment accomplished using the R package Pathview [142]. We defined synergistic and antagonistic gene regulation by memory in all DEGs using the following equation:

$$\Delta AB_{memory} = \frac{AB - (\emptyset + \Delta A\emptyset + \Delta B)}{(\emptyset + \Delta A\emptyset + \Delta B)}$$

$$\Delta AB_{memory} > 0.25 = Synergy;\ \Delta AB_{memory} < -0.25 = Antagonism$$

Here, we compare the gene expression due to sequential stimulus of ligand A and B (AB) to the expected gene expression if the effects of A and B were independent normalized (the "null hypothesis") by the expected gene expression. The expected gene expression term is shown as the gene expression from naïve, media treated cells (∅) plus the change in gene expression from treatment with ligand A followed by media (ΔA∅) plus the change in gene expression from treatment with ligand B only (ΔB). If ΔAB_{memory} was 25% greater than expected, we considered it synergy, and if ΔAB_{memory} was 25% less than expected, we considered it antagonism.

GO and KEGG overrepresentation analysis on groups of synergistic and antagonistic genes was performed using gProfiler [143]. Enriched TFs were identified using the ENCODE ChIP-seq database in ChEA3 [144].

Ct values were calculated using software defaults and normalized to glyceraldehyde-3-phosphate dehydrogenase (GAPDH) expression to produce ΔCt values. ΔCt values were subtracted from the ΔCt values from control samples to calculate the ΔΔCt as a proxy for fold change expression over control.

ATAC sequencing analysis

ATAC peaks were aligned to a reference genome (GRCm38) and called using MACS2 [145]. Peaks from all samples were merged into a single file using iterative overlap peak merging as described in Corces & Granja et al. [146], and all raw peaks quantified using featureCounts [139]. Peaks were normalized and differentially open chromatin sites compared to media control were identified using edgeR and limma [140,141]. Open peaks were annotated using the R package ChIPseeker [147] and enriched transcription factor binding motifs identified from the JASPAR2022 database [148] using the R package monaLisa [149]. All TFs with logFC enrichment > 1 were considered significant and a complete list of enriched TFs can be found in the supplemental information. Genomic tracks were visualized using the R package Rtracklayer [150].

RESULTS

PART I: NFκB MEMORY COORDINATES TRANSCRIPTIONAL RESPONSES TO DYNAMIC INFLAMMATORY STIMULI – *CELL REPORTS* 2021[b]

Introduction

Exposure to pathogenic stimuli results in acute secretion of inflammatory cytokines, followed by a gradual rise and fall in anti-inflammatory cytokines and growth factors [25,27,151,152]. The sequence (temporal ordering) of these stimuli provides information about the local tissue environment to nearby cells, and disruption of this progression is linked to pathology. For example, inflammatory signals in sepsis and chronic inflammation dramatically reshape the innate immune response to subsequent challenges [34,152–154]. Furthermore, efforts to engineer the inflammatory response in adjuvant therapy require understanding how prior exposure alters subsequent stimulus responses [155,156].

Despite the diversity of inflammatory signals, many of these converge on few signaling networks with shared intracellular kinases and activated transcription factors. Pathogenic ligands which activate the Toll-like receptor (TLR) family and pro-inflammatory cytokines secreted by host macrophages all converge on a small set of key inflammatory transcription factors, including the canonical NFκB family transcription factor RelA [57,136,137]. Patterns of NFκB activation over time, or activation dynamics, transmit information about stimulus identity and coordinate the subsequent inflammatory response. Ligands induce distinct dynamics of NFκB nuclear translocation, which facilitate accurate information transmission from extracellular signals to

[b] Most of this section is adapted from Wang AG, Son M, Kenna E, Thom S, and Tay S. NF-κB memory coordinates transcriptional responses to dynamic inflammatory stimuli. *Cell Reports* 40(7):111159. (2022)

expression of response genes [78,157]. NFκB dynamics reshape the accessible chromatin landscape of the cell and regulate gene expression induced by each stimulus [50,74]. However, it is unknown how prior signal exposure alters NFκB dynamics. If prior stimuli induce distinct feedback responses which modulate a signaling network, it raises the possibility that activation dynamics can encode information about both the cell's current stimulus and prior history.

Previous studies of innate immune signaling focused on population-level effects of stimulus history at timescales of days to weeks [30,34,43,152]. These studies report that innate immune memory can induce both priming, where response to subsequent stimulus is stronger [43,153], and tolerance, where the subsequent response becomes attenuated [34,158,159]. However, innate immune memory at short timescales is poorly studied due to the difficulties in strict control of stimulus timing and continual cell monitoring. Furthermore, population averaged read-outs often blur single cell dynamics and may not represent the actual cellular response.

Here, we explored how prior stimulus history alters subsequent signaling responses in the NFκB signaling network by combining automated microfluidic stimulation with live cell imaging (Figure 4a). We found that prior stimuli produced distinct attenuation patterns in subsequent NFκB signaling dynamics through differential regulation of negative feedbacks. These patterns encode information about the cell's prior history, showing that the NFκB network stores information about the temporal sequence of environmental signals and transmits that information in the inflammatory response.

Prior ligand history influences NFκB activation to subsequent stimuli

We focused on the interactions between four inflammatory ligands, tumor necrosis factor alpha (TNFα), interleukin 1β (IL-1β), lipopolysaccharide (LPS), and PAM2CSK4 (PAM). TNFα and IL-1β are key pro-inflammatory cytokines which are secreted by sentinel cells and which activate TNFR and IL1R respectively [160]. LPS is a cell wall component of Gram-negative bacteria which activates TLR4, while PAM is a synthetic analogue of bacterial lipopeptides which activates TLR2/6 [137]. Thus, LPS and PAM represent pathogen signals, which would trigger local secretion of TNFα and IL-1β in an infection scenario. Signaling for LPS, PAM, and IL-1β share the receptor-associated adaptor protein MyD88 and downstream components, including IRAK1 (Fig 1B) [58]. In contrast, TNFα signaling acts through a different set of receptor-associated intermediaries [136]. All these pathways converge at activation of IκB-kinase (IKK), which mediates nuclear translocation of RelA [136,137]. Multiple levels of negative feedback regulate this network, including autoinhibitory phosphorylation of IRAK1 and several transcriptionally regulated negative feedback proteins, such as A20 and IκBε (Figure 4b) [83,84,89,99,102]. Each of these negative feedback proteins targets different components in the NFκB signaling network (Figure 4b) [84].

To characterize how prior histories shape the NFκB response to a subsequent ligand, we used a microfluidic platform to provide sequential stimuli to RelA$^{-/-}$ NIH/3T3 fibroblasts (3T3s) expressing a RelA-DsRed fusion protein (Figure 4a) [102,124]. By continuously imaging 3T3s in this platform, we evaluated NFκB dynamics under a series of stimuli without disrupting the cells (Figure 4c-d). To establish a baseline for comparison between history of the same and different ligands, we stimulated cells with the same ligand four times. In general, prior stimulus with a ligand weakened subsequent responses to the same ligand, which is consistent with previous work with repeated ligand stimulus [99,102,161]. LPS and PAM only produced a response after the first

stimulus, while TNFα and IL-1β exhibited weak responses after the second to fourth stimulus depending on dose (Figure 5a-c). We then systematically profiled the effects of prior history by stimulating cells with non-repeating sequences of all four ligands. This approach

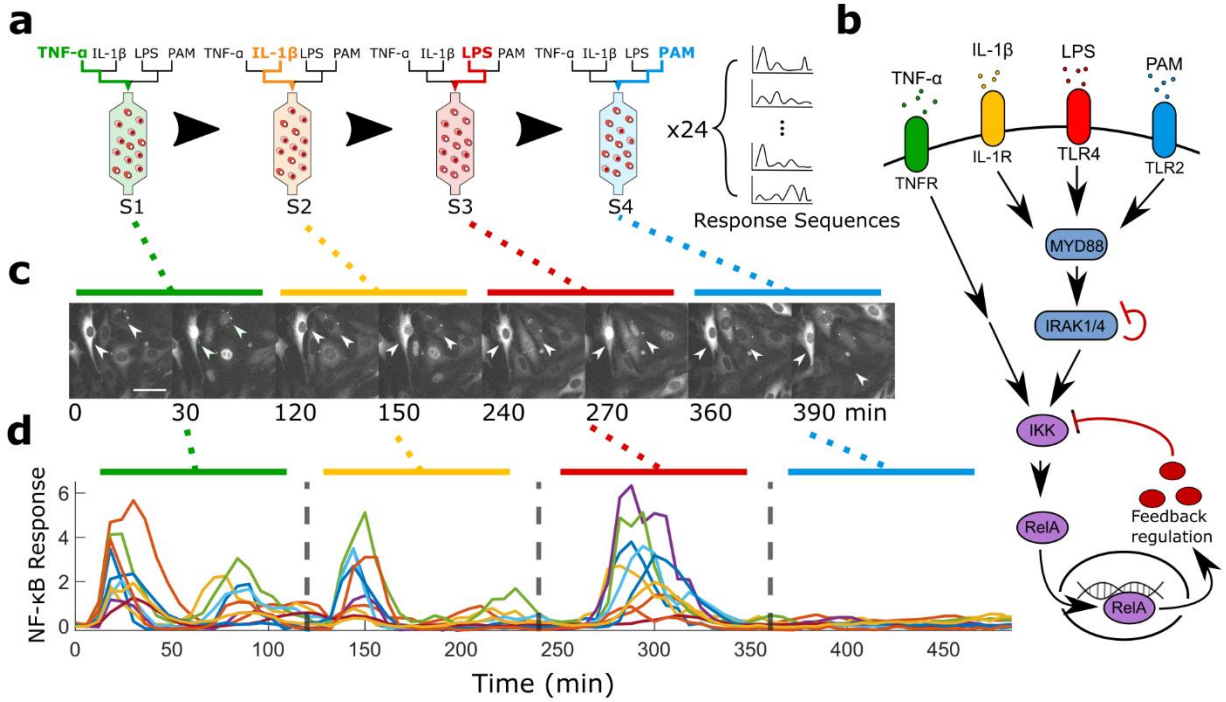

Figure 4. **Microfluidic live cell imaging tracks single cell NFκB responses through multiple sequential stimuli.**

a) Schematic representation of experimental conditions and microfluidic imaging set up. RelA-DsRed tagged 3T3s were stimulated with non-repeating combinations of 4 ligands with in an automated microfluidic cell culture device. **b)** Schematic representation of TNFα (TNFR), IL-1β (IL-1R), LPS (TLR4), and PAM (TLR2) signaling converging on activation of RelA. **c)** Representative grayscale images of RelA nuclear translocation during stimulation with mid dose TNFα (0 min), IL-1β (120 min), LPS (240 min), and PAM (360 min). RelA nuclear translocation in single cells (white arrows) is shown. Scale bar 50 microns. **d)** Quantification of nuclear/cytoplasmic NFκB over imaging interval. Gray dashed lines indicate when new stimulus was provided.

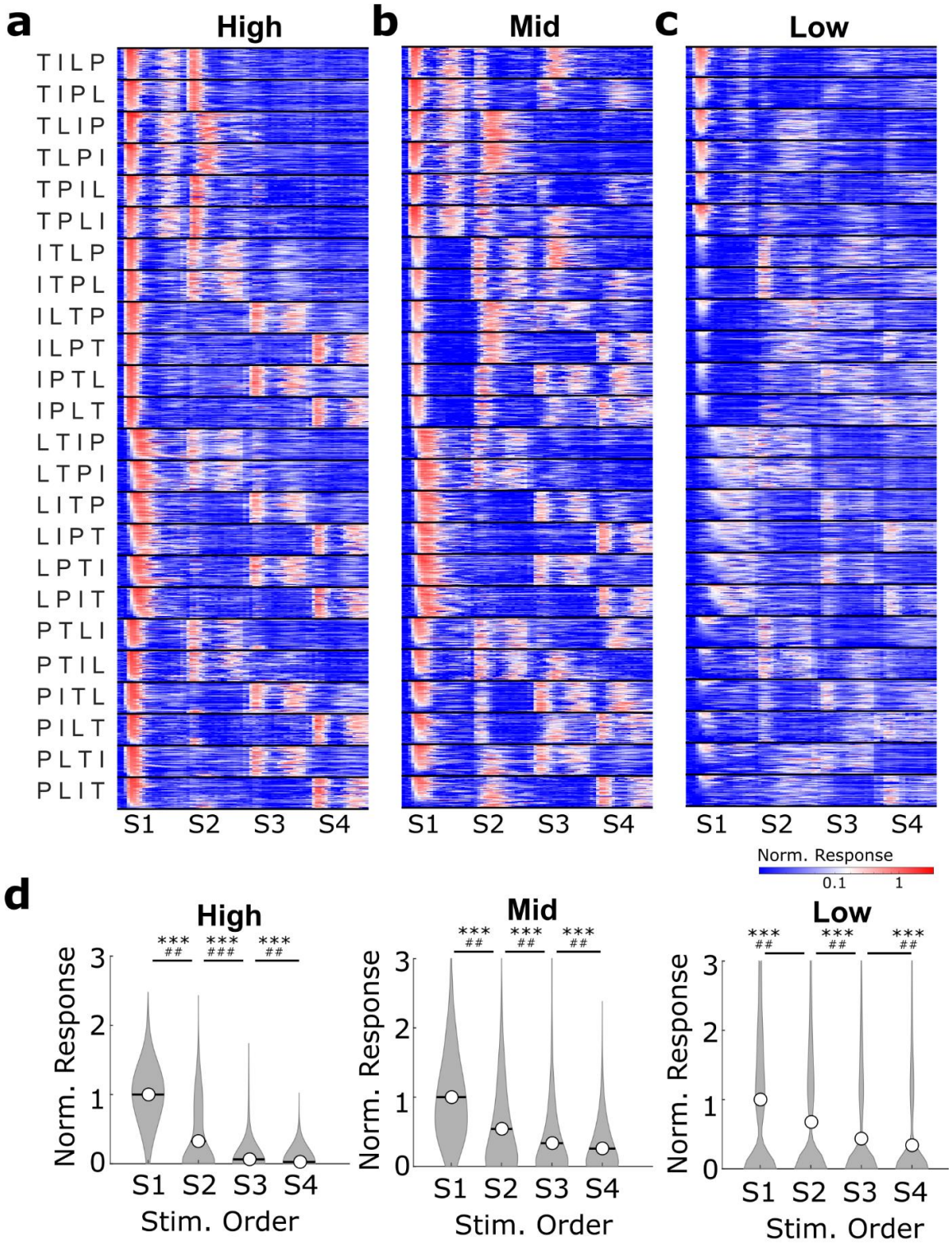

Figure 5. Single-cell NFκB activation traces reveal ligand and dose specific attenuation of signaling by prior stimuli.

Figure 5, continued

a-c) NFκB response dynamics over 2 hours of stimulus for each ligand. 50 randomly selected single-cell traces from two independent replicates are displayed for each condition. Each row shows the nuclear NFκB level of a single-cell measured by time-lapse microscopy, and x-axis shows the time. Heatmap columns are arranged from the first stimulus (S1) to the fourth stimulus (S4). Stimulus orders are shown to the left of the first heatmap, where T stands for TNFα, I for IL-1β, L for LPS, and P for PAM. Heatmap for response to four consecutive feedings with the same ligand are shown above the combinatorial orders. Heatmap colors are normalized based on the high dose S1 response to each ligand. **d)** Single cell responses from S1-S4, normalized to the mean of corresponding S1 response (>2000 cells for each condition). Open circle and line show the mean. Bonferroni corrected Wilcoxon rank sum test p-value < 10^{-4} (***). Fold change difference between sample means > 1 (#), > 1.25 (##), or >4 (###).

produced 24 unique stimulus conditions. The first stimulus (S1) is provided to cells without prior inflammatory ligand exposure, and thus induces a "naïve" response. However, the second, third and fourth stimuli (S2-4) would induce NFκB responses affected by one, two, or three prior ligands, respectively. We used the response to a particular ligand at S1 as a baseline for comparing how different prior stimulus sequences change the response to that ligand. Additionally, to test how stimulus dose changes prior history effects, we calibrated high, mid, and low doses for each ligand based on the percentage of activated cells (Figure 6a-e), then repeated the 24 stimulus sequences for each dose. In our initial dataset of 72 conditions, we analyzed more than 10,000 single cells (Figure 5a-c, Figure 6f-Figure 8) with a range of prior histories and stimulus doses.

To observe general trends in ligand response, we first examined how the response to a specific ligand changed depending on its order in a stimulus sequence. All single cell responses in each sequence position were grouped by ligand and normalized to the mean S1 response for that ligand (Figure 5a-c, Figure 9a-c). When we compared the amplitude changes over the four sequence positions, we observed that response for each ligand decreased from S1 to S4 (Figure 5d). Even in low dose conditions, where response heterogeneity results in highly variable response amplitudes, ligand responses decreased from S1 to S4. Similar trends were observed when quantifying the area under the curve (AUC) of the response instead of the maximum response amplitude (Figure 9d). From these observations, we concluded that prior exposure history primarily attenuates signaling responses to subsequent ligands. However, we also noted that distinct patterns of attenuation existed depending on ligand identity and dose. Even at high dose, where attenuation was strongest, cells responded to TNFα stimulus irrespective of prior

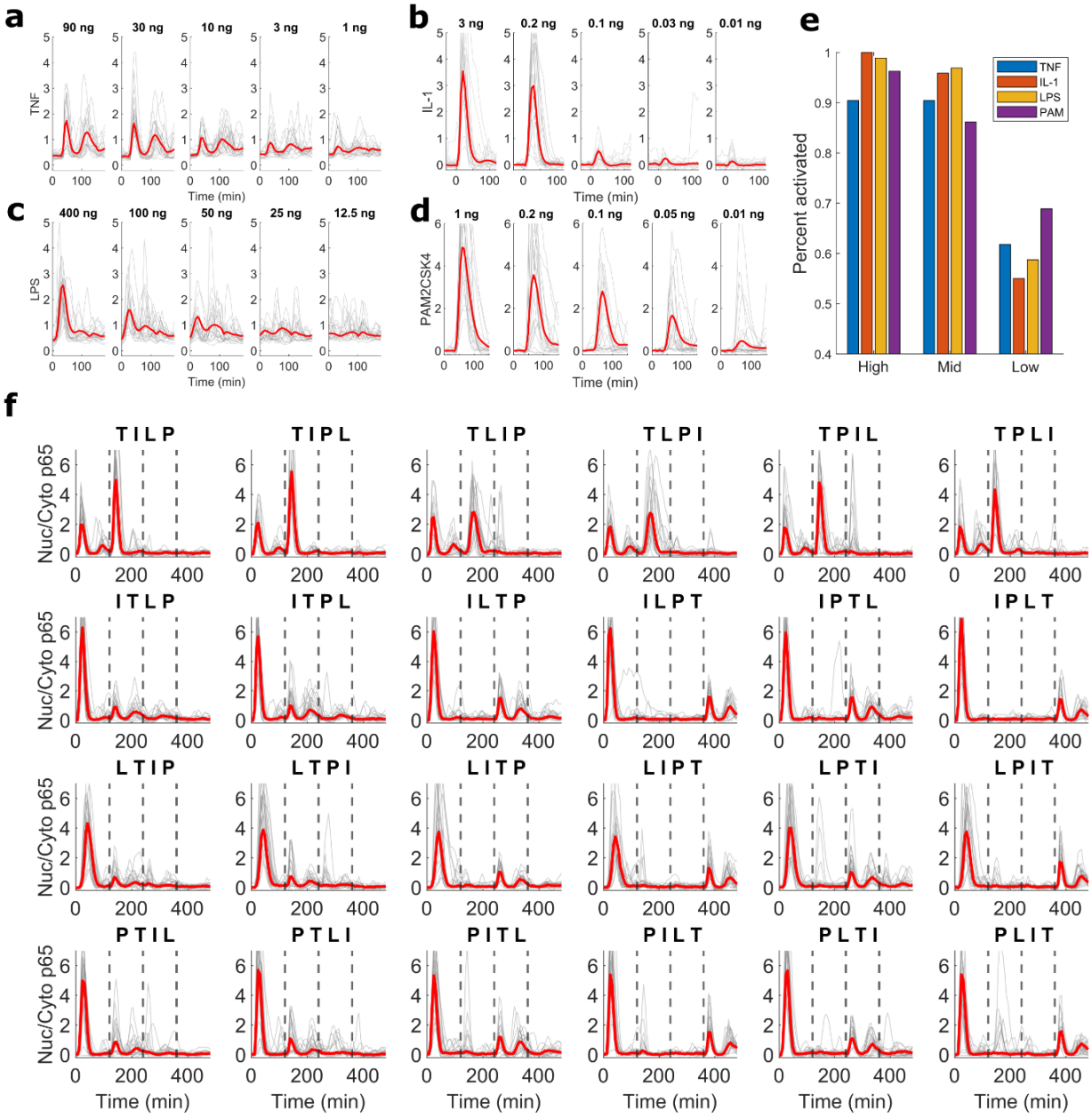

Figure 6. NFκB response to varying doses of ligand stimulus.

20 randomly selected single cells (gray lines) and mean (red line) are shown for each stimulus condition: **a)** TNFα, **b)** IL-1β, **c)** LPS, or **d)** PAM. **e)** Percent activated for selected dose ranges – high (> 95% activated, TNFα 90 ng/mL, IL-1β 3 ng/mL, LPS 400 ng/mL, PAM 1 ng/mL), mid (85-95% activated, TNFα 30 ng/mL, IL-1β 0.2 ng/mL, LPS 100 ng/mL, PAM 0.2 ng/mL), low (50-70% activated, TNFα 3 ng/mL, IL-1β 0.05 ng/mL, LPS 12.5 ng/mL, PAM 0.01 ng/mL). Maximal activation percentage for TNFα is ~90% so high dose of TNFα showed lower percent activation than high dose of other ligands. F) NFκB response to all 24 high dose

Figure 6, continued

combinations of TNFα (T, 90 ng/mL), IL-1β (I, 3 ng/mL), LPS (L, 400 ng/mL), PAM (P, 1 ng/mL). 20 randomly selected single cells from > 200 cells (gray lines) and mean (red line) shown for each stimulus condition. Dotted lines indicate the timing for second, third, or fourth stimulus.

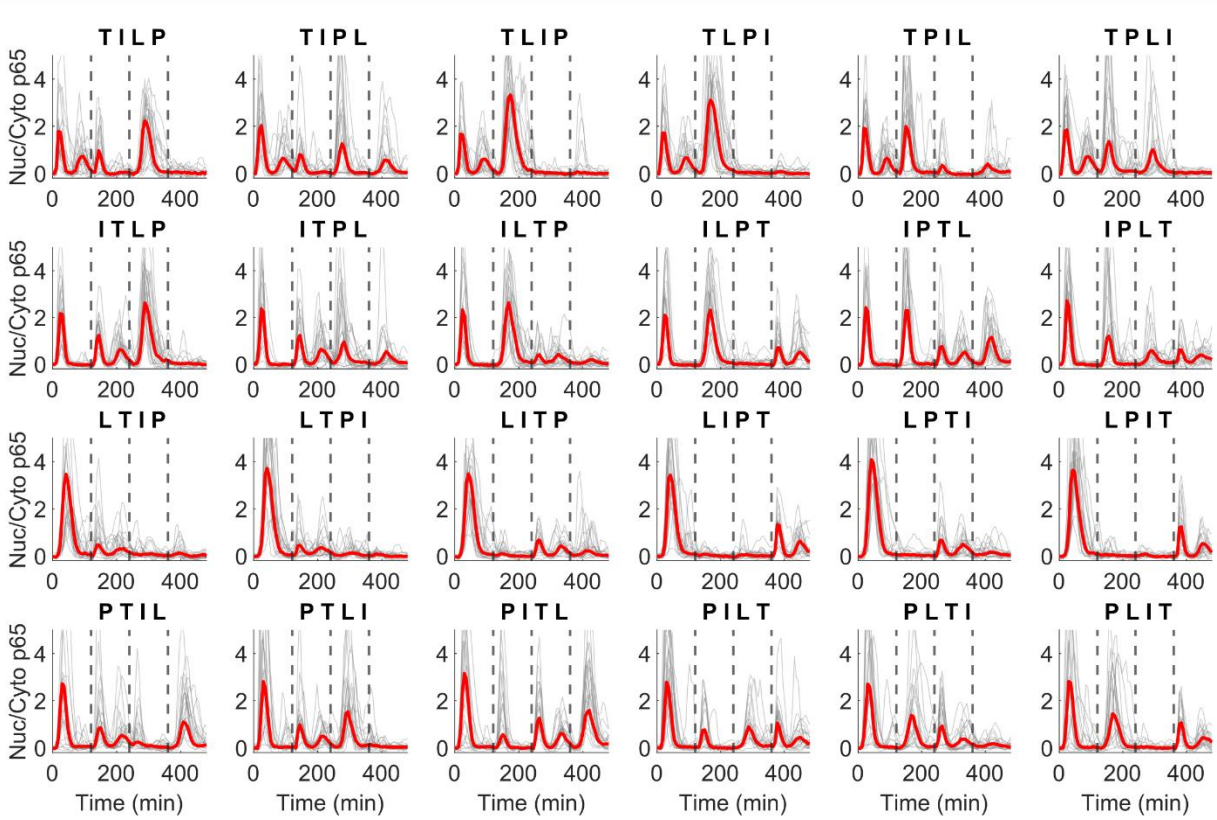

Figure 7. NFκB response to all 24 mid dose ligand combinations.

TNFα (T, 30 ng/mL), IL-1β (I, 0.2 ng/mL), LPS (L, 100 ng/mL), PAM (P, 0.2 ng/mL) provided in indicated orders. 20 randomly selected single cells from > 200 cells (gray lines) and mean (red line) shown for each stimulus condition. Dotted lines indicate the timing for second, third, or fourth stimulus.

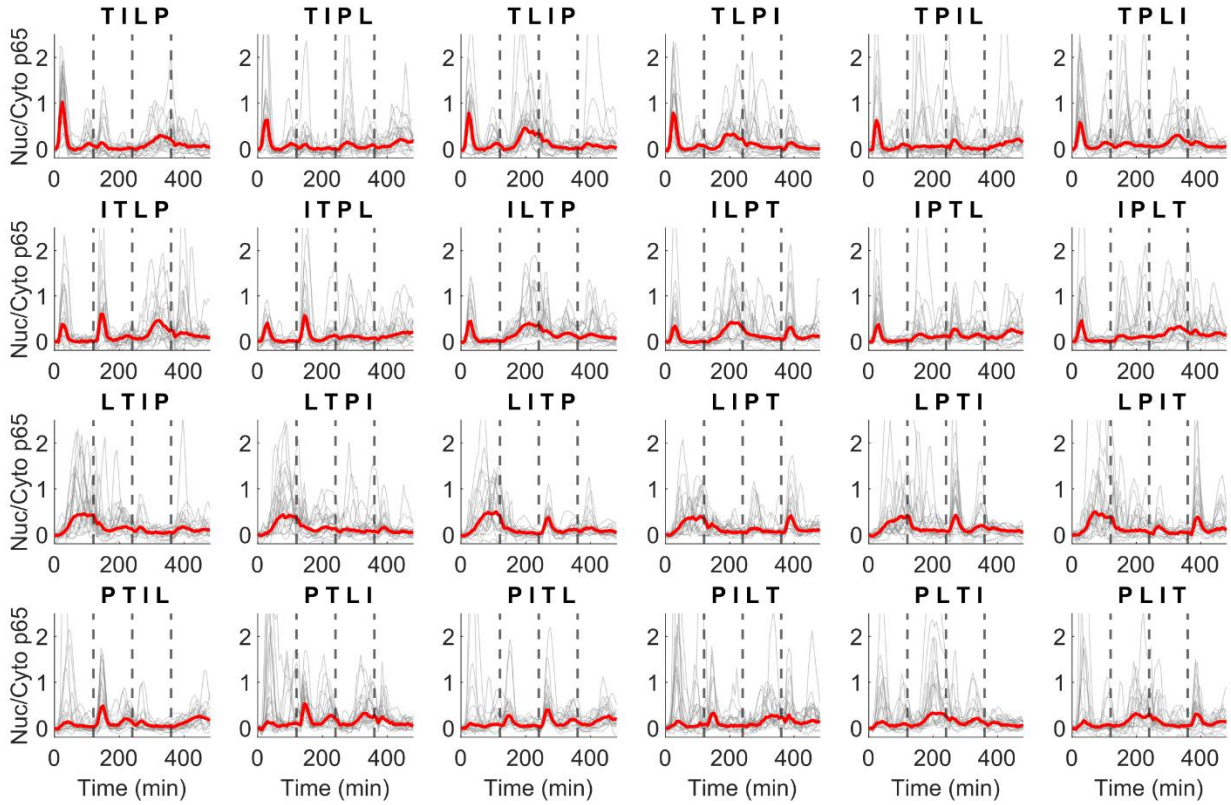

Figure 8. NFκB response to all 24 low dose combinations

TNFα (T, 3 ng/mL), IL-1β (I 0.05 ng/mL), LPS (L 12.5 ng/mL), PAM (P, 0.01 ng/mL) provided in indicated orders. 20 randomly selected single cells from > 200 cells (gray lines) and mean (red line) shown for each stimulus condition. Dotted lines indicate the timing for second, third, or fourth stimulus.

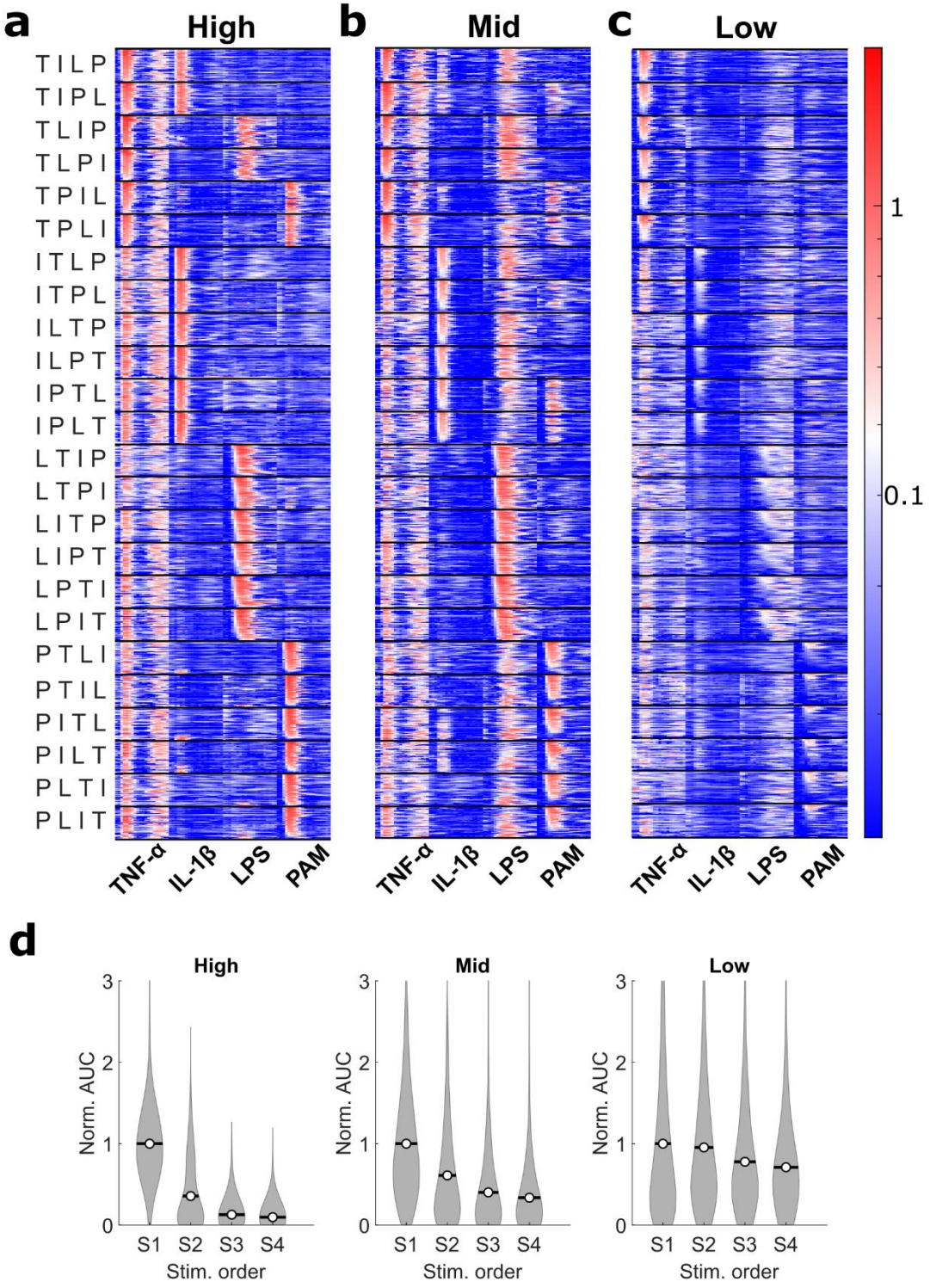

Figure 9. NFκB response dynamics over 2 hours of stimulus for each ligand.

Figure 9, continued

Each stimulus interval is normalized to the mean peak amplitude of the naïve (S1) response at high dose and plotted in heatmaps (50 randomly selected traces for each condition). Heatmap columns are arranged based on the stimulus ligand regardless of its order in the sequence. Stimulus orders are shown to the left of the first heatmap from S1 to S4, where T stands for TNFα, I for IL-1β, L for LPS, and P for PAM. Plots shown for high **(a)**, mid **(b)**, and low **(c)** dose. **d)** Single cell area under the curve (AUC) from S1-S4, normalized to the mean of corresponding S1 AUC (>2000 cells for each condition). Open circle and line show the mean.

history (Figure 5a, Figure 9a). At mid and low dose, each ligand displayed different history responses. LPS and TNFα responses exhibited the weakest attenuation, with some level of stimulus response retained across most conditions, while IL-1β and PAM responses showed large variability in response depending on prior stimulus history (Figure 5b-c, Figure 9b-c). Thus, particular histories of ligand exposure can alter subsequent stimulus responses in a consistent and predictable manner.

The NFκB network reflects information about prior ligands in the subsequent response

If particular ligand histories alter subsequent response dynamics in a distinctive manner, it would be possible to characterize a cell's prior history through its response to subsequent stimuli. However, the regulation of a genetic network is inherently noisy, resulting in diverse response to identical stimulus at the single cell level and over time [122,162,163]. This variability may impact how accurately individual cells can reflect prior history in subsequent responses. Thus, we needed to address single cell variability in characterizing how effectively prior history is reflected in subsequent response.

We used information theory to characterize the distinguishability of NFκB responses to different stimulus orders despite single cell noise. In information theory, the maximum information transmittable by a noisy network is described by the channel capacity (CC) (Figure 10a). In our case, the CC represents the maximum distinguishability of groups in a population response. Therefore, the CC can be used to quantify the accuracy of signal transduction in the NFκB network [78,129,164,165]. We first measured the CC of the NFκB network in distinguishing all 24 stimulus conditions in each dose. If the NFκB network did not retain information about prior history, we would expect the CC to stay the same or decrease from S1 to S4, since the effect of

noise is enhanced with signal attenuation (Fig 5d) [166]. However, we found that CC increased from S1 to S2 despite attenuation (Figure 10b). Even later in the stimulus sequence at S3 and S4, where attenuation became more pronounced, the CC still remained above the baseline at S1. These observations indicate that, even though the same four ligands are used for stimulation in each sequence, more distinguishable responses are present in S2 ─ 4. Thus, the NFκB signaling network retains information about prior history and coordinates subsequent stimulus responses based on prior exposure.

To investigate how prior history affected the response for each ligand, we quantified the CC for each ligand at positions S1−4. We grouped the samples based on ligand and sequence position and calculated the CC among the samples within each group (Figure 10c). Ligands unaffected by prior history would produce identical responses and a CC of zero, while ligands for which prior history changes activation dynamics would see an increase in CC at S2-4. We found that the CC specific to each ligand generally rose at S2 and remained elevated at S3-4. In other words, more distinct response behaviors are present in S2-4, indicating that cell's response to a specific ligand is significantly changed based on the cell's prior history. However, TNFα at high dose and LPS at low dose gained little information from prior history, which reflected our observations that prior history only weakly attenuated signaling in those samples (Figure 5a, c, Figure 9a, c). Nonetheless, the general trend of increased CC at S2-4 compared to S1 suggests that the NFκB network encodes information about prior history in subsequent responses.

We also noted that the dynamics of the NFκB response play a major role in accurate information transmission from prior history. When we compared the CC using response amplitudes at multiple timepoints to the CC using a single feature (the response amplitude when

the mean was at its peak), we found that the CC from a single feature (Figure 10b red lines, 10d) are substantially lower than the CC from the dynamic measurement (Figure 10b blue lines, 10d). This indicates that alteration of NFκB activation dynamics plays a role in transmitting information about prior history [129].

We then investigated which ligand responses were most distinguishable from each other by calculating the mutual information between a pair of ligand responses. We focused on the naïve responses to a ligand at S1 and following another ligand at S2, resulting in a comparison of 16 conditions for each dose (Figure 10e). In the comparison matrix, mutual information patterns at low and mid dose were primarily driven by differences between TNFα or IL-1β response dynamics and LPS or PAM response dynamics (e.g., comparing TNFα and LPS). However, response to IL-1β or PAM following LPS (LI or LP) also were distinguishable from almost every other response at mid dose. At high dose, the pattern of mutual information changed such that all TNFα responses became highly distinguishable from other samples. Likewise, the naïve and TNFα exposed responses to IL-1β, LPS, and PAM also became distinguishable from same responses following either IL-1β, LPS, or PAM (e.g., TI vs LI or TL vs IL). This shift in mutual information patterns between low, mid, and high doses suggests that fundamentally distinct mechanisms could potentially mediate the effects of prior history in these dose ranges. Overall, these mutual information analyses confirmed that the NFκB response is distinguished based on ligand sequence at the single cell level.

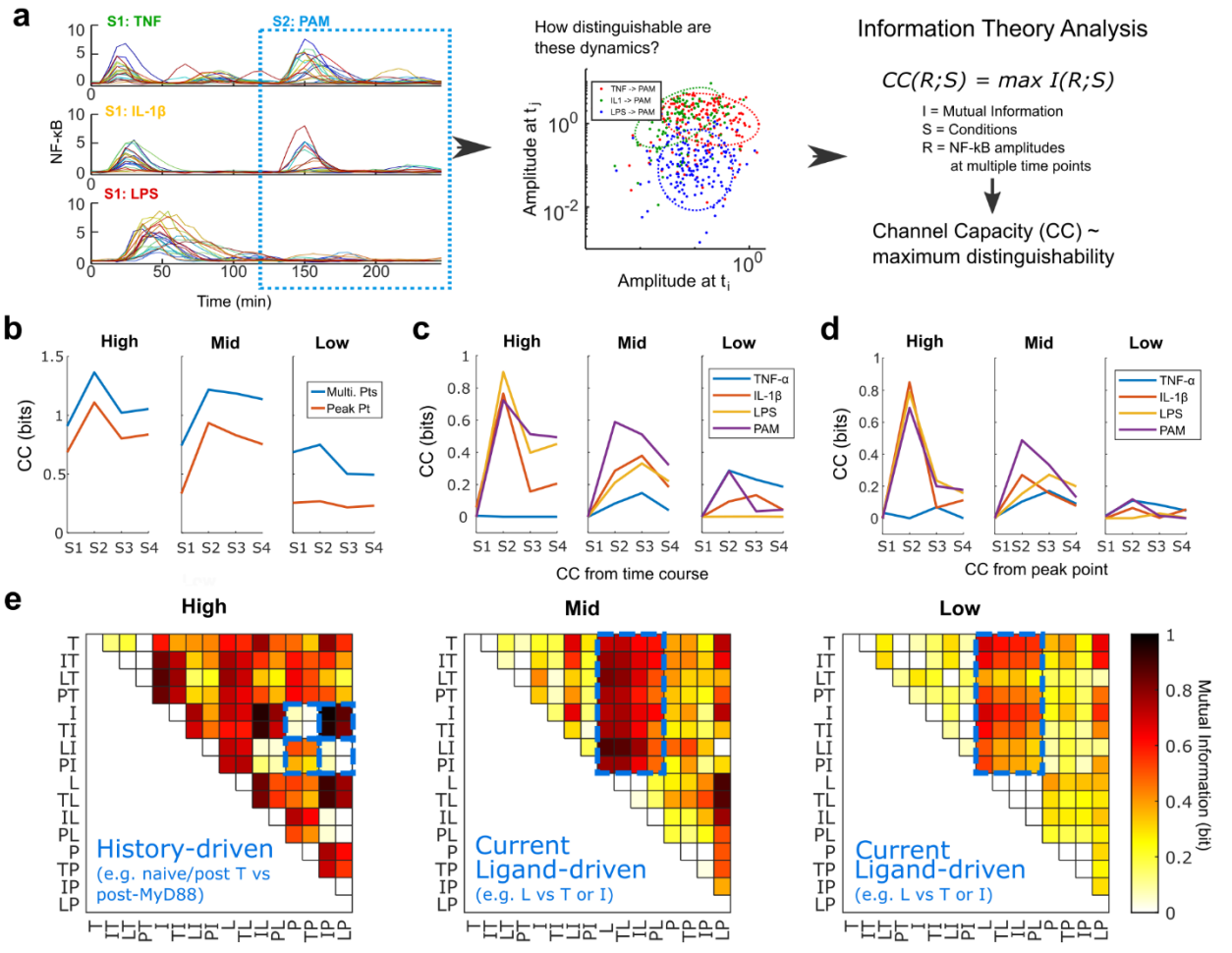

Figure 10. Information about prior stimulus history is reflected in the dynamics of subsequent NFκB responses.

a) Schematic representation of information theory analysis. Nuclear NFκB levels at six different time points (20, 30, 40, 50, 70, and 90 min) from multiple conditions are used as inputs to calculate the mutual information between conditions. Channel capacity (CC) represents the maximum mutual information between conditions. **b)** Distinguishability among all samples at S1-4. CC is calculated from the 6-dimension vector (blue line) and compared to the CC from a single feature (red line) **c)** CC among samples exposed to the indicated ligand at S1-4 calculated using the 6-dimension vector. CC in S2-4 indicates how accurately the NFκB network reflects the prior history in the response to the indicated ligand. **d)** As in **c)**, CC among all samples with the same ligand at each sequence interval but calculated using a single feature. **e)** Mutual information (MI) between ligand response dynamics (S1 and S2 only). T, I, L, P indicates the order of the stimulus. MI of 1 indicates complete distinguishability between two conditions.

Prior stimuli attenuate subsequent NFκB response in a ligand- and dose- dependent manner

To study how information about prior history is stored in the NFκB network, we investigated how different stimuli produced different patterns of attenuation (Figure 4c). At all three dose ranges, TNFα signaling was only weakly attenuated by prior stimulus, while the attenuation of LPS, PAM, and IL-1β signaling varied depending on the dose and identity of the prior ligand (Figure 5a-c, Figure 9a-c). LPS, PAM, and IL-1β signaling all utilize a MyD88-dependent signal transduction pathway, including the shared signaling intermediary IRAK1 (Figure 4b) [137]. IRAK1 has been reported to regulate itself through autoinhibitory phosphorylation, which limits subsequent activation of IRAK1 by other stimuli[84]. Thus, we hypothesized that prior MyD88-dependent signaling attenuates subsequent signaling in the same pathway, but that TNFα is independent from this inhibition.

To test this hypothesis, we focused on how a single prior ligand affects the following response, i.e., how the S1 ligand response changes the S2 ligand response (Figure 11a-c). The LPS response was delayed as both an S1 ligand and an S2 ligand (Figure 11a-c) despite sharing the same intracellular molecular pathway as PAM and IL-1β [78,86,157]. This feature has been linked to ligand-specific control of IKK activation dynamics, and has been proposed to be due to modulation of IKK cycling rates [63,86]. Indeed, we found that different IKK cycling rates could result in the delayed LPS response we observed experimentally (Figure 15e). We found that, following TNFα stimulus, the response to MyD88-dependent ligands was weakly attenuated (Figure 11d, blue). Likewise, the response to TNFα following MyD88-dependent stimuli was weakly attenuated (Fig 11d, green). In contrast, MyD88-dependent ligands attenuated subsequent signaling by other MyD88-dependent ligands in a dose-dependent manner (Figure 11d, red). At high and mid doses,

exposure to MyD88-dependent ligands resulted in significantly attenuated signaling from other MyD88-dependent ligands compared to previous TNFα exposure. Taken together, these results indicate that a prior history of TNFα signaling minimally affected MyD88-dependent signaling and vice versa, while a prior history of MyD88-dependent signaling inhibited the response to other MyD88-dependent ligands in a dose-dependent manner.

If shared negative feedback is the primary cause of attenuation for subsequent MyD88-dependent signaling, each MyD88-dependent ligand should equally attenuate subsequent MyD88-dependent ligands. Although LPS is known to also utilize a MyD88-independent module mediated by TRIF and TRAM [79,167], we found that the MyD88-independent pathway for LPS had minimal influence in these cells, as knocking out MyD88 was sufficient to abolish all response to LPS (Figure 12a-c). Thus, we expected LPS, PAM, and IL-1β to equally inhibit the response to each other. At high dose, all three MyD88-dependent ligands indeed strongly attenuated subsequent responses (Figure 11e). In contrast, at mid and low doses, only LPS strongly attenuated subsequent MyD88-dependent signaling (Figure 11e, red), while IL-1β and PAM allowed significantly stronger subsequent responses (Figure 11e, blue, green). Thus, at high dose, attenuation between LPS, PAM, and IL-1β occurred symmetrically, while at mid and low doses, attenuation became asymmetric. Prior LPS stimulus inhibited subsequent IL-1β/PAM response but not vice versa. Similarly, when we compared the JNK responses to MyD88-dependent ligands following either IL-1β or LPS stimulus, we saw that symmetric attenuation took place at high dose, but at mid dose, only LPS maintained strong attenuation of MyD88-dependent JNK activation (Figure 12f-h). These data reproduced the asymmetry in attenuation

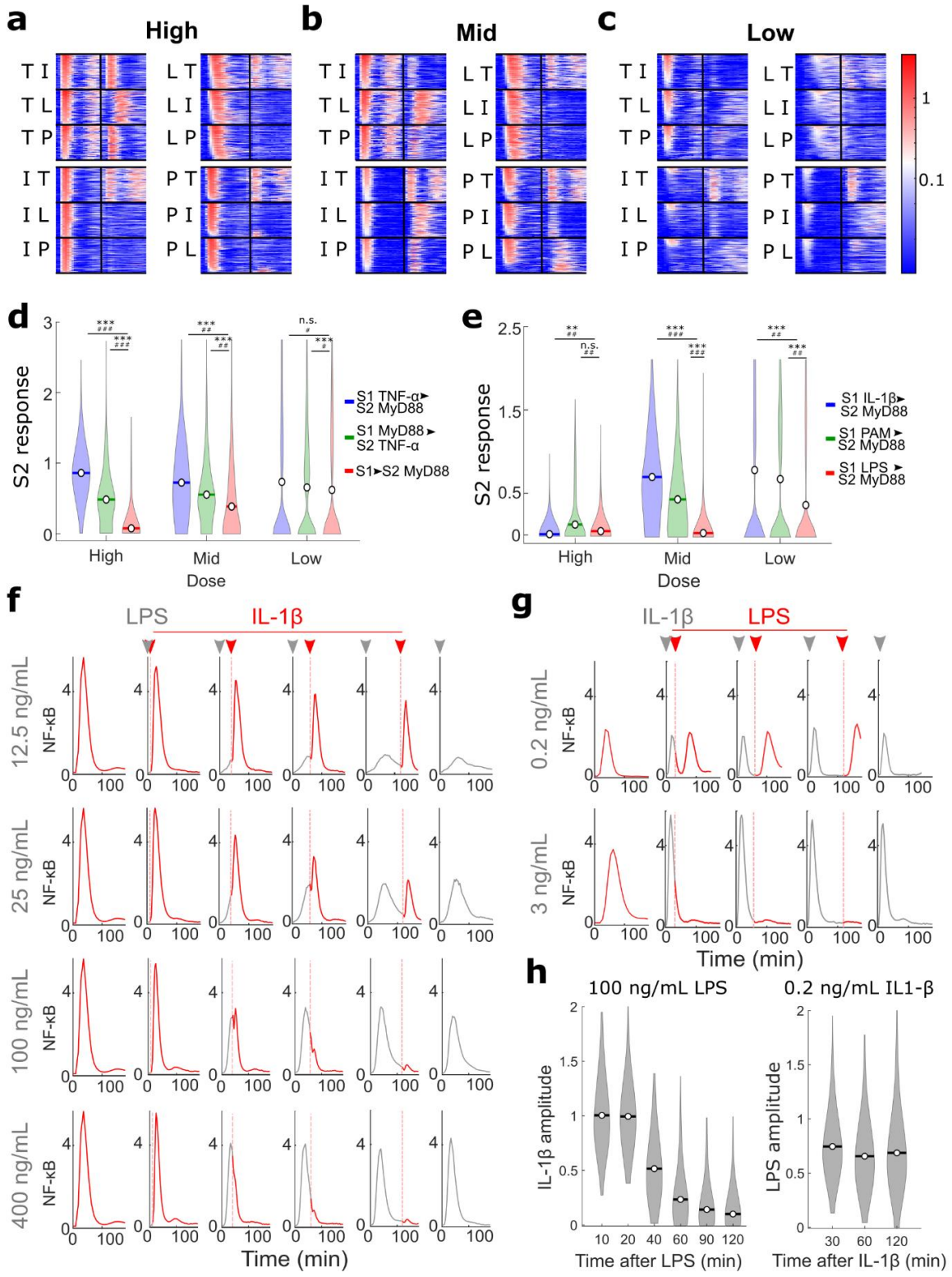

Figure 11. Ligand and dose specific effects of prior history differentiate TNFα from MyD88 dependent ligands and differentiate among MyD88 dependent ligands.

Figure 11, continued

a-c) NFκB response dynamics over 2 hours of stimulus for each ligand normalized to the mean amplitude of the naïve (S1) high dose response. 50 single-cell traces randomly selected for each condition. All sequences of S1 and S2 ligands shown. All 9 sequences shown at high **(a)**, mid **(b)**, and low **(c)** dose. **d)** Violin plot comparing the normalized S2 responses of the MyD88-dependent ligands (LPS, PAM, IL-1β) following either TNFα (blue) or another MyD88-dependent ligand (red) or the TNFα response following a MyD88 dependent ligand (green) (> 650 cells per condition). Open circle and line show the mean. **e)** Violin plot comparing the normalized S2 MyD88-dependent responses following IL-1β (blue), PAM (green), and LPS (red) stimulus at high, mid, and low doses (> 340 cells per condition). Bonferroni corrected Wilcoxon rank sum test p-value > 10^{-2} (n.s.), < 10^{-2} (*), < 10^{-3} (**), < $1*10^{-4}$ (***). Fold change difference between sample means > 1 (#), > 1.25 (##), or >4 (###). **f)** Plot of mean trace for conditions where LPS is provided at 0 min (gray arrowhead) and switched to 3 ng/mL (high dose) IL-1β after the indicated time (red arrowhead). Gray region and red regions of trace indicate NFκB response during LPS stimulus interval and after replacement with IL-1β, respectively. Entirely red traces in the left column show an only IL-1β response and entirely gray traces in the right column show an only LPS response. Each mean trace represents > 100 single cells from 2 biological replicates. **g)** Plot of mean traces for conditions where 0.2 and 3 ng/mL (mid and high dose) IL-1β are provided at 0 min and switched to 100 and 400 ng/mL (mid and high dose) LPS, respectively, after the indicated time. Gray region and red regions of trace indicate NFκB response during IL-1β stimulus interval and after replacement with LPS, respectively. As in **(f)**, entirely red traces in the left column show an only LPS response and entirely gray traces in the right column show an only IL-1β response. Each mean trace represents > 100 single cells over 2 biological replicates. **h)** Violin plot comparing the normalized response for 3 ng/mL IL-1β following 100 ng/mL LPS or the response for 100 ng/mL LPS following 0.2 ng/mL IL-1β. Each plot is derived from > 100 cells per condition over 2 biological replicates. Open circle and line show the mean.

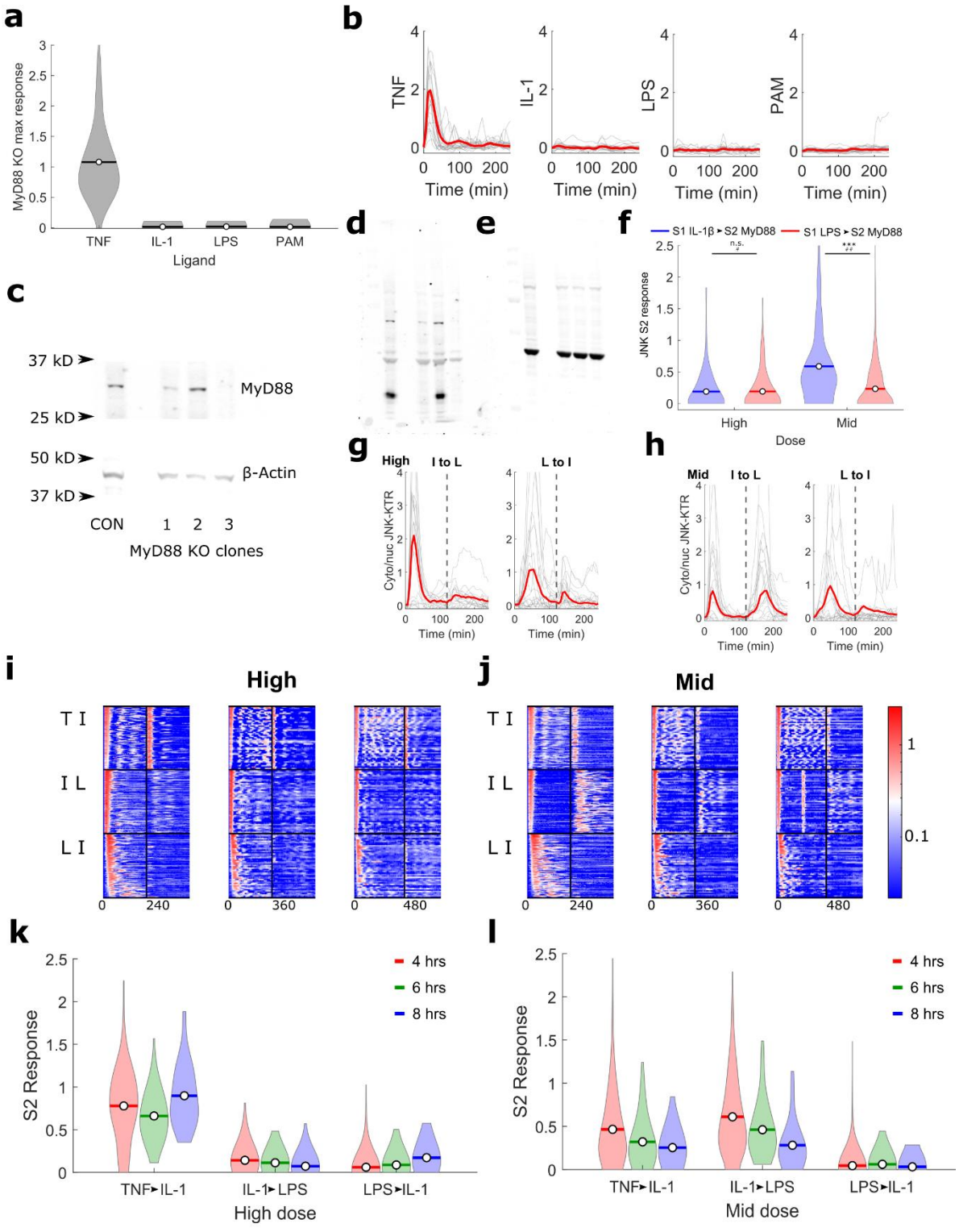

Figure 12. MyD88 is critical for IL-1β, LPS, and PAM responses.

Figure 12, continued

a) Max response following stimulation by the indicated ligand in MyD88$^{-/-}$ cells normalized to max response following stimulation in WT cells. **b)** NFκB traces for stimuli response shown in **(a)**. 20 randomly selected single cells from > 200 cells (gray lines) and mean (red line) shown for each stimulus condition. **c)**. Western blot confirming successful knockout of MyD88 by CRISPR-Cas9. Three isolated single cell clones following CRISPR-Cas9 targeting of *Myd88* showing either frameshift mutations in both copies (clone 1, 3) or in one copy (clone 2) were probed for MyD88 and β-actin by western blot. Based on expression levels, MyD88 KO clone #3 was used for subsequent experiments. **d-e)**. Full western blots for MyD88 **(d)** and β-Actin **(e)**. **f)** Violin plot comparing JNK response to MyD88-dependent ligands following 2 hours of IL-1β (blue) or LPS (red) stimulus at high and mid dose normalized to naïve response. Each condition shown from > 300 single cells. **g)** JNK response traces following stimulus with high dose LPS (L) or IL-1β (I) for 120 minutes switching to the other ligand (dashed vertical line). Data shown for 20 randomly selected single cells (gray lines) and population mean (red line) from > 200 cells. **h)** Same as **g)** at mid dose. **i-j)** NFκB response dynamics over 4-8 hours of stimulus for each ligand normalized to the mean amplitude of the naïve (S1) response. 50 single-cell traces randomly selected for each condition. Sequences at high **(i)** and mid **(j)** dose shown after 4, 6, and 8 hours of stimulus. **k-l)** Violin plot comparing the normalized S2 responses of the indicated stimulus pairs after 4 (red), 6 (green), or 8 (blue) hours of stimulus from > 50 cells per condition at high dose **(k)** or mid dose **(l)**. The 8 hour stimulus was fed twice, once at 0 minutes and once at 240 minutes to prevent cell starvation. Open circle and line show the mean.

observed in our NFκB measurements and suggest that asymmetric prior history effects may be broadly applicable in multiple inflammatory signaling pathways. Despite the highly shared pathways between LPS, PAM, and IL-1β, prior LPS effects differ from prior PAM or IL-1β effects in a dose dependent manner.

Although our results suggest asymmetry in short term history effects between MyD88-dependent ligands, innate immune signaling occurs on a range of timescales. Thus, we sought to understand the temporal range under which this asymmetry persists and extended the duration between S1 and S2 to 4, 6, and 8 hours (Figure 12i-l). At these longer durations, we still observed similar ligand and dose specific attenuations. TNFα only weakly attenuated MyD88-dependent signaling through IL-1β, while LPS and IL-1β attenuated each other symmetrically at high dose. At mid dose, LPS still strongly attenuated IL-1β, but not vice versa. At longer time intervals, both TNFα dependent attenuation of IL-1β and IL-1β dependent attenuation of LPS strengthened, which suggests that longer duration stimuli may weaken the asymmetry between ligand histories. Nonetheless, the overall trends at increased duration were consistent with our findings after 2 hours of stimulus, which indicates that these effects persist at longer durations.

Slow LPS-dependent negative feedback induces distinct attenuation in subsequent response

While autoinhibition of IRAK1 can explain symmetric attenuation at high ligand dose [84], as IRAK1 is shared by each of the MyD88-dependent ligands (Figure 4b), it could not explain our results at mid and low doses. Asymmetric cross-attenuation at mid and low doses suggests the existence of an additional negative feedback mechanism which would be more strongly activated by LPS stimulation than by IL-1β or PAM.

To study the characteristics of asymmetric attenuation of MyD88-dependent signaling, we examined how rapidly attenuation takes place upon stimulation with LPS. The timescale of attenuation can inform where in a signaling network the feedback acts. For example, rapid attenuation is unlikely to be driven by transcription and translation of downstream feedback genes. We stimulated cells with various doses of LPS (12.5 – 400 ng/ml), then stimulated the cells with high dose of IL-1β (3 ng/ml) after 10-120 minutes of LPS stimulus (Figure 11f, Figure 13a). Attenuation of IL-1β signaling by high dose LPS (400 ng/ml) was fast and strong, rapidly suppressing the subsequent IL-1β response at all times except the shortest time interval (10 min). As IRAK1 is shared in the early part of the signaling pathway, this observation was consistent with rapid autoinhibition of IRAK1. However, following lower doses of LPS, the IL-1β response became gradually attenuated depending on duration of LPS stimulus (Figure 11f, h).

On the other hand, when we stimulated first with IL-1β, then LPS, we did not observe gradual attenuation. Similar to high dose LPS, high dose IL-1β still produced immediate and strong attenuation of the LPS response, suggesting autoinhibition of IRAK1 still plays a major role in subsequent attenuation (Figure 11g, Figure 13b). Increasing duration of stimulus with mid dose IL-1β, however, had no impact on attenuation of LPS signaling (Figure 11g). To compare the difference between prior stimulation with LPS and IL-1β more clearly, we normalized the responses to the second stimulus to the corresponding naïve responses (Figure 11h). As expected, the response to IL-1β following LPS gradually decreased over time, while LPS response following IL-1β remained consistent over time. These results suggest that an additional activation-time dependent negative feedback process is differentially regulated by each MyD88-dependent ligand.

This time dependence led us to hypothesize that this additional feedback response relies on NFκB dependent gene expression.

Ligand-specific attenuation in MyD88-dependent signaling depends on activation of IKK

To test whether NFκB translocation and subsequent gene expression is necessary for asymmetric and ligand-dependent attenuation, we targeted the signaling intermediary IKK. IKK controls the activation and translocation of NFκB into the nucleus through degrading the inhibitory protein IκBα (Figure 4b). Using PS1145, a reversible small molecule inhibitor of the IKK-β subunit[79,168], we blocked signaling downstream of IKK activation. Due to the reduced activity of IKK, pretreating cells with 40 μM PS1145 significantly reduced NFκB translocation by LPS stimulation (Figure 13c-d). To test the impact of IKK inhibition for attenuation of subsequent signaling events, we washed cells to remove the drug after LPS stimulation and restimulated with 3 ng/mL (high dose) IL-1β. Cells treated with PS1145 showed significantly stronger NFκB responses to subsequent IL-1β stimulus compared to untreated cells (Figure 14a). Thus, aspects of NFκB signaling downstream of IKK activation, e.g., NFκB nuclear translocation and NFκB-mediated gene expression, play a major role in LPS-dependent attenuation of subsequent signaling. Through these inhibition studies, we show that asymmetric attenuation of MyD88-dependent signaling depends on IKK activation and subsequent NFκB nuclear translocation, suggesting that this asymmetry depends on NFκB-mediated gene expression.

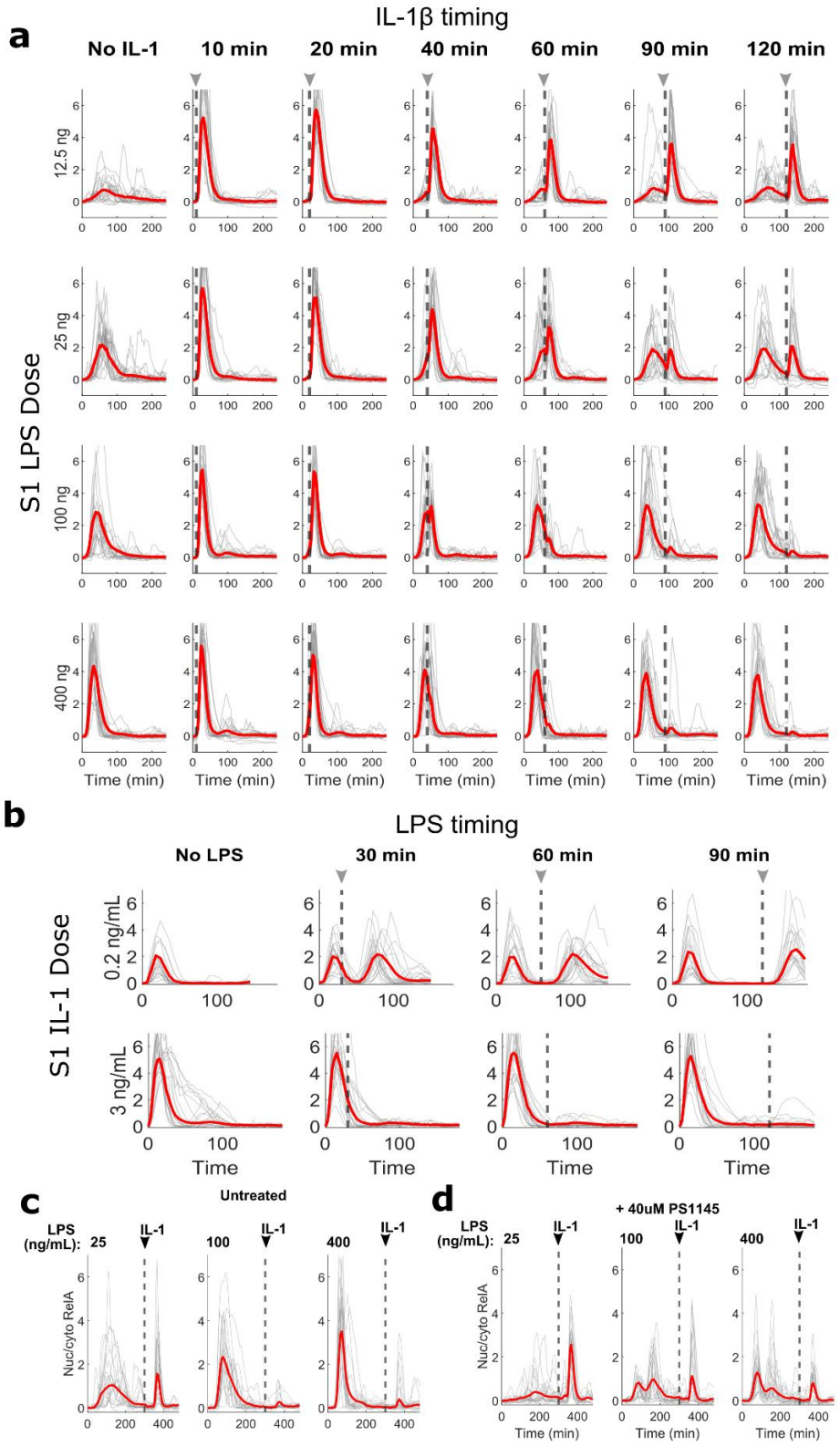

Figure 13. NFκB traces for time-resolved stimulation and IKK inhibition.

Figure 13, continued

a) Time resolved LPS switching to 3 ng/mL IL-1β or **b)** IL-1β switching to LPS (100 ng/mL top, 400 ng/mL bottom). First stimulus was introduced at 0 minutes and dashed gray line indicates when the second stimulus was introduced. 20 randomly selected single cells (gray lines) and mean from > 100 cells (red line) shown for each stimulus condition. **c-d)** NFκB response traces from untreated cells **(c)** or cells pretreated with 90 minutes of 40 μM PS1145 stimulation **(d)**. Cells were then exposed to LPS at the indicated dose for 240 minutes (+ 40 μM PS1145 for treated cells), washed with media twice for 15 minutes each, and stimulated with 3 ng/mL IL-1β. The dashed vertical line shows when IL-1β was supplied. Data shown for 20 randomly selected single cells (gray lines) and population mean (red line) from > 120 single cells.

Mathematical modeling with negative feedback produces ligand and dose-specific attenuation

Our data give rise to a model where, at high dose, IRAK1 auto-inhibition results in symmetric attenuation of Myd88-dependent signaling, while at moderate and low doses, differential transcription of downstream negative regulators produces asymmetric attenuation. To study whether a network topology with these two motifs is sufficient to reproduce our observed prior history effects, we incorporated these two feedbacks into the NFκB network model and studied the change in network dynamics when stimulated with different ligand sequences.

To focus on the role of these two negative feedbacks, we minimized the network topology by converging all kinases not involved in negative feedback or the translocation of NFκB [100]. Then, we expanded this minimal NFκB model by adding network components connecting three receptors (TNFR, IL-1R, and TLR4) and incorporating autoinhibition of IRAK1 and ligand-dependent inhibition downstream of NFκB (Figure 14b). To model the greater transcription of negative regulators following LPS stimulation compared to IL-1β and TNFα (Figure 14a, 16c) [74], we set the LPS-dependent inhibition arising from NFκB dependent transcription to be four-fold that of IL-1β or TNFα. Even with these expansions, our model uses only 20 parameters and successfully reproduced our experimental observations (Figure 14c-e). At high dose of IL-1β or LPS, strong activation of IRAK1 resulted in rapid inactivation, which prevented NFκB activation by subsequent MyD88 ligands (Figure 14c). However, TNFα does not affect IRAK1 and only weakly attenuates subsequent signaling due to induction of downstream feedback (Figure 14e).

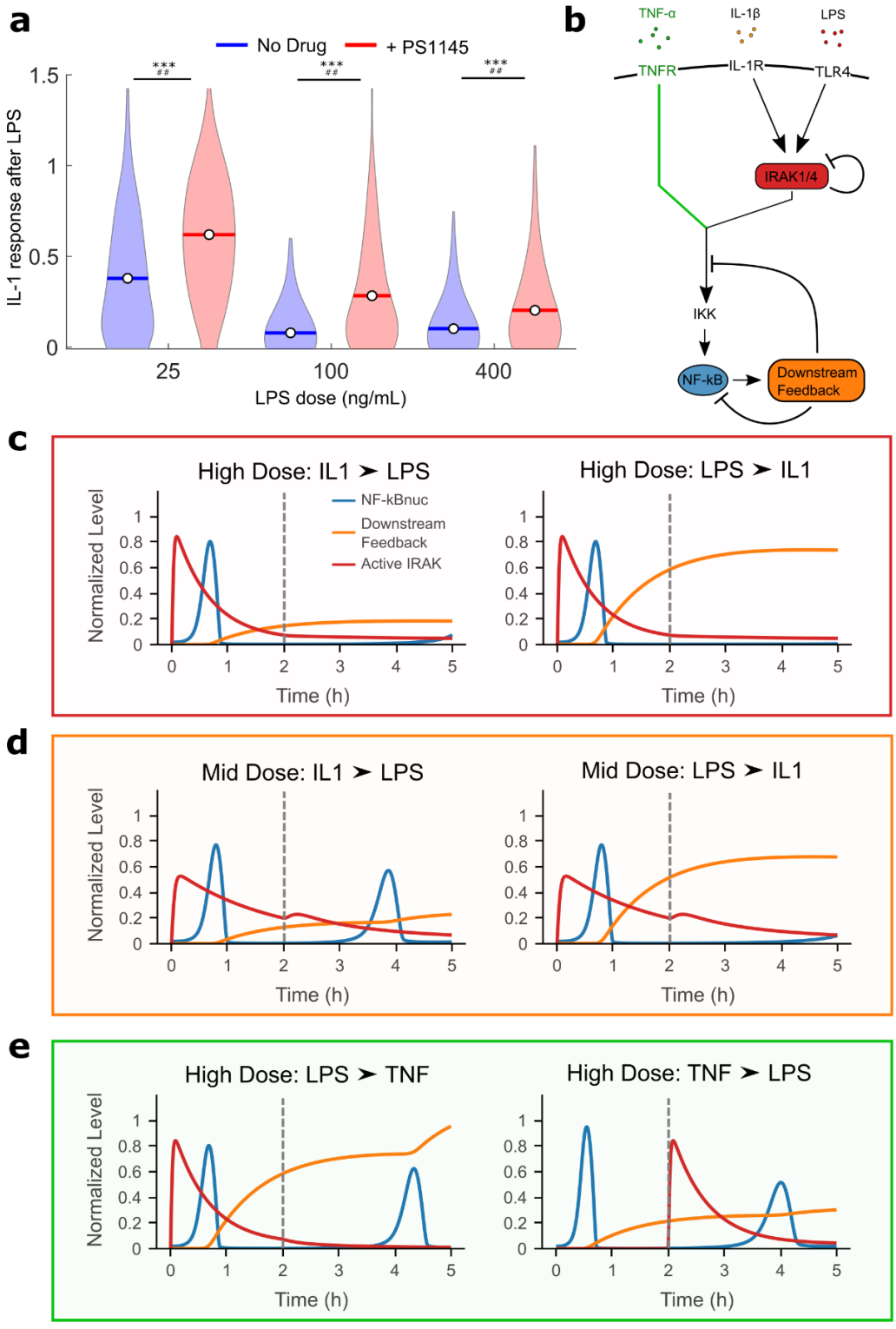

Figure 14. Differential regulation of downstream feedback controls ligand specificity of tolerance.

Figure 14, continued

a) Violin plot comparing IL-1β maximum response following LPS treatment normalized to naïve for untreated (blue) and PS1145 pre-treated (red) cells. Pre-treated cells were exposed to 40 μM PS1145 stimulated with LPS at the indicated concentration, washed and stimulated with 3 ng/mL IL-1β. Each condition shown from > 120 single cells over 2 biological replicates. **b)** Diagram illustrating the NFκB network model used for the simulation. Two negative components, IRAK1 autoinhibition and nuclear NFκB dependent attenuation, are highlighted in red and orange. The TNFα signaling pathway (green) utilizes different kinases to activate IKK than the MyD88 dependent ligands. **c-e)** Simulated network responses to different sequences of stimuli. The blue lines show the dynamics of nuclear NFκB, the red lines for active IRAK1, and the orange lines for the downstream feedback component. Gray dashed vertical line indicates time of simulated replacement of ligands.

In contrast, at mid dose, IL-1β induced weaker activation of IRAK1 and resulted in modest inactivation of itself, allowing activation of IRAK1 by subsequent LPS stimulus (Figure 14d). Partial inactivation of IRAK1 by LPS stimulus combined with induction of transcriptional feedback prevented subsequent MyD88-dependent signaling (Figure 14d). Thus, in this dose range, differential engagement of downstream feedback plays a critical role in differentiating LPS and IL-1β signaling and promoting asymmetric response. Additionally, we simulated other six combinations of sequential stimuli (Figure 15a), which reproduced the remaining experimental results.

An alternative mechanism for attenuation is the saturation of signaling molecules shared with the prior stimulus. This possibility is unlikely in our mid and low dose situations, as NFκB signaling was not saturated and clear asymmetry between ligands with comparable NFκB responses existed. However, at high dose, saturation of NFκB signaling suggested that reservoirs of intermediaries may be depleted. While this is difficult to test experimentally, our simulation suggests this mechanism may be possible. Negative feedback on IRAK1 occurs in the form of auto-inactivation. As a result, high dose stimulus triggers rapid inactivation of the IRAK1 population, leading to depletion of available IRAK1 (Figure 15a). Although reservoirs of downstream modules like IKK are still available, depletion of IRAK1 prevents further activation through the MyD88-dependent pathway (Figure 15b). Thus, saturation and depletion of shared upstream intermediaries like IRAK1 may play a role in attenuation under saturating signaling conditions. At mid dose, however, both IRAK1 and IKK are available following both IL-1β and LPS stimulus (Figure 15c-d). Our simulation demonstrates how a simple network motif with a

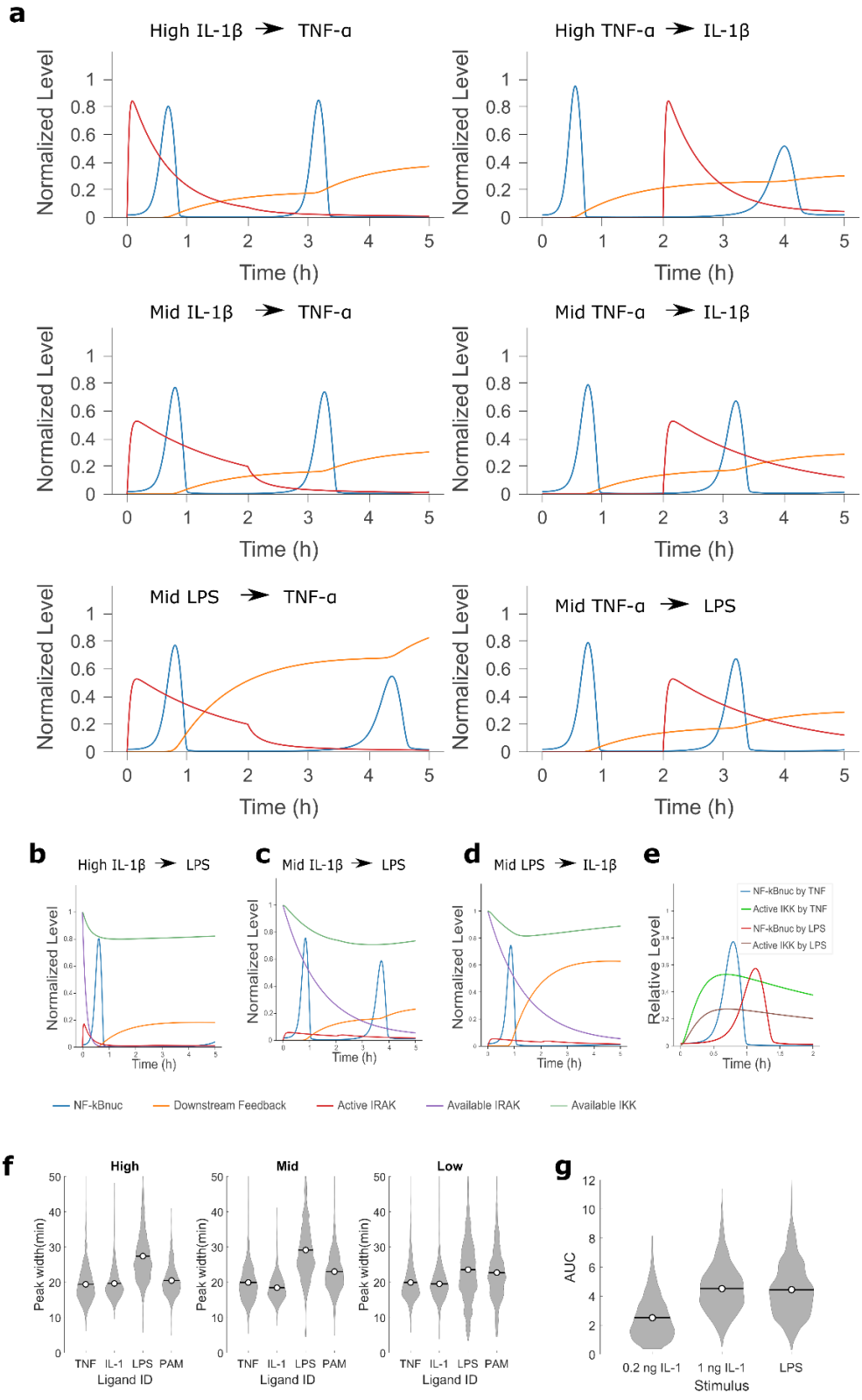

Figure 15. Additional simulations of NFκB behavior.

Figure 15, continued

a) Each subplot shows the simulated NFκB, active IRAK, and downstream feedback dynamics in response to the other sequences of stimuli. The blue lines show the dynamics of nuclear NFκB, the red lines for active IRAK1, and the orange lines show the dynamics for the downstream feedback component. **b-d)** Expanded detail from selected simulated conditions including available IRAK1 (purple) and IKK (green) at every time interval. Note that active IRAK is scaled to total IRAK instead of max active IRAK as in other simulation examples. **e)** Simulation of possible IKK cycling mechanism for delayed LPS signaling. TNF signaling (base model parameters) and LPS signaling (a_R doubled, μ halved) resulting in activation of IKK and translocation of NFκB is shown, demonstrating dependence of activation timing on IKK cycling parameters. **f)** Quantification of S1 peak width for each ligand from sequential stimulation data (S2-4). Width is defined as time-interval between half-maximal response on either side of the maximal response. **g)** Area under the curve (AUC) for the indicated stimulus responses. AUC calculated as trapezoidal approximation of integral over the stimulus interval.

few negative feedbacks acting on different nodes can retain information about stimulus history and coordinate subsequent inflammatory signaling.

MyD88-dependent ligands differentially regulate NFκB negative feedback response genes

Our computational and experimental results suggest that NFκB-induced negative feedbacks are differentially regulated by MyD88-dependent ligands. To confirm this model, we profiled gene expression through RNA sequencing following 2 h of stimulation with mid dose LPS, PAM, or IL-1β. Compared to unstimulated cells, we found a total of 609 differentially expressed genes (DEGs) following LPS stimulus, 166 following PAM stimulus, and 108 following IL-1β stimulus. Almost all DEGs induced by IL-1β and PAM were also induced by LPS, while DEGs by IL-1β and PAM showed little overlap (Figure 16a). Differences in gene expression between these three ligands were primarily driven by magnitude of up or down-regulation, rather than regulation of different genes (Fig 16b). In general, upregulation of gene expression by LPS was stronger than upregulation by PAM, which was itself stronger than by IL-1β. These differences in the magnitude of gene expression suggest that MyD88 dependent ligands indeed differentially regulate expression of NFκB response genes despite highly shared pathways.

We then focused on which genes were most differentially regulated by MyD88 ligands. We found that many known negative regulators of NFκB signaling were upregulated 2- to 4-fold in response to LPS stimulus compared to IL-1β stimulus (Fig 16c). Many of these regulatory genes act to directly sequester NFκB or inhibit the activities of shared upstream signaling components [49]. Thus, these negative regulators likely affect subsequent signaling by other MyD88 ligands. We also found that the most differentially expressed genes between LPS and IL-1β are signaling proteins, indicating that these transcriptional differences give rise to different functional outcomes

between LPS and IL-1β signaling (Fig 16d). For example, some of the most differentially regulated genes were well-known proteins secreted by activated fibroblasts, including the growth factors *Csf2* and *Csf3* and the cytokines *Cxcl2* and *Cxcl3* [169–171].

It is surprising that LPS and IL-1β induce different gene expression patterns despite similar intracellular pathways. Ligand-specific NFκB activation dynamics may be involved in differentiating these expression patterns. LPS consistently produced a longer NFκB activation duration than a comparable dose of IL-1β (Figure 15f). The duration of NFκB activation has been shown to differentially regulate transcription of NFκB response genes [50,74], possibly explaining differences between IL-1β and LPS induced gene expression. However, longer activation duration also increases the total nuclear NFκB over time.

To examine if total nuclear NFκB, as measured by the area-under-the-curve (AUC) of the NFκB response, can explain the differential gene expression by different ligands, we quantified gene expression in cells stimulated with mid dose IL-1β and LPS (0.2 ng/mL and 100 ng/mL, respectively) and a higher dose of IL-1β (1 ng/mL). Mid dose IL-1β produced lower AUC than mid dose LPS did, while 1 ng/mL IL-1β produced a similar AUC to mid dose LPS (Figure 15g). If higher total nuclear NFκB explains stronger gene expression by mid dose LPS than by mid dose IL-1β, 1 ng/mL IL-1β should induce comparable downstream gene expression. Through reverse-transcription quantitative PCR (RT-qPCR), we profiled the transcription of three differentially expressed negative feedback regulators, *Nfkbia, Nfkbie,* and *Tnfaip3*. We found that for *Nfkbia* and *Tnfaip3*, expression was significantly increased in the 100 ng/ml LPS sample compared to both 0.2 ng/ml and 1 ng/ml IL-1β samples (Figure 16e). 0.2 ng/mL IL-1β stimulus produced weaker expression of *Nfkbia* and *Tnfaip3* compared to untreated cells after 2 hours of stimulus. Because

these are early NFκB target genes which are rapidly transcribed and degraded following activation of NFκB, this result is likely due to targeted degradation after an initial burst of transcription [101]. Importantly, even IL-1β stimulus which induced comparable NFκB response AUC to mid dose LPS did not increase transcription of negative regulators of NFκB to the level of LPS stimulation.

Similarly, we profiled five secreted proteins which were also highly differentially expressed between LPS and IL-1β stimulus, *Csf2, Csf3, Cxcl2, Cxcl3,* and *Il23a* (Figure 16e). Each of these genes except *Csf3* was significantly upregulated following LPS stimulation compared to both IL-1β doses. These results suggest that AUC cannot explain the differential downstream expression we observed, but that NFκB dynamic features, likely including activation duration, drive the differential downstream expression between LPS and IL-1β. Similar to what we observed using qPCR, the greater number of DEGs following LPS stimulus may be explained by the difference in activation duration between the LPS and IL-1β response. Overall, our downstream analyses demonstrate that each MyD88-dependent ligand differentially regulates downstream gene expression, and that differences in negative feedback expression can store prior ligand information to control subsequent NFκB signaling.

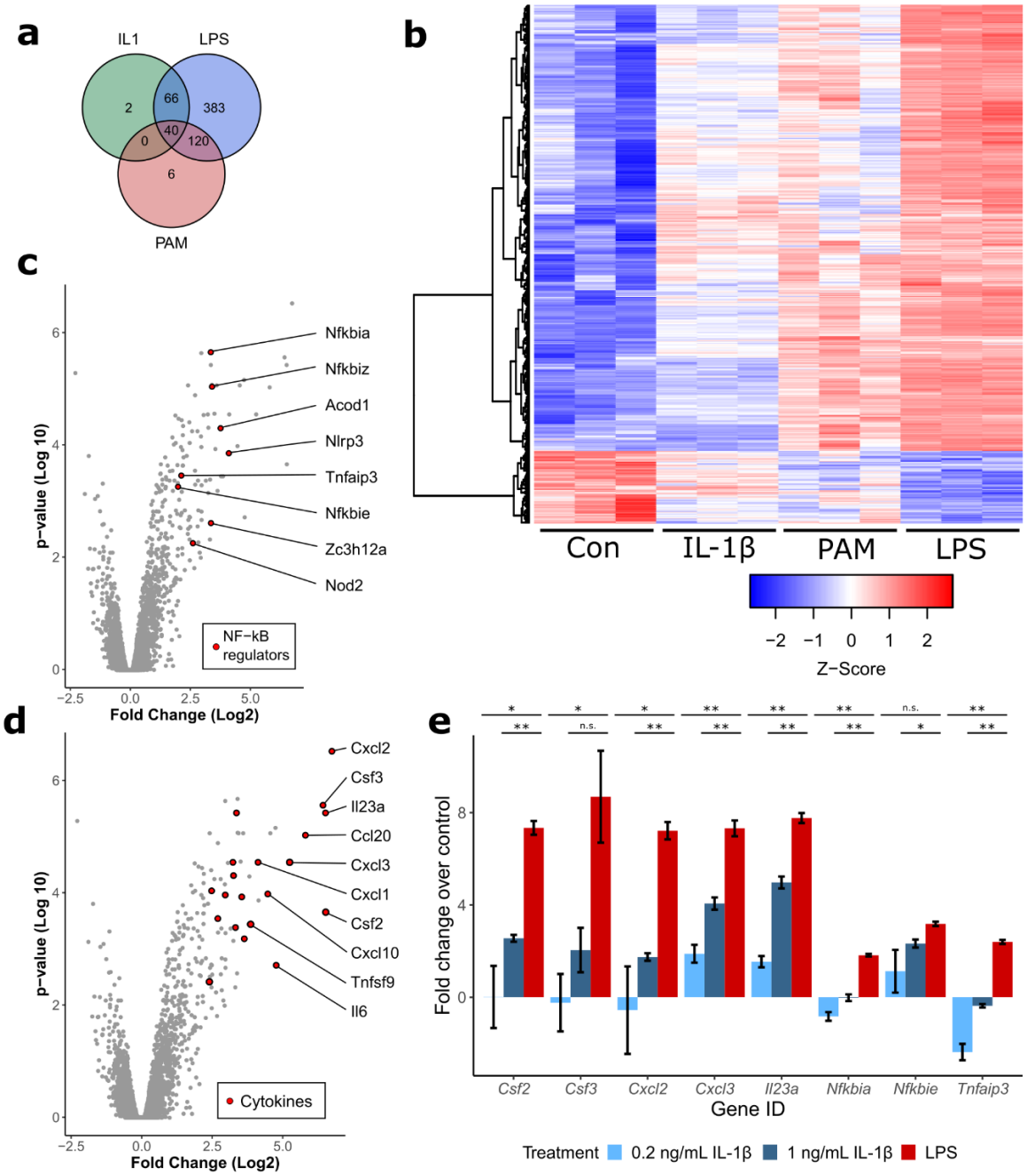

Figure 16. Myd88-depenent genes differentially regulate downstream cytokines and negative feedback regulators.

a) Venn diagram showing overlap of differentially expressed genes (DEGs) between IL-1β, LPS, and PAM after 2 hours of stimulus. **b)** Heatmap of DEGs for MyD88-dependent ligand treated cells. RNA-sequencing was performed in triplicate. Each row shows the normalized expression (z-score) of a single gene. Dendrogram shows linkage based on Ward's method. **c-d)** Volcano

Figure 16, continued

plot showing log2(fold change) and -log10(P value) for DEGs between LPS and IL-1β stimulus Among the DEGs with adjusted p-value < 0.01 and fold change > 4, genes annotated as NFκB negative regulators (GO:0032088) **(c)** or cytokines (GO:0005125) **(d)** are colored in red. All differentially expressed regulators and top ten differentially expressed cytokines are labeled. **e)** qRT-PCR data following for a subset of highly differentially expressed cytokines and NFκB negative regulators stimulation with 0.2 ng/mL (light blue), 1 ng/mL (dark blue) IL-1β, or 100 ng/mL LPS (red). Gene expression is normalized to basal gene expression for unstimulated cells. Data shown as mean fold change over unstimulated cells +/- S.E.M. from 3 replicates. Benjamini-Hochberg adjusted P value < 0.05 (*) or <0.01 (**).

RESULTS PART II: MULTI-LEVEL ENCODING OF SIGNALING MEMORY IN MACROPHAGES – *IN PREPARATION*

Introduction

Inflammation due to infection or injury produces dynamic fluctuations in the levels of foreign pathogens, pro-inflammatory cytokines, and anti-inflammatory cytokines over hours or days [172]. Prior stimuli contextualize immune responses to subsequent signals in the inflammatory cascade and produce cellular memory (Figure 17a) [173]. Macrophages are critical immune sentinel cells which sense pathogen and coordinate local and systemic immune responses [174]. Macrophage contextualization of prior inflammatory signals plays a key role in innate immune memory, and dysfunction in macrophage memory plays a role in pathogenic conditions like sepsis and chronic inflammation [173].

However, memory shapes macrophage responses in contradictory ways (Figure 17b). Prolonged exposure to bacterial lipopolysaccharide (LPS) attenuates subsequent organismal and cellular responses to inflammatory stimulus, producing tolerance [31,34,42]. However, exposure to low-dose LPS can potentiate stronger responses upon restimulus, producing priming [175–177]. Few studies have systematically profiled memory encoding by inflammatory stimuli to identify rules underlying cellular decisions towards priming or tolerance[159].

Furthermore, although single cell heterogeneity shapes innate immune responses to infection and inflammation[112–114], study of innate immune memory rely on population-level studies. Bulk cytokine secretion and endpoint RNA or protein measurements are unable to study how prior stimulus can produce memory states in individual cells. Profiling innate immune

memory in single cells could reveal distinct classes of encoded memory and develop principles for engineering innate immunity.

The canonical NFκB pathway is one of the central nodes for signaling from many inflammatory stimuli[22]. It is unclear how passing sequential signals through this shared information bottleneck contributes to memory. Temporal dynamics of NFκB nuclear localization encode information about the identity, dose, and duration of a particular stimulus [78,129,178]. Furthermore, NFκB dynamics are shaped by stimulus history [102], which may encode memory temporally despite the information bottleneck. Recently developed transgenic mouse models have shown how NFκB dynamics play a role in primary immune cells and disease states [50,78,179,180]. These advances enable study of innate immune memory at a single cell level and application of these questions to *in vivo* disease models.

In this work, we systematically profile the effects of stimulus identity, dose, and duration on NFκB activation dynamics to restimulus in bone-marrow derived macrophages. We show that NFκB dynamics encode both priming and tolerance, that *in vivo* endotoxemia is also encoded in NFκB dynamics, and that single cell memory can be determined based on response to prior stimulus. Our mathematical modeling showed that initial macrophage heterogeneity and ligand-dependent feedback can explain deterministic single cell behavior. Using transcriptomics and chromatin accessibility profiling, we show how a combination of altered NFκB dynamics and ligand-specific changes in chromatin state give rise to memory-informed transcriptional outputs. Altogether, this work shows how remodeling at multiple levels of signaling work together to encode innate immune memory in macrophages.

Sequential stimulus with inflammatory ligands results in distinct NFκB activation dynamics

Systematic screening of single-cell innate immune memory is technically challenging and requires high throughput, time-resolved, non-perturbative stimulation, and continuous, single-cell resolution readouts. Automated microfluidic live cell imaging resolves these concerns by increasing simultaneous throughput, culturing and stimulating cells, and providing real-time readouts of cell state (Figure 17c). Leveraging these strengths, we used microfluidics to profile innate immune memory in primary bone marrow derived macrophages generated from transgenic mice expressing RelA-mVenus ($RelA^{v/v}$) (Figure 17e) [78,102].

We chose six prototypical NFκB-activating ligands, including pro-inflammatory cytokines (TNFα, IL-1β), bacterial molecules and analogs (CpG, PAM2CSK4 (PAM), LPS), and viral analogs (PolyI:C). Signal transduction for these ligands relies on several intracellular pathways before converging on activation of NFκB (Figure 17d) [137]. We stimulated cells with one of these ligands (Ligand A) at varying doses for 4 or 8 hours, followed by either 10 ng/mL TNFα or 1 ng/mL LPS (Ligand B) (Figure 17f). TNFα is an acute pro-inflammatory cytokine has a largely independent signaling pathway and LPS is bacterial molecule which shares many pathway intermediaries with all ligands except TNFα. Testing all parameter combinations gave us a total of 78 memory conditions. We tracked nuclear translocation of the canonical NFκB transcription factor RelA in single cells during stimulation with Ligand A and Ligand B (Figure 17g). Distinct NFκB activation dynamics were visible among the 78 conditions (Figure 18a-b, Figure 19a-f).

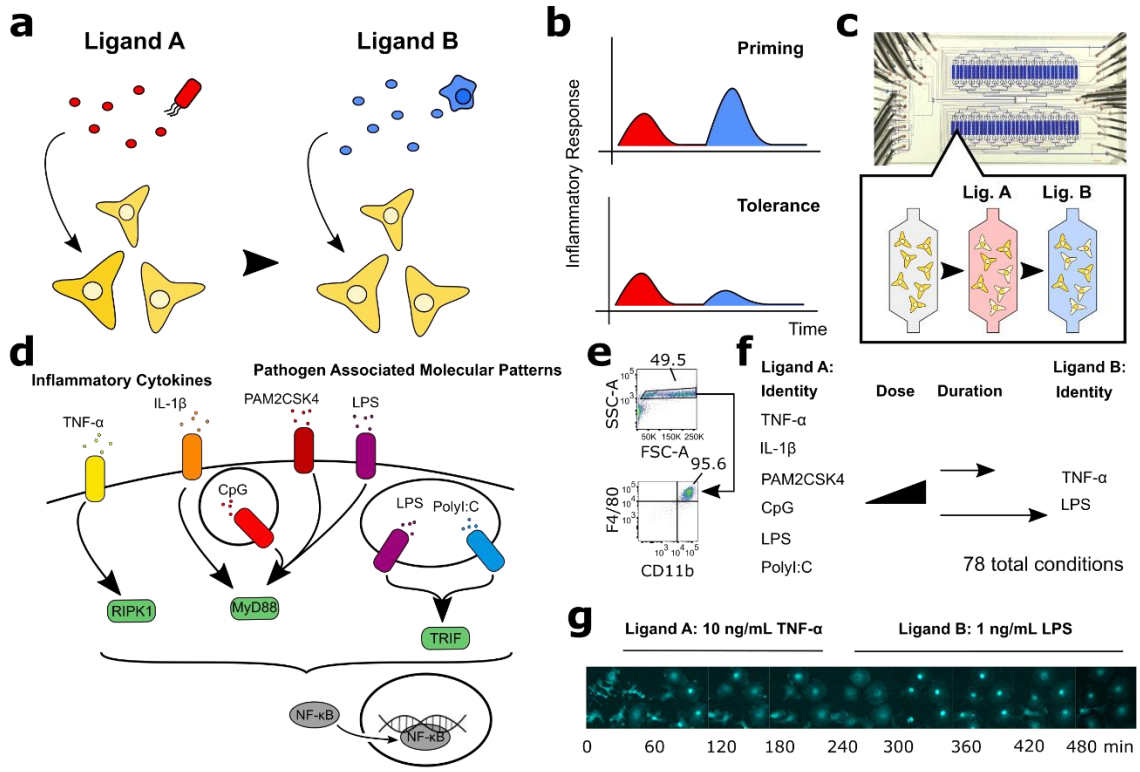

Figure 17. Microfluidics enables high throughput screening of memory encoded in NFκB dynamics.

a) Sentinel cells experience complex temporal stimulus dynamics during acute inflammation. **b)** Priming and tolerance are models of innate immune memory. **c)** Automated microfluidics enables high throughput stimulation and continuous tracking of single cells over sequential stimuli. **d)** Signaling for diverse proinflammatory cytokines and pathogenic molecules converge on several intracellular pathways and ultimately nuclear translocation of NFκB. e) Flow cytometry validation of bone marrow derived macrophage. **f)** High throughput screening parametrizes effect of ligand identity, dose, and duration on memory. **g)** Live cell imaging of macrophages from $RelA^{v/v}$ mice over multiple stimuli.

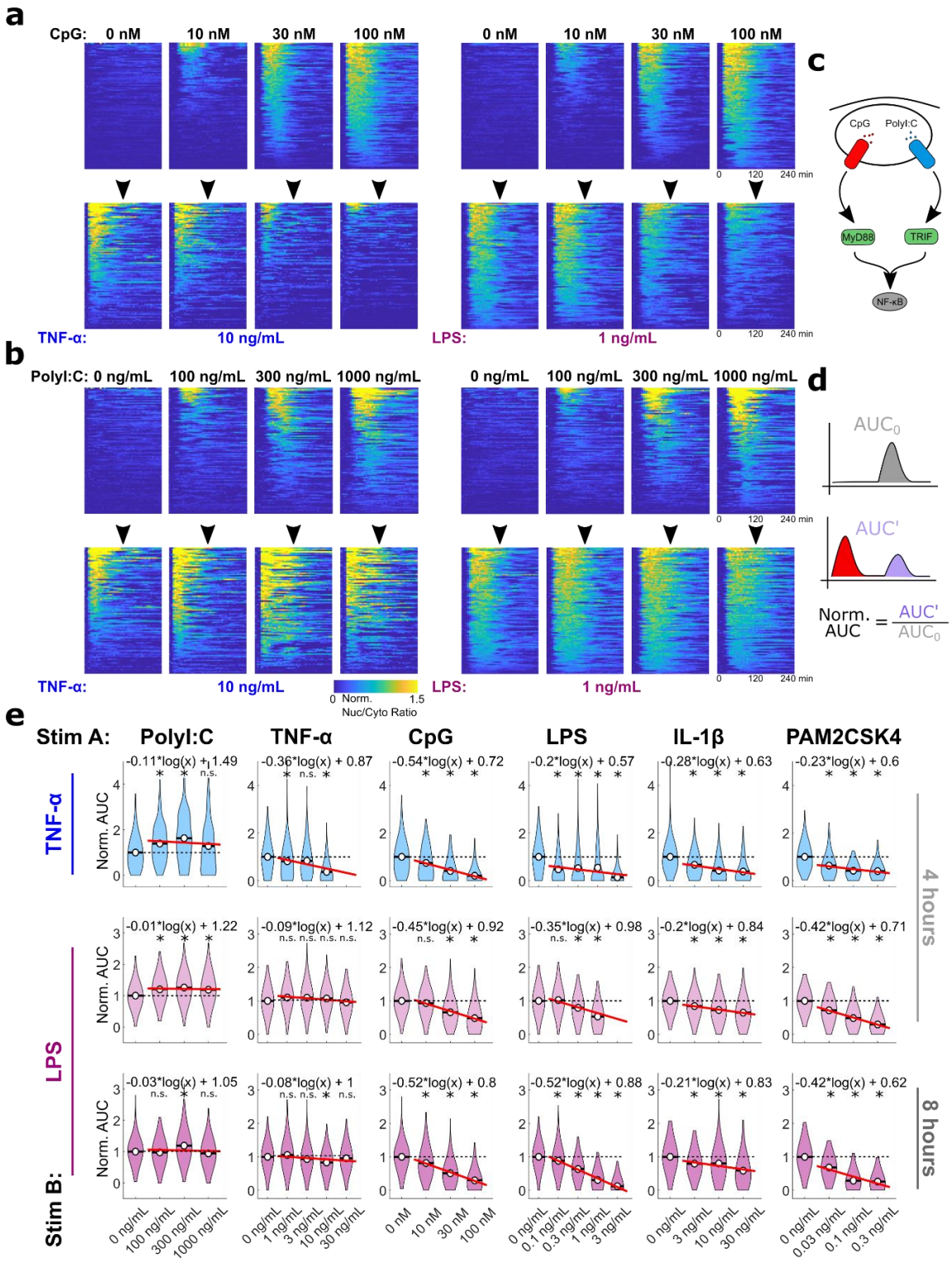

Figure 18. Stimulus identity, dose, and duration shape innate immune memory to produce both priming and tolerance.

Figure 18, continued

a-b) NFκB responses to different doses of CpG **(a)** or PolyI:C **(b)** for four hours (upper plots) followed by either TNFα or LPS (lower plots). Single cell tracemaps show 100 random traces sorted by activation magnitude over 240 minutes of stimulus. Color indicates normalized nuclear/cytoplasmic ratio, with 1 being the mean amplitude at the highest dose (Stimulus A) or with no prior ligand (Stimulus B). **c)** CpG and PolyI:C transduction pathways. **d)** Method for calculating normalized AUC. Stimulus B AUC following Stimulus A (AUC') is normalized by mean AUC_0 of the naïve Ligand B response. **e)** Quantified normalized AUC for TNFα (blue) or LPS (purple) response following stimulus A at the indicated dose for four (light shading) or eight hours (dark shading). y-intercept of log-linear regression fit shows normalized AUC at lowest dose and slope indicates overall trend. Black dashed line shows AUC at baseline (normalized to 1). Open circle shows mean. n > 100 single cells over two independent preparations for each condition. * $p < 1*10^{-2}$ by Wilcoxon rank-sum test with Bonferroni correction.

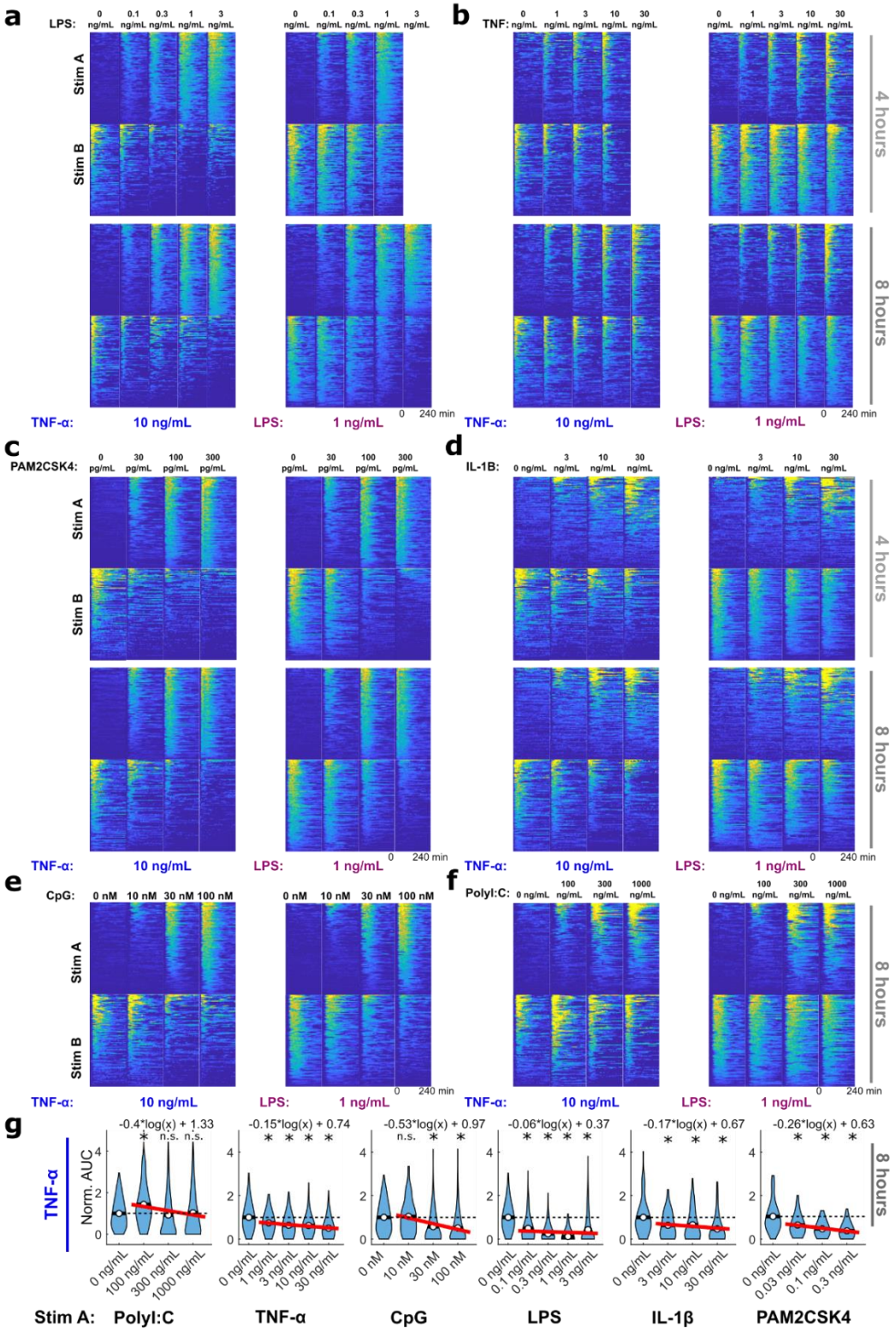

Figure 19. NFκB dynamics in response to varying Ligand A identity, dose, and duration and Ligand B identity.

Figure 19, continued

a-f) NFκB responses to different doses of LPS **(a)**, TNFα **(b)**, PAM2CSK4 **(c)**, IL-1β **(d)**, CpG **(e)**, or polyI:C **(f)** (upper plots) followed by TNFα or LPS (lower plots). Single cell tracemaps shown as 100 random traces sorted by activation magnitude over 240 minutes of stimulus. Color indicates normalized nuclear/ cytoplasmic ratio, with 1 being the mean amplitude at the highest dose (Stimulus A) or with no prior ligand (Stimulus B). Light grey groups are from 4 hours of Stimulus A, and dark grey groups are from 8 hours of Stimulus A (Delivered as two 4 hour pulses). g) Quantified normalized AUC for TNFα (blue) stimulus following stimulus A at the indicated dose for eight hours. y-intercept of log-linear regression fit to normalized AUC at lowest dose and slope indicates dose-dependent trend. Black dashed line indicates an AUC of 1 (unchanged from naïve). Black line and open circle show mean. n > 100 single cells over two independent preparations for each condition. * $p < 1*10^{-2}$ by Wilcoxon rank-sum test with Bonferroni correction.

For example, we considered the macrophage responses to 4 hours of CpG and polyI:C followed by either TNFα or LPS (Figure 18a-b). Both CpG and polyI:C require endocytosis prior but signal through TLR9-MyD88 or TLR3-TRIF and associated intracellular pathways, respectively, before ultimately triggering NFκB translocation (Figure 18c) [137]. For CpG, we observed a clear attenuation of cellular response to both TNFα and LPS as the CpG response increased (Figure 18a), while increased polyI:C response potentiated responses by increasing activation amplitude and durations (Figure 18b). Thus, we concluded that NFκB dynamics encoded ligands-specific memory effects, including both tolerance and priming.

Ligand-specific memory encodes dose- and duration- dependent tolerance and priming

To quantify and compare memory effects between conditions, we normalized NFκB response area-under-the-curve (AUC) from pre-treated cells to the naïve AUC for the same stimulus (Figure 18d). We considered stimuli with a response AUC below naïve to be tolerance and those with a response AUC above naïve to be priming. In this way, we confirmed that CpG stimulus tolerized subsequent TNFα and LPS signaling, and that polyI:C stimulus primed subsequent signaling. We did not observe dose-dependent shifts from priming to tolerance or vice versa, which indicated that memory was ligand-specific in our dose range (Figure 18e, Figure 19g). However, high doses of tolerogenic stimuli resulted in greater tolerance, showing that tolerance was dose-dependent. PolyI:C, the only ligand to produce priming, only showed weak dose-dependency.

Generally, memory affected subsequent TNFα and LPS stimulus similarly, which was unlike previously reported overlap-dependent memory in the NFκB network[84]. TNFα, however, tolerized only subsequent TNFα restimulus, which may be due to pathway specific negative

feedback [99]. PolyI:C priming was also stronger for TNFα than LPS. Increasing stimulus duration resulted in a greater magnitude of tolerance at higher doses, but largely the same patterns (Figure 18e, Figure 19g). Priming weakened with longer stimulus duration, suggesting that priming by polyI:C may be transient. Our initial screen thus identifies ligand-specific priming and tolerance with dose- and duration-dependent strengthening of tolerance and duration-dependent weakening of priming.

After examining population level response using AUC, we considered potential features of the dynamic trace itself. We focused on peak amplitude and duration, as measured by late AUC, which are key aspects of the NFκB trace (Figure 20a-b) [78]. Priming the TNFα response by polyI:C increased both amplitude and late AUC, while priming of the LPS response primarily increased late AUC (Figure 20c). In contrast, CpG-induced tolerance of both TNFα and LPS decreased both amplitude and late AUC (Figure 20d). Thus, we concluded that memory reshapes activation dynamics of NFκB signaling by modulating both the amplitude and duration of signaling.

After focusing on population-level effects, we asked whether these phenotypes could encode information about memory state in single cell activation dynamics. Mutual information quantifies the level of distinguishability between two populations and thus can characterize the accuracy of signal transduction in a signaling network [78,129]. When we compared TNFα activation dynamics after four hours of prior stimulus, mutual information ranged from 0.03 to 0.9 bits, *i.e.* from nearly indistinguishable to completely distinguishable (Figure 21a). TNFα following polyI:C was particularly distinct due to priming. Similarly, TNFα after eight hours and LPS after four or eight hours all displayed distinct patterns of mutual information (Figure 21b-d).

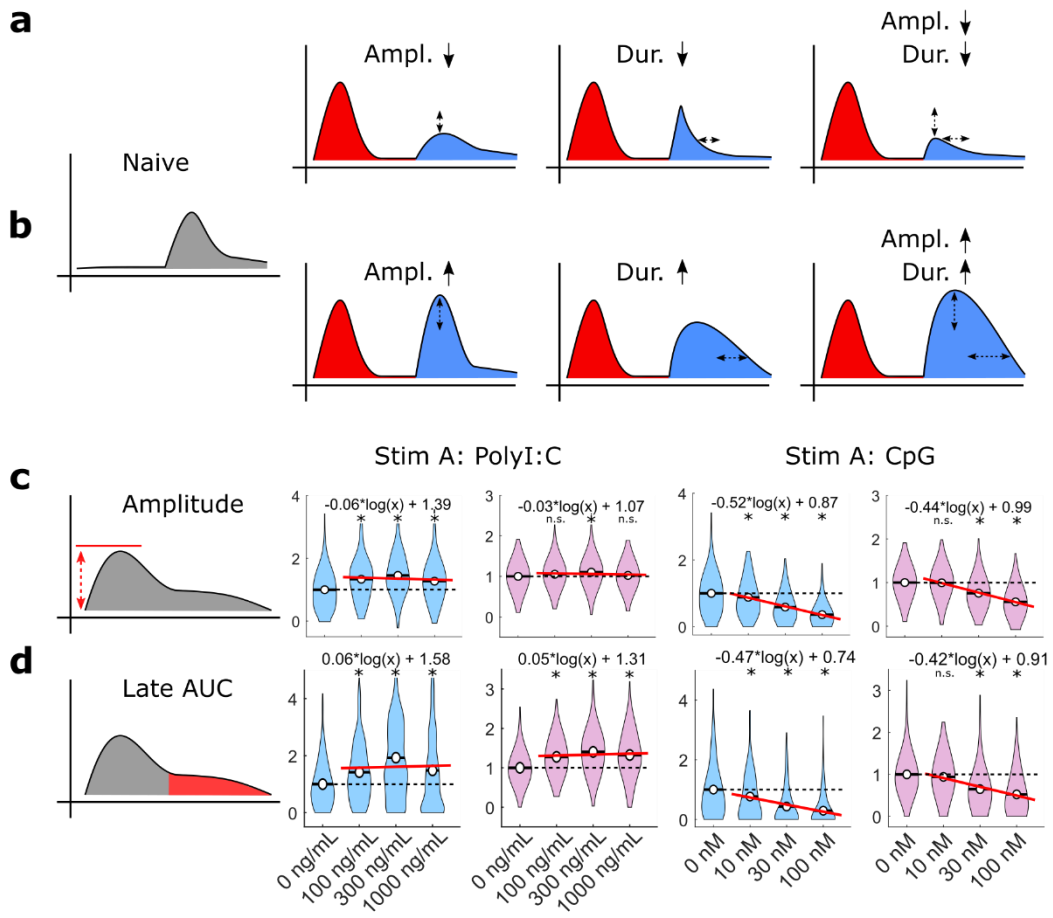

Figure 20. Dynamical features of the NFκB response are altered by ligand memory.

a-b) Conceptual models for how amplitude and duration of ligand responses can be altered in the context of tolerance **(a)** or priming **(b)**. **c-d)** Quantification of normalized amplitude **(c)** and late AUC **(b)** from Stimulus B response (TNFα blue, LPS purple) following Stimulus A (polyI:C or CpG) at the indicated doses. Black dashed line indicates no change from the naïve response, open circle and line indicate mean. n > 100 single cells over two independent preparations for each condition. * $p < 1*10^{-2}$ by Wilcoxon rank-sum test with Bonferroni correction.

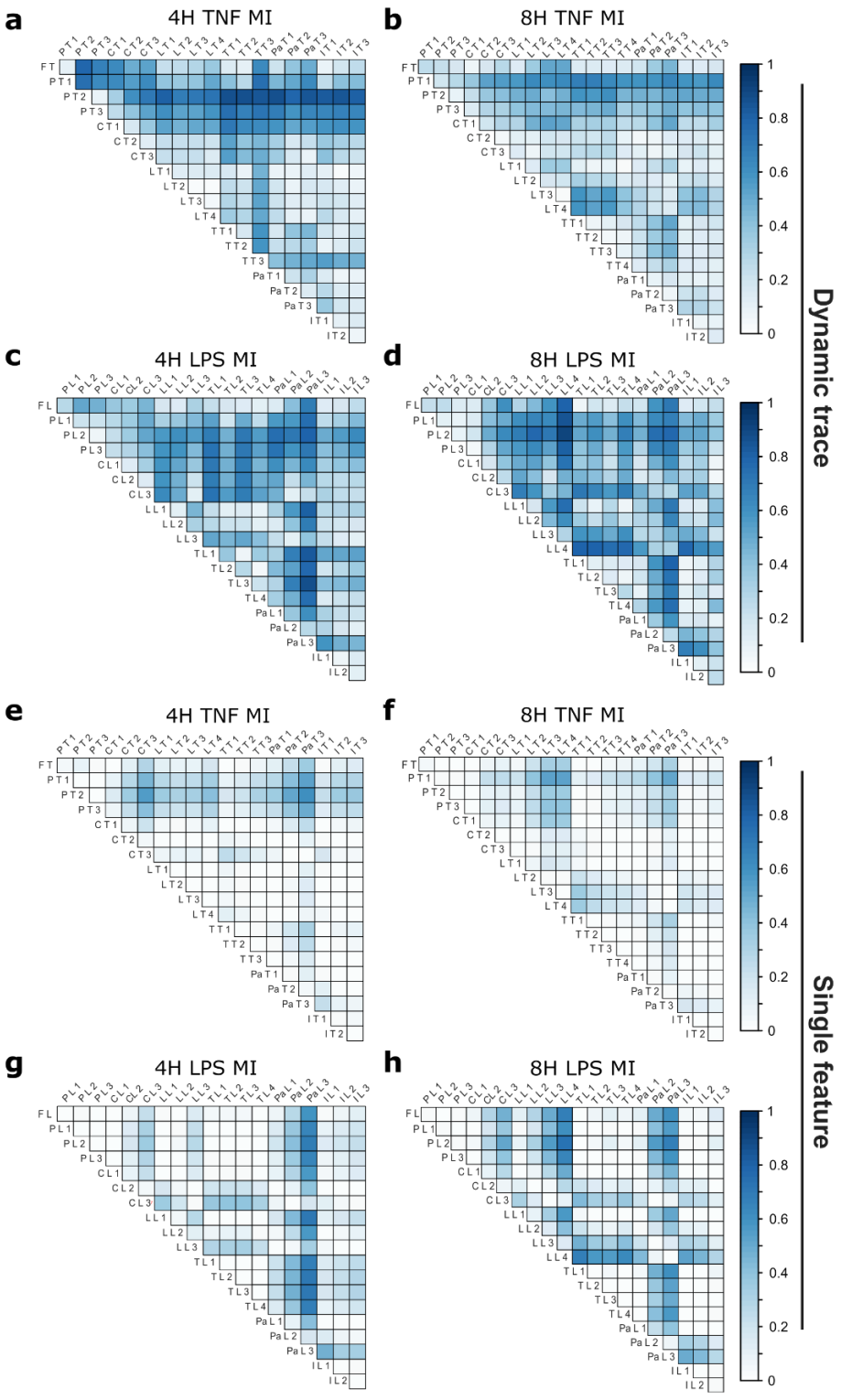

Figure 21. Mutual information between different memory conditions based on information theory.

Figure 21, continued

a-d) Mutual information (MI) calculated from dynamic vector of 20 evenly spaced timepoints over the 4 hour stimulus interval. All conditions compared within one heatmap are the same Ligand B after 4 **(a, c)** or 8 **(b, d)** hours of Ligand A. Ligand A dose ordered from lowest (1) to highest (3 or 4). MI shown in bits where 1 indicates full distinguishability and 0 indicates indistinguishability. **e-h)** Same MI calculations but from a single feature (maximum amplitude) instead of a dynamic vector.

LPS responses showed particularly strong distinguishability following the highest doses of LPS or PAM. Importantly, using a key feature (maximum amplitude) instead of a dynamic trace resulted in far lower distinguishability between conditions in almost all cases (Figure 21e-h). Taken together, these results show that distinct memory states can produce highly distinguishable NFκB responses dynamics to identical stimuli.

NFκB dynamics encode memory of *in vivo* inflammatory challenge in adult macrophages

After observing that memory alters NFκB activation dynamics in bone-marrow derived macrophages, we asked whether *in vivo* acute inflammation also induces similar memory in adult macrophages. Murine endotoxin tolerance is a classic model of innate immune memory where sublethal endotoxemia protects against lethal rechallenge [31], and the role of macrophage memory in this phenomenon has been well described [34,42,181]. Sepsis induced immunosuppression is a related, clinically important phenomenon [182]. We hypothesized that network changes following endotoxin challenge also encode memory as altered signaling dynamics.

We calibrated a model of sublethal endotoxemia via peritoneal injection of LPS (Figure 23a), followed by isolation and microfluidic culture of primary peritoneal macrophages from endotoxin and saline-treated mice (Figure 22a, Figure 23b-d). Peritoneal macrophages cultured without stimulus showed minimal activation and good adaptability to microfluidic culture (Figure 22b, e). Treatment with TNFα and LPS revealed clear differences in NFκB activation dynamics. While nearly all macrophages from saline-treated mice activated following stimulation, response to TNFα is significantly attenuated and response to LPS is completely abolished in macrophages from endotoxin-treated mice (Figure 22c-e). Endotoxemia also significantly delayed and increased the heterogeneity in the time to activation following

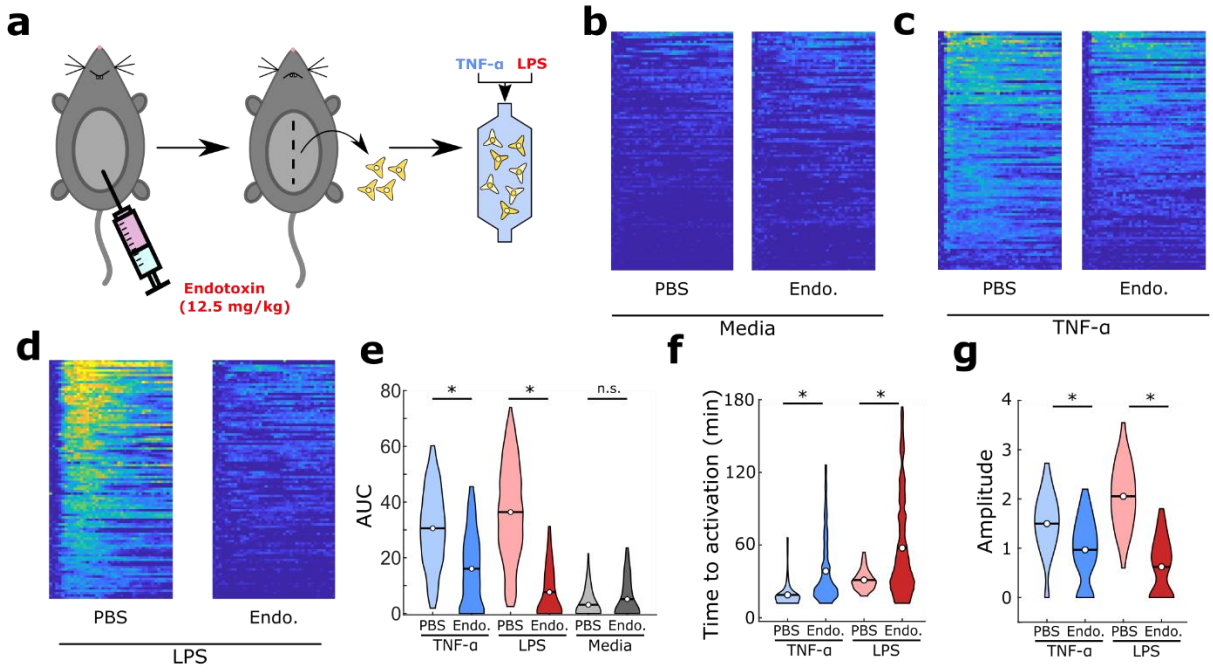

Figure 22. *In vivo* endotoxin tolerance is encoded in adult macrophages through altered NFκB dynamics.

a) Schematic for endotoxemia and adult macrophage retrieval. b-d) NFκB dynamics in adult peritoneal macrophages from mice injected with PBS or endotoxin. 100 random traces selected from >200 cells **(b)** or >600 cells **(c-d)** over 3 mice/condition. **b)** Baseline NFκB dynamics. **c)** NFκB dynamics following 10 ng/mL TNFα. **d)** NFκB dynamics following 1 ng/mL LPS. **e-g)** Violin plot of total AUC **(e)**, time to activation **(f)**, or activation amplitude **(g)** over 4 hours for each condition. Open circle shows mean. * p-value < $1*10^{-10}$, n.s. p-value > 0.01 by Wilcoxon ranked sum test with Bonferroni correction.

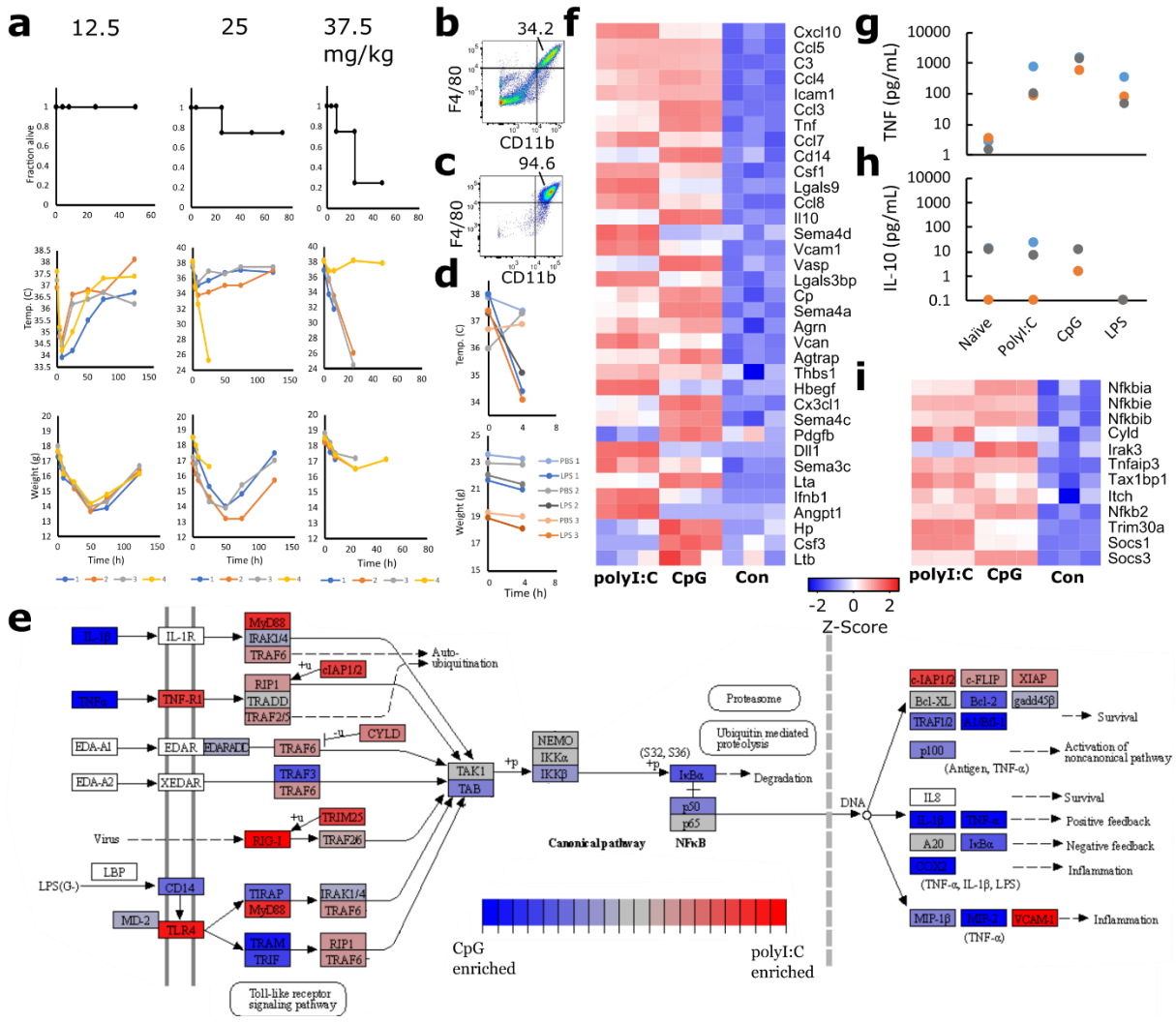

Figure 23. Validation of an *in vivo* endotoxemia model and profiling of state differences due to polyI:C and CpG stimulation.

a) Measurement of dose-dependent morbidity and mortality due to endotoxemia. 12.5, 25, or 37.5 mg/kg of LPS in PBS were injected i.p. in 4 6-8 week old mice per condition. Kaplan-Meier curve, rectal temperature, and weight were recorded for mice in each group. **b-c)** Flow cytometry showing enrichment of F4/80^{+} CD11b^{+} peritoneal macrophages **(c)** from peritoneal lavage **(b)** using negative selection. **d)** Measured weight and temperature for mice used for NFκB dynamics measurements following induction of endotoxemia. Each experiment used a pair of littermates where one was treated with 12.5 mg/kg LPS and the other with an equivalent quantity of PBS i.p. 3 independent pairs were used for the experiment. Mice were taken for extraction of peritoneal macrophages after 4 hours of stimulation. **e)** Gene expression enrichment for key members of the NFκB signaling network following CpG or polyI:C treatment based on KEGG map 04064 using Pathview. **f)** Heatmap of upregulated secreted signaling molecules with expressed receptors in

Figure 23, continued

bone-marrow-derived macrophages following four hours of CpG or polyI:C treatment. **g-h)** ELISA measurements of secreted TNFα **(g)** or IL-10 **(h)** following 4 hours of the indicated stimulus. Data shown are from three independent stimulations. **i)** Heatmap of upregulated negative feedback regulators in the NFκB network following 4 hours of stimulation with polyI:C or CpG.

treatment with TNFα and LPS (Figure 22f) and reduced the amplitude of activation (Figure 22g). We concluded that innate immune memory phenotypes like endotoxin tolerance can indeed be encoded by adult macrophages in altered NFκB dynamics.

Interestingly, TNFα activation dynamics in peritoneal macrophages showed an extended activation plateau instead of an activation pulse (Figure 22c). Endotoxemia attenuated LPS-induced dynamics more strongly than TNFα-induced dynamics (Figure 22c-d), while TNFα was generally more attenuated than LPS in bone-marrow derived macrophages (Figure 18e). These results suggest that signaling networks may be wired in adult macrophages to produce different activation dynamics and that the physiological context of endotoxemia may shape memory differently from *in vitro* stimulation.

Single cell innate immune memory can be determined by response to prior stimulus

Next, we asked whether innate immune memory can be encoded on the level of single cells. Our microfluidic setup allowed us to investigate whether an individual macrophage response to stimulus A and to stimulus B are correlated. We chose four hours of CpG to LPS or polyI:C to TNFα as our test cases for priming and tolerance, and used maximum response amplitude and time to activation as the key features which differentiated single cell responses to CpG and polyI:C. Within the population of cells exposed to CpG and polyI:C, both features are heterogeneous and encode key information about maximum signaling flux and pathway activated (Figure 24a-c). We clustered cells into five subpopulations of >100 cells based on these features for both CpG and polyI:C response (Figure 24b). We thus defined subpopulations of cells based on dynamic response to stimulus A for further analysis of memory effects.

k-means clustering grouped cells based on activation amplitude (Groups 1-3) and time (Groups 4-5) in response to CpG (Figure 24d-e). Group 1 captured the strong, early responders and group 5 captured the weak, slow responders and non-responders. When we plotted traces for each group, we saw that LPS responses appeared negatively correlated with CpG response (Figure 24d-e). The strongest LPS responders were in the weak CpG response groups, and the strong CpG responders largely did not activate to LPS restimulus. Indeed, quantification of LPS AUC showed notably stronger LPS response in groups 4 and 5 (Figure 24e). We concluded that single cell tolerance is correlated with CpG response strength and speed, such that strong CpG responders are more attenuated to subsequent LPS stimulus.

We then turned to information theory to quantify whether memory states in each group were sufficiently different to encode distinguishable information in the subsequent response to LPS. Mutual information between groups 4-5 and groups 1-3 reached up to 0.44 bits despite coming from identical treatment conditions (Figure 24f). Thus, subpopulations of cells with different responses to CpG induce memory states which can be distinguished by their subsequent response to restimulus. We concluded that tolerance is largely deterministic in single cells and positively correlated with CpG response strength.

We used the same analysis approach for polyI:C response. In group 4 and 5, which showed weak polyI:C response, cells did not respond strongly to subsequent TNFα, suggesting that subpopulations of polyI:C response may correlate with priming on a single cell level (Figure 24g). When we quantified the TNFα AUC in each group, groups 1-3 were indeed priming, while groups 4 and 5 were unchanged or slightly tolerized (Figure 24h), although significant heterogeneity existed across all groups. Notably, group 3 and 4 had similar polyI:C AUC but

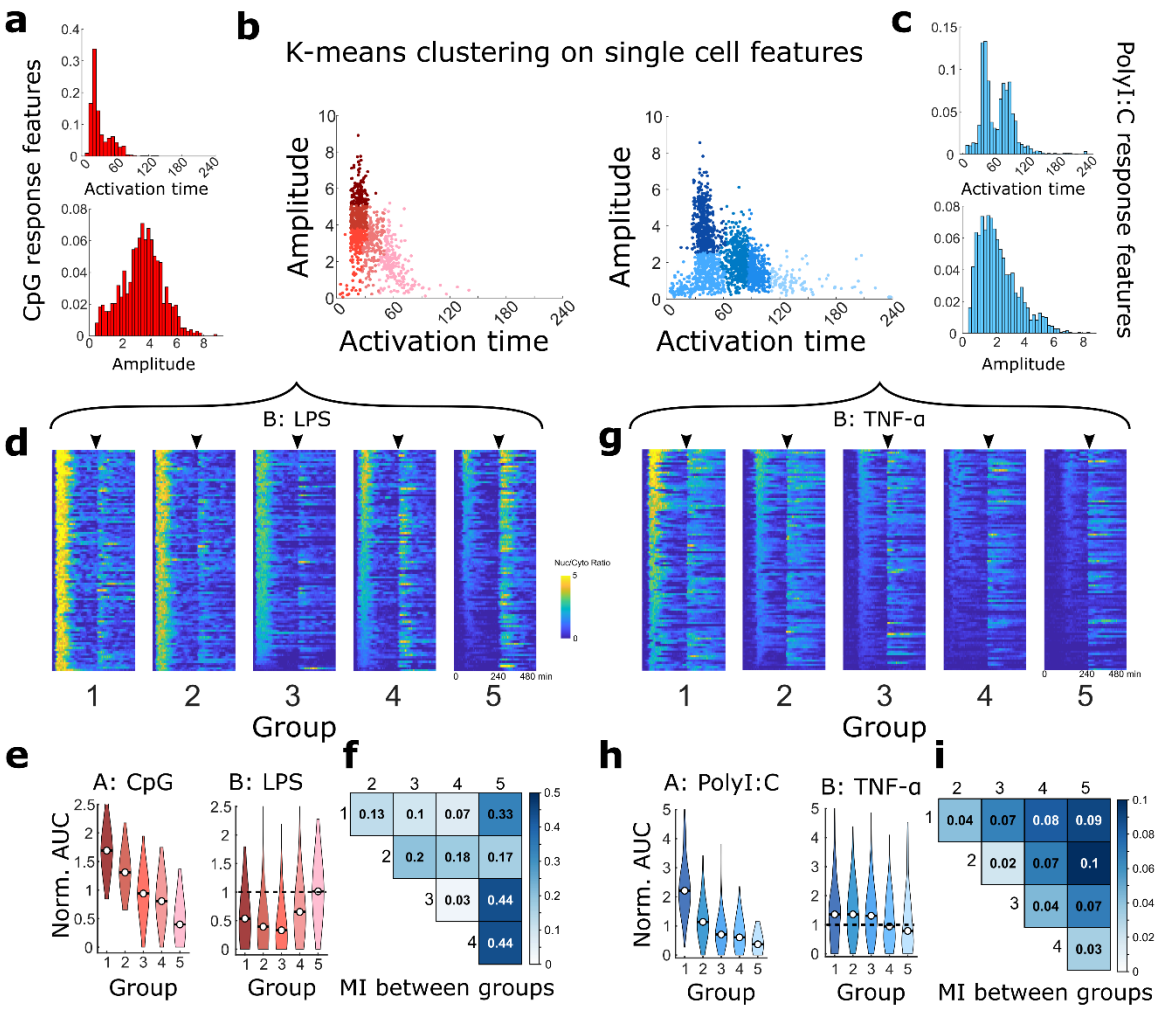

Figure 24. Single cell analysis reveals subpopulations of innate immune memory based on response to initial stimulus.

a) Histograms of single-cell distribution for key features of the heterogeneous response to 300 nM CpG. Population fraction is on the y-axis. **b)** k-means clustering of single cells based on polyI:C (blue) or CpG (red) trace behavior. Scored using cityblock distance and best score of five initializations used. **c)** Same as **(a)** for 1000 ng/mL polyI:C. **d)** Traces from single cells stimulated with CpG to LPS in groups from **(b)**. **e)** Quantification of normalized AUC within each group for CpG and subsequent LPS response. Normalized to mean AUC for CpG or naïve LPS response. Open circle indicates mean, dotted line indicates baseline TNFα response. **f)** Mutual information between LPS responses from each group. **g)** Traces from single cells stimulated with polyI:C to TNFα in groups from **(b)**. **h)** Same as **e)** for polyI:C and subsequent TNFα responses. **i)** Same as **(f)** for groups by polyI:C response

different priming, suggesting that key information is encoded in the different time to activation between these groups (Figure 24b). Turning once again to information theory, we found weak mutual information up to 0.1 bit between each group's TNFα responses (Figure 24i). Thus, we concluded that distinct priming states exist in subpopulations of polyI:C treated macrophages and can be identified by single cell NFκB response, but that this relationship only weakly deterministic.

Innate immune memory is independent of paracrine TNFα and IL-10 secretion

Memory encoded in NFκB dynamics implies dynamic changes in the signaling networks which regulate these dynamics due to prior stimulus. To characterize these network changes and search for potential modules encoding priming and tolerance, we profiled the transcriptome of macrophages treated with CpG or polyI:C. We identified differentially regulated genes related to NFκB signaling (Figure 23e) and upregulated ligands with expressed receptors (Figure 23f) [183]. We hypothesized that paracrine signaling, especially through TNFα and IL-10, could affect memory. TNFα signaling can tolerize cells to subsequent TNFα stimulus (Figure 18e) [102], and IL-10 is a known inhibitor of NFκB signaling [92]. Secreted TNFα is detectable following four hours of stimulation, and while IL-10 was below the detection limit of ELISA, the low chamber volume in the microfluidic device could magnify the effects of any locally secreted IL-10 (Figure 23g-h) [184].

We added excess soluble TNFR1 during stimulation with polyI:C or CpG to block block paracrine signaling by secreted TNFα, followed by washout and stimulus with exogenous TNFα or LPS. We observed a marked decline in late-activating cells and lower late AUC under both polyI:C and CpG stimulus (Figure 25a-b), which is consistent with activation to paracrine TNFα

resulting in late and extended NFκB activation (Figure 24c) [78]. CpG-treated cells exhibited similar tolerance irrespective of TNF blocking, suggesting little role for paracrine TNFα in tolerance. Surprisingly, TNFα priming was strongly increased following polyI:C with excess TNFR1. This observation suggests that polyI:C-induced priming amplifies the macrophage response to local TNFα secretion, and that without paracrine TNFα signaling macrophage responses to exogenous TNFα are stronger.

Similarly, we blocked IL-10 paracrine signaling by adding excess soluble IL10R during stimulation by CpG. We observed no significant changes in subsequent TNFα or LPS response (Figure 25c), which led us to conclude that IL-10 does not play a major role in inducing the tolerance we observed. Due to these results, we concluded that innate immune memory at our timescales was primarily mediated intracellularly with little role for paracrine signaling.

Network modeling suggests induced feedbacks control priming and tolerance

Based on the differentially regulated genes we identified (Figure 23e), we were particularly interested in known negative and positive regulators of NFκB signaling. Many negative regulators of NFκB signaling in macrophages are stimulus-induced feedback and encode memory of prior stimuli, including A20, IRAKM, and IκBδ [87,91,102,132,185,186]. These negative feedback proteins were upregulated by both polyI:C stimulus and CpG stimulus (Figure 23h). Interestingly, key intermediary proteins TNFR1 and positive regulator of TNFα signaling cIAP1 [187] were upregulated for TNFα signaling and TLR4 and Myd88 were upregulated for LPS signaling (Figure 23e). These observations led us to hypothesize that

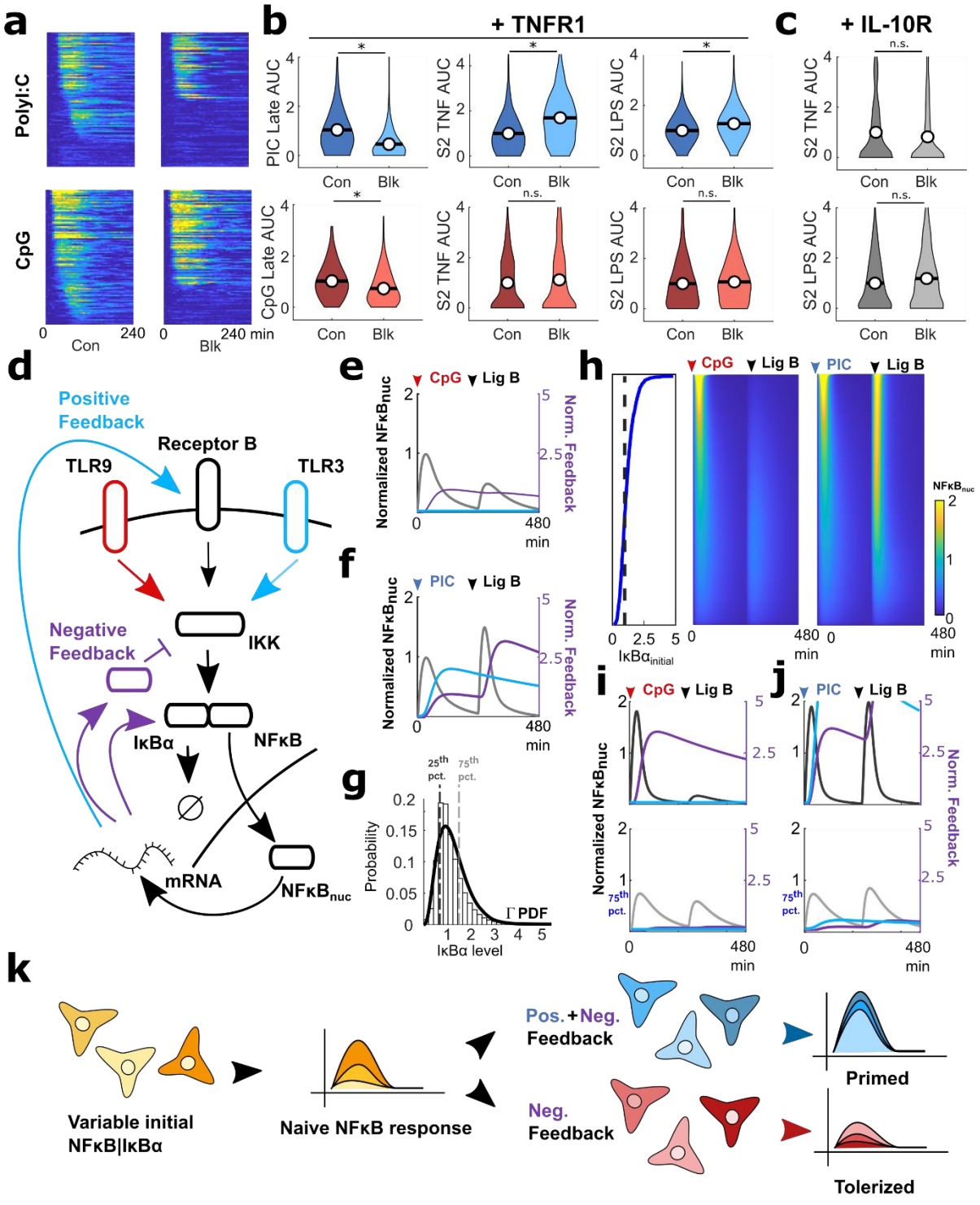

Figure 25. Mathematical modeling suggests single-cell memory is encoded directly in altered intracellular signaling networks.

Figure 25, continued

a) Traces from single cells stimulated with 300 ng/mL polyI:C or CpG with 0 (Con) or 13 (Blk) μg/mL TNFR1. **b)** Violin plots showing change in late AUC due to TNFα block (left), and AUC from restimulus with TNFα (middle) or LPS (right). **c)** Violin plots showing AUC from CpG to TNFα or LPS with 0 (Con) or 6.5 ug/mL IL10R (Blk). b-c) * p val. < 0.01 by Wilcoxon ranked sum test with Bonferroni correction from > 200 individual cells. **d)** Simplified design of computational NFκB circuit (full network in Figure 26a). NFκB-dependent feedback is shared (purple arrows) or polyI:C specific (blue). **e-f)** Simulation of nuclear NFκB (grey), negative feedback (purple), and positive feedback (blue) levels reproducing mean behavior from CpG to LPS **(e)** and polyI:C to TNFα **(f)**. **g)** Experimental distribution of IκBα levels in single naïve macrophages from flow cytometry (histogram) fit to a Γ distribution (black line, a=3.83, b=294). IκBα level normalized to median, dark grey and light grey lines show 25^{th} and 75^{th} percentile IκBα levels respectively. **h)** Simulated single-cell NFκB traces for CpG or polyI:C to Lig. B based on initial NFκB|IκBα level. $NF\kappa B|I\kappa B\alpha_{initial}$ for each trace sorted in ascending order and shown in line plot at left. **i-j)** Simulation of nuclear NFκB, negative feedback (purple), and positive feedback (blue) levels using 25^{th} and 75^{th} percentile IκBα levels (dark and light grey NFκB traces respectively). Simulation for CpG **(i)** or polyI:C **(j)** to Lig. B. **k)** Schematic model of memory encoding at a single cell level due to extrinsic noise and IκBα heterogeneity.

tolerance is encoded by negative feedback regulators, but that priming increases key protein levels to overcome negative feedback.

To test this hypothesis, we turned to mathematical modeling of the NFκB network. While exceptional NFκB network models have been generated [90,100,101], few model the interplay between sequential stimuli. To achieve this, we developed a simplified mathematical model which captures relationships between signal transduction from different ligands over time (Figure 25d) [102]. In this model, network topology is functionally equivalent at the receptor level, so we used the same receptor to represent TNFR and TLR4 as "Receptor B". We simulated the impact of negative feedback through an NFκB-induced inhibitor of IKK activation which acts as several known negative feedback proteins (Figure 26a). We also included positive feedback through polyI:C-induced upregulation of Receptor B. We fit this model to the mean amplitudes from experimental traces of each condition (Figure 19c). The resultant model with 15 equations and 26 parameters successfully reproduced both CpG-induced tolerance (Figure 25e) and polyI:C-induced priming (Figure 25f) of response amplitude. A circuit topology with shared negative feedback acting on the IKK node and polyI:C specific positive feedback acting on the receptor node is therefore sufficient to produce both tolerance and priming.

Single-cell encoding of innate immune memory can be determined by initial conditions

To identify key parameters and species which control memory in the NFκB network, we varied each parameter 100-fold (Figure 26b). The model was sensitive to IKK cycling parameters and degradation rates, as well as initial conditions of key species. The most sensitive parameter, however, was the initial amount of NFκB associated with IκBα (NFκB|IκBα). Initial IκBα and NFκB levels have been shown to predict single cell variability in the NFκB response [123]. This led

us to hypothesize that heterogeneous initial NFκB|IκBα could control single-cell variability in response to stimulus A and resultant memory states.

To test this hypothesis, we first profiled the distribution of IκBα levels in naïve macrophages. These levels matched a gamma distribution (Figure 25g), consistent with theoretical and measured protein distributions in single cells [163,188]. Using this distribution, we simulated tolerance and priming in 1000 single cells using identical parameters as in the bulk model, but with initial NFκB|IκBα levels chosen randomly according to the fitted distribution. This simulation produced response traces strikingly like experimental trends (Figure 25h). Initial responses were heterogenous, as cells with higher initial NFκB|IκBα levels produced stronger responses to initial stimulus. Strong responders to CpG were highly tolerized in response to ligand B due to high negative feedback, while weak responders were largely unchanged (Figure 25h, i). Likewise, strong responders to polyI:C were strongly primed in response to ligand B, while weak responders showed weaker priming (Figure 25h, j). Thus, our simulation results map onto our experimental data showing that stronger responders to CpG and polyI:C induce strong memory states, while weak responders induce little to no memory. Taken together, these results suggest that heterogeneity in a single initial condition can give rise to dramatically different memory states at the single cell level (Figure 25k).

Here, we show that a computational model fit for mean behavior can recapitulate key features of single cell innate immune memory simply by varying one initial condition. This observation demonstrates that complex single cell behaviors over extended durations can be governed by simple differences in initial protein abundances.

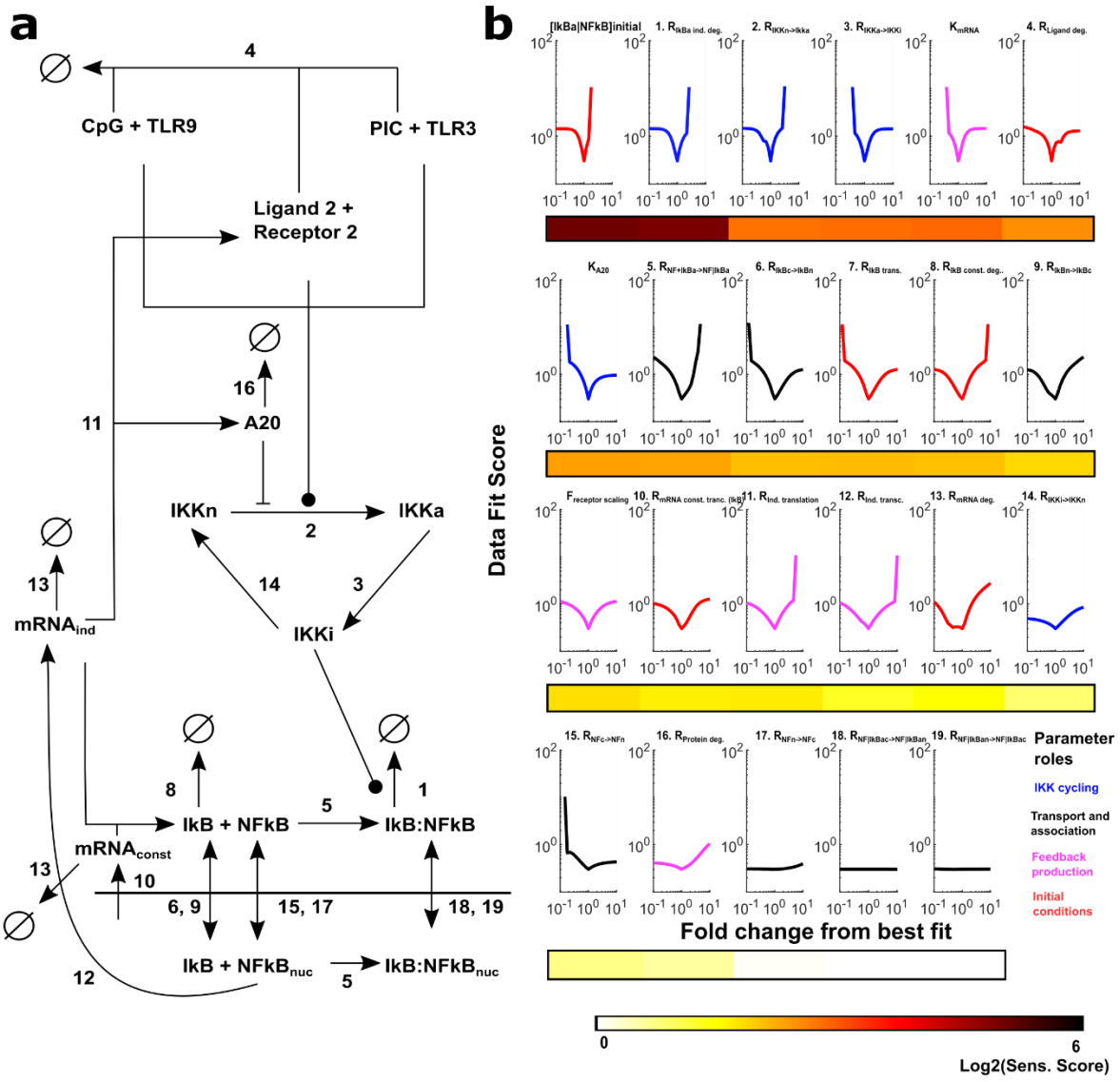

Figure 26. Parameter sensitivity for NFκB memory mathematical model.

a) Detailed network diagram for model showing all equations and rate parameters (numbered). **b)** Parameter sensitivity results from scanning 100x around the best-fit parameter. Data fit score calculated as deviation from experimental means for priming and tolerance. Color indicating sensitivity score quantifies rate of change or "steepness" of the well around the best-fit point. Parameters organized by sensitivity score and color coded by class of parameter.

Memory-dependent differences in NFκB dynamics are encoded in transcriptional output

We then asked whether memory encoded in NFκB dynamics can also be reflected in cell state differences using transcriptomic profiling. We used four cases of memory, polyI:C/CpG to TNFα/LPS, which represent both priming and tolerance. Genes were classified by whether they were synergistically or antagonistically regulated by prior stimulus (Figure 27a). Since NFκB dynamics are strengthened following priming and weakened following tolerance, we expected tolerance to produce more antagonism and priming to produce more synergy. Consistent with our expectations, we identified 214 synergistically regulated transcripts and 366 antagonistically regulated transcripts for CpG to TNFα stimulus, compared to 572 synergistic and 394 antagonistic transcripts for polyI:C to TNFα (Figure 27b-c). We repeated this analysis for polyI:C/CpG to LPS and found similar numbers of synergistic transcripts, but over 30% more antagonistic transcripts for CpG to LPS (Figure 28a-b). We then identified cellular processes associated with synergy and antagonism using overrepresentation analysis. Synergistic transcripts from all conditions were enriched for immune and inflammatory responses, while those due to priming were also enriched for NFκB and TNF signaling (Figure 27d). Similarly, antagonistic transcripts from all conditions were enriched for cell adhesion and signal transduction, but those associated with tolerance were more enriched for immune processes, NFκB signaling, and TNF signaling (Figure 27e). Taken together, these results suggest that while memory globally increases a subset of genes associated with inflammatory signaling, genes specific to NFκB and TNF signaling are synergistically regulated by priming but antagonistically regulated by tolerance.

Based on these results, we identified transcription factors (TFs) associated with synergy and antagonism in each condition. We used the ChEA3 algorithm to identify overrepresented TFs based on published ENCODE CHIP-seq data [144] . Synergistic transcripts for both polyI:C and CpG to TNFα share a large fraction of enriched TFs, including NFκB (RelA), AP-1 (Jun, JunD), and interferon-related (Stat1/2) TFs, though these TFs were generally more enriched following polyI:C (Figure 27f). In contrast, antagonistic transcripts largely did not share enriched TFs, with CpG specific TFs including many of those involved in NFκB and JNK signaling (Figure 27g). Applying the same analysis to the polyI:C and CpG to LPS conditions also showed shared TFs among the synergistic genes and more distinct TFs among antagonistic transcripts (Figure 28b-c). Taken together, these results suggest that priming and tolerance both synergistically regulate targets of signaling pathways involved in inflammatory signaling (e.g. NFκB, AP-1), but that tolerance also antagonistically regulates a subset of targets involved in the same pathways.

Unexpectedly, we found that seven TFs were overrepresented in both synergistic and antagonistic transcript sets for CpG to TNFα. This overlap suggests memory controls which genes are transcribed by active TFs in addition to regulation of TF activation at the network level. To profile which expression programs are turned on and off by memory, we looked at cellular processes associated with the 96 synergistic and 325 antagonistic transcripts regulated by at least one of the seven shared TFs. We found that synergistic transcripts were enriched for IFN-γ signaling and proliferation, while antagonistic transcripts were enriched for metabolism, NFκB signaling, and MAPK signaling (Figure 27h). Although no IFN-γ is transcribed, the term may reflect Stat1/2 activation by secreted IFN-β (Figure 27f, Figure 23f). Thus,

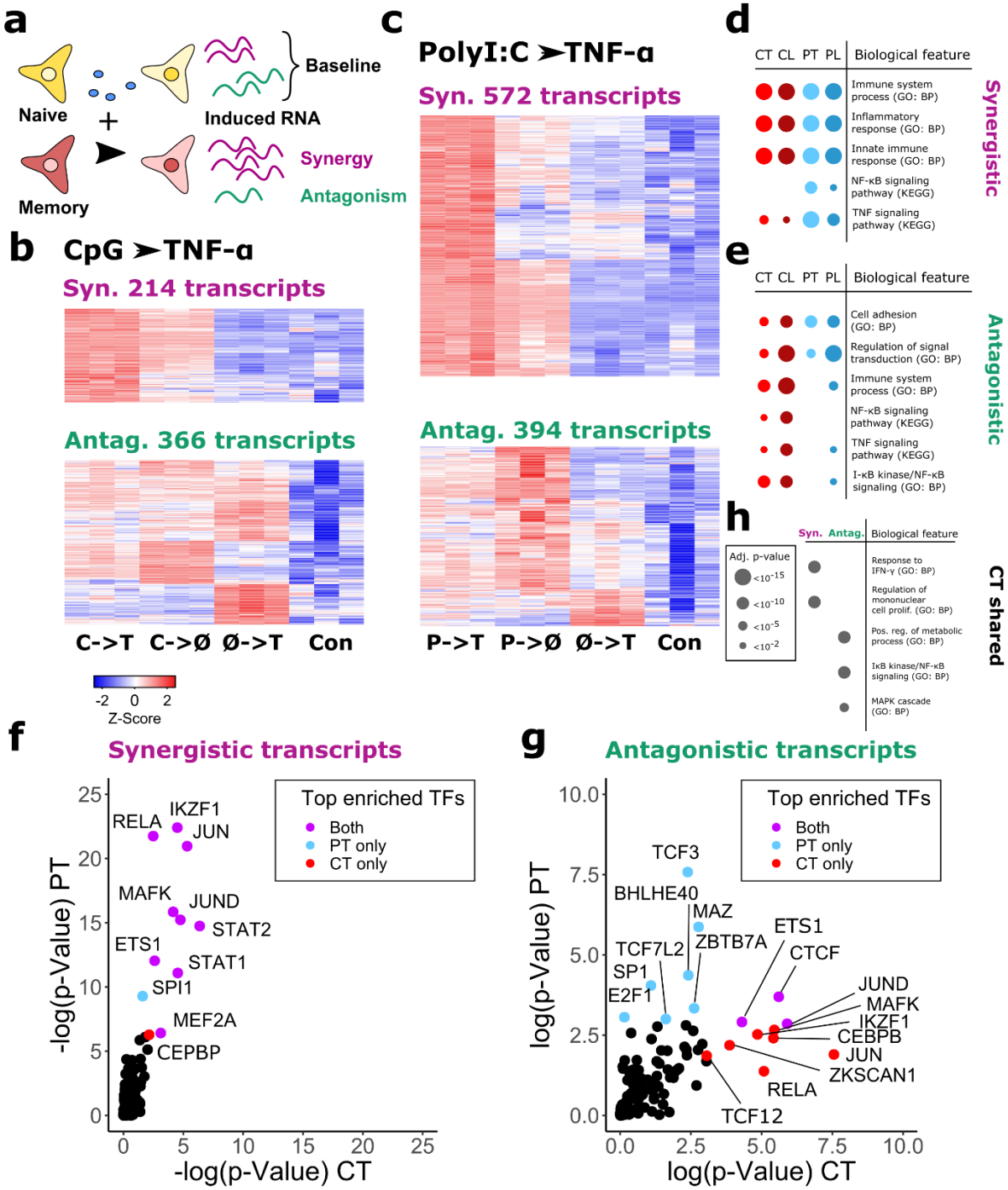

Figure 27. Gene expression profiling reveals distinct transcriptomic changes due to tolerance or priming.

a) Approach for determining memory-based synergy and antagonism in gene expression. **b)** Heatmaps of synergistically or antagonistically upregulated genes for CpG to TNFα. RNA-seq

Figure 27, continued

was performed in triplicate and each row is one gene. **c)** Same as **(b)** for polyI:C to TNFα. **d-e)** p-values from overrepresentation analysis of synergistic **(d)** or antagonistic **(e)** genes for the indicated treatment conditions. Gene sets from either GO: BP or KEGG databases. Size of circle corresponds to adjusted p-value. **f)** Scatterplot of overrepresented TFs from synergistically regulated genes following either CpG to TNFα (CT) or polyI:C to TNFα (PT). Top 10 TFs for each condition colored based on whether they are overrepresented for PT (blue), CT (red), or both PT and CT (purple). Enrichment p-values based on ChEA3 using the ENCODE TF target library. **g)** Same as **(f)** for antagonistically regulated genes following either CT or PT. **h)** Overrepresentation analysis for CT genes regulated by TFs enriched in both synergistic and antagonistic gene sets. p-values shown for GO:BP terms associated with synergistic genes or antagonistic genes regulated by the same TFs. Size of circle corresponds to adjusted p-value.

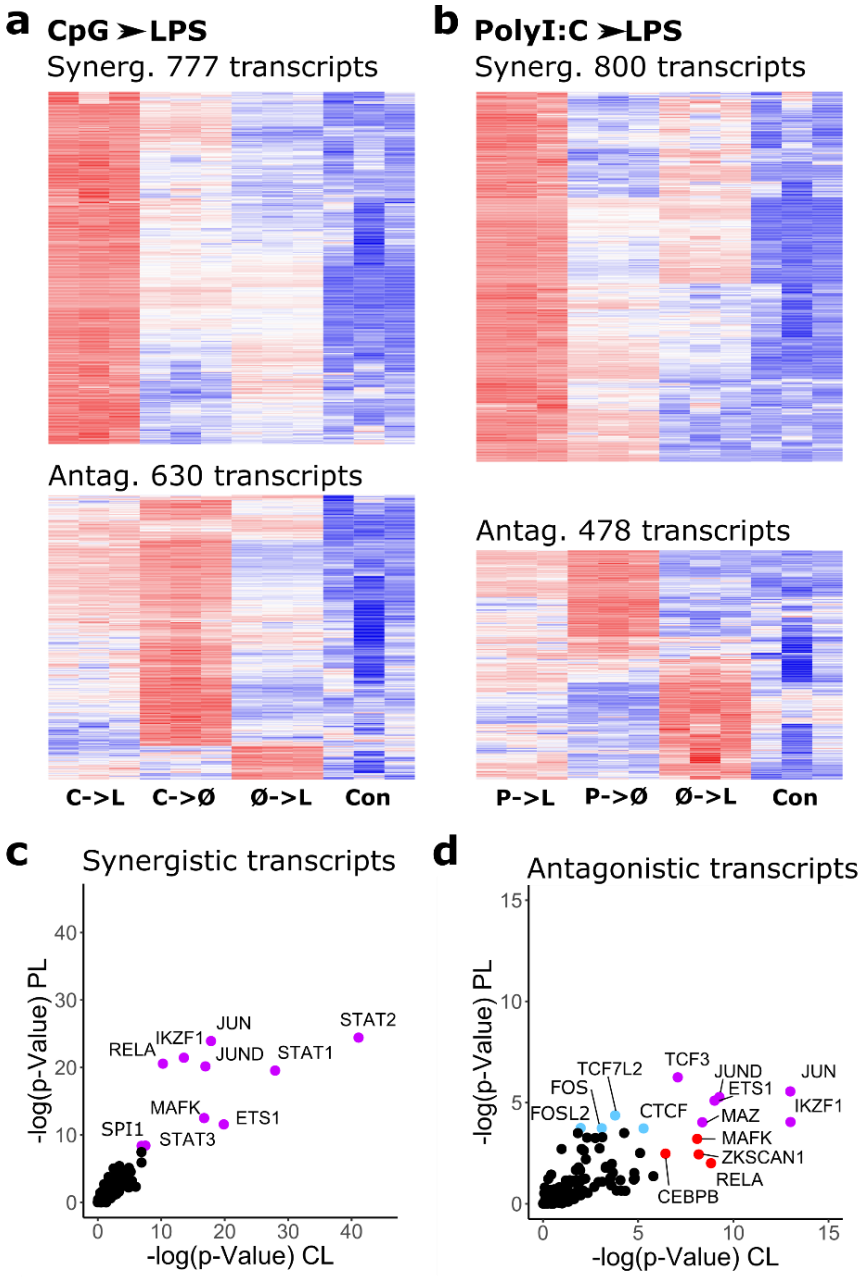

Figure 28. Gene expression profiling of memory effects on LPS-induced transcription.

a) Heatmaps of synergistically or antagonistically upregulated genes for CpG to LPS. RNA-seq was performed in triplicate and each row is one gene. **b)** Same as **(a)** for polyI:C to LPS. **c)** Scatterplot of enriched transcription factors based on synergistically regulated genes following either CpG to LPS (CL) or polyI:C to LPS (PL). Top 10 transcription factors for each condition colored based on whether they are enriched for PL (blue), CL (red), or both PL and CL (purple). Enrichment p-values based on ChEA3 using the ENCODE TF target library **d)** Same as **(c)** for antagonistically regulated genes following either CL or PL.

memory may “fine tune” TF activity to synergize particular gene programs and antagonize others.

Chromatin accessibility dynamics tune transcription factor targets following activation

Dynamic chromatin accessibility could explain how one TF can regulate both synergistic and antagonistic transcripts. Chromatin accessibility rapidly changes after exposure to inflammatory stimulus [189] and remodeling of promoters and enhancers could tune the transcriptional response to subsequent stimuli. Differential promoter accessibility for a key TF could give rise to both synergy and antagonism despite identical TF dynamics (Figure 29a). We performed ATAC-seq, which profiles accessible chromatin, on single and sequential stimulus conditions to test this possibility.

We observed that four hours of CpG and polyI:C treatment indeed produced distinct changes in chromatin accessibility (Figure 29b). Hierarchical clustering identified regions with increased accessibility after polyI:C treatment, CpG treatment, and after both, along with two groups which became less accessible (Figure 30a-b). Interestingly, all three upregulated groups showed enrichment for κB and activated protein 1 (AP-1) motifs, consistent with TF overrepresentation in transcriptomic data (Figure 29b). The polyI:C-specific and shared groups were enriched for interferon stimulated regulatory elements (ISREs), while the CpG-specific group was enriched for c/EBP motifs. These observations correspond with activation of NFκB, JNK, and p38 signaling by both polyI:C and CpG, while polyI:C induces an interferon program. c/EBP activation by CpG has not been described, but the c/EBP family of TFs coordinates initial responses to inflammatory stimuli and controls myeloid differentiation [190]. Thus, stimuli remodel the accessible chromatin landscape of macrophages in a signal-specific manner.

We then asked whether differential peak accessibility correlated with synergistic gene expression. We identified genes with upregulated promoter peaks (+/- 3000 bp from the TSS) following polyI:C and found that a larger fraction of synergistic transcripts for polyI:C to TNFα/LPS than antagonistic transcripts had increased promoter accessibility (Figure 29c). Likewise, genes with upregulated promoter peaks following CpG included a larger fraction of synergistic transcripts for CpG to TNFα, though the fraction of synergistic and antagonistic transcripts for CPG to LPS was more similar (only 27% vs 22%). Altogether, these observations led us to conclude that chromatin accessibility contributes regulating to synergy and antagonism in transcription.

Surprisingly, we saw enrichment of RelA motifs in all three groups with increased peak accessibility (Figure 29b). We asked whether regulation of RelA sites by neighboring TFs could explain the different regulatory modes for one TF motif. Indeed, RelA motifs co-occur with ISREs in polyI:C upregulated RelA peaks (60% compared to 31% of CpG peaks) (Figure 29d). Likewise, 66% of CpG upregulated RelA peaks also contained a c/EBP motif, compared to 33% of polyI:C peaks. The co-occurrence of AP-1 motifs with RelA is quite similar across all groups (57% to 67%) (Figure 29d). These also motif "signatures" correspond to synergistic transcripts. For example, *Ifi44* primarily contains RelA motifs and ISREs in the promoter region and is synergistic for polyI:C to TNFα stimulation (Figure 29e). *Cp* contains RelA and c/EBP motifs and is synergistic for CpG to TNFα (Figure 29f). *Traf2* is synergistic for both conditions and

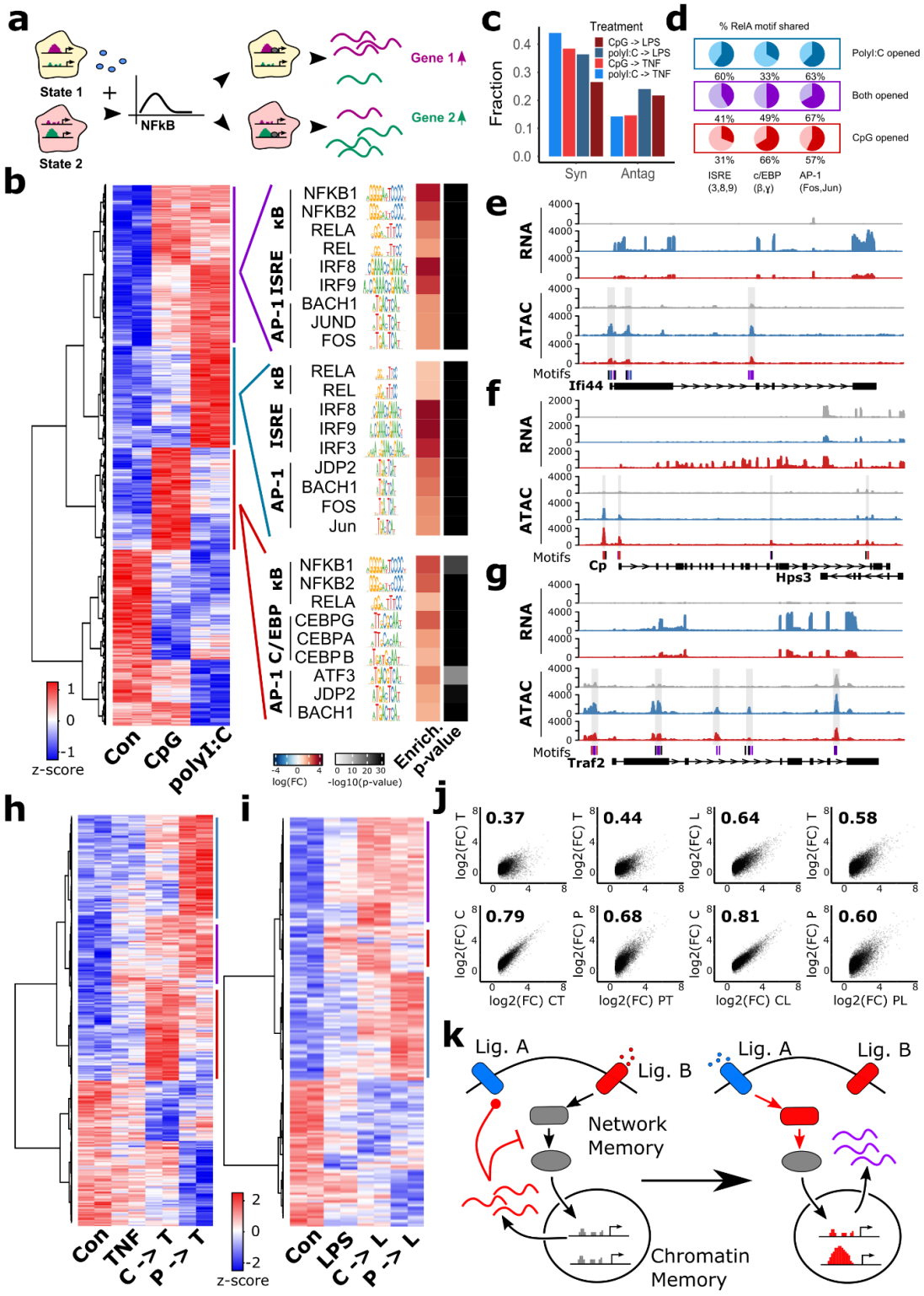

Figure 29. Chromatin accessibility is associated with tolerance- and priming-specific memory effects.

Figure 29, continued

a) Model of how state-dependent chromatin accessibility alters transcriptional output. **b)** Heatmap of differential accessibility following CpG or polyI:C stimulus. Groups clustered using the Ward algorithm. A subset of enriched motifs for each group are shown on the side. **c)** Barplot showing fraction of synergistic or antagonistic transcripts for each treatment condition with increased promoter accessibility following polyI:C or CpG treatment. Increased accessibility after polyI:C or CpG used depending on first stimulus. **d)** Fraction of differentially open RelA peaks (MA0107.1) which share Irf3, 8, and 9 motifs (MA0652.1, MA0653.1, MA1418.1), c/EBP β and γ motifs (MA0838.1, MA0466.1), or Fos and Jun motifs (MA0476.1, MA0488.1) **e-g)** Tracks from RNA-seq (media – grey, P->T – blue, C->T – red) and ATAC-seq (media – grey, polyI:C – blue, CpG – red) for synergistic genes in P->T (e), C->T **(f)**, or both **(g)**. RelA motifs (black), Irf3 and Irf8 motifs (blue), c/EBPγ motifs (red), and Fos motifs (purple) shown below tracks. Called peaks shaded in grey. **h-i)** Differential peak accessibility for TNF, C->T, and P->T **(h)** or LPS, C->L, and P->L **(i)** compared to media control. Groups clustered using the Ward algorithm. **j)** Scatterplots comparing fold-change in accessibility for upregulated regions for C->T, P->T, C->L, and P->L, to the same peaks following indicated conditions. Spearman correlation coefficient for each comparison shown above. **k)** Summary model: Feedback encoded memory in the signaling network and chromatin encoded memory combine to produce transcriptional outcomes.

contains RelA and AP-1 motifs. (Figure 29g). These observations suggest that stimulus-specific tuning of epigenetic accessibility may be due to cooperation between transcription factors.

We then turned to whether stimulus induced changes in chromatin accessibility can be overwritten by subsequent restimulus. We profiled chromatin accessibility of all four polyI:C/CpG to TNFα/LPS memory conditions and identified differentially accessible regions (Figure 29h, i). We identified similar groups as before by clustering, with shared, polyI:C upregulated, and CpG upregulated groups. ISREs were enriched in polyI:C upregulated groups, c/EBP motifs in CpG upregulated groups, and κB and AP-1 motifs were generally enriched (Figure 30c-d). The similarity between treatment with just polyI:C or CpG and the four sequential conditions made us question the importance of the second TNFα/LPS stimulus in chromatin accessibility. We compared the correlation between chromatin accessibility from sequential stimulus to the chromatin landscape from just the initial or the subsequent stimulus (Figure 29k). Correlation between sequential stimuli and the initial CpG/polyI:C chromatin landscape was generally much stronger than correlation with the LPS/TNFα landscape, the only exception being polyI:C to LPS, which correlated equally well to both polyI:C and LPS. We concluded that initial stimulus exposure plays a lasting role in determining chromatin accessibility landscape for a cell and is difficult to overwrite by subsequent stimulus exposure.

Here, we show that stimulus induced chromatin accessibility changes on the timescale of hours can shape memory-dependent transcriptional responses. We identify stimulus specific TF motifs which tune both chromatin accessibility and synergistic transcription. Finally, we show that initial inflammatory exposure produces lasting effects which persist even after re-exposure with another stimulus.

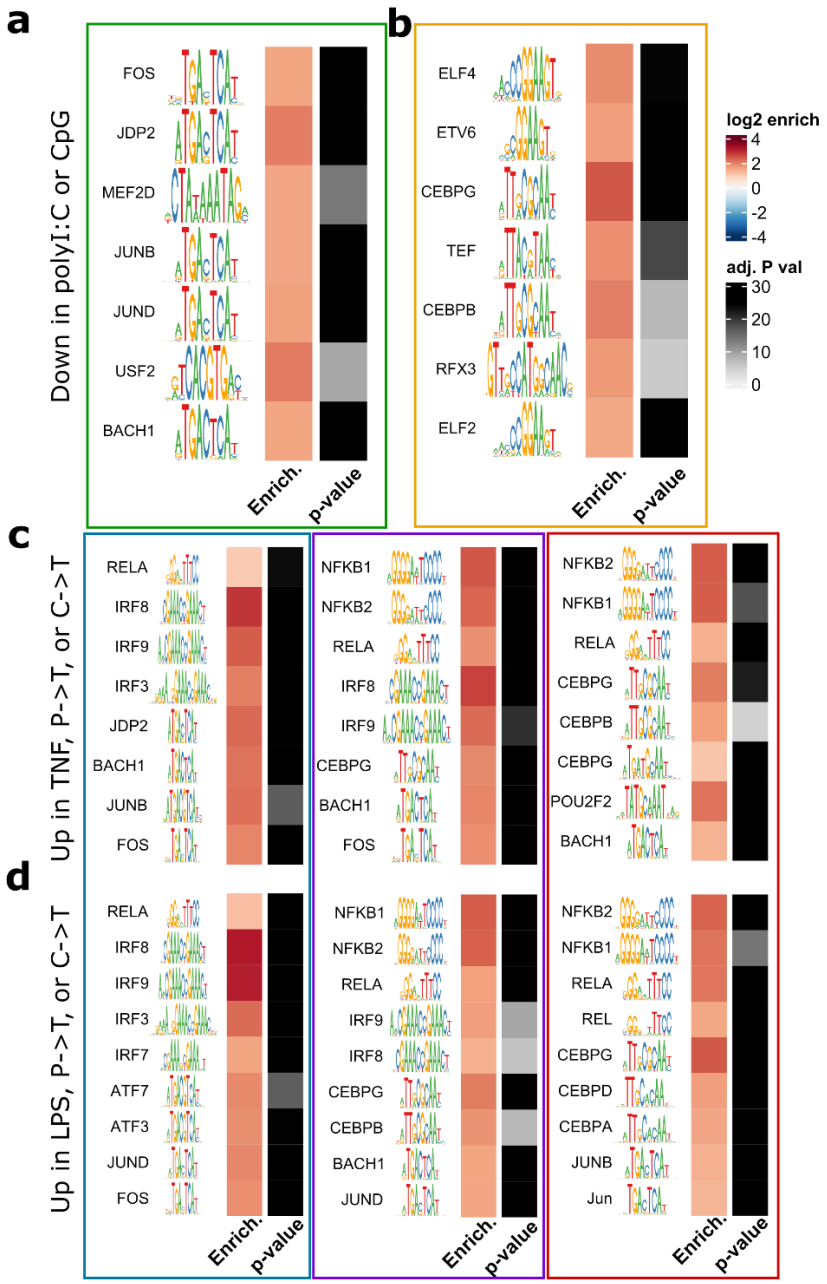

Figure 30. Enriched TF motifs in different groups of differentially regulated chromatin regions.

a-b) Enriched motifs for group 4 (less accessible in both polyI:C and CpG) **(a)** or group 5 (less accessibly in only polyI:C) **(b)** from Figure 29b. **c)** Enriched motifs for group 1 (blue – more accessible in P->T), group 2 (purple – more accessible in both P ->T and C->T), and group 3 (red – more accessible in C -> T) from figure 7h. **d)** Enriched motifs for group 1 (purple – more accessible in both P ->L and C->L), group 2 (red – more accessible in C -> L), and group 3 (blue – more accessible in P->L) from Figure 29i.

DISCUSSION

Overview

The work presented in this thesis systematically profiles signaling memory in the context of NFκB activation dynamics in fibroblasts and macrophages and shows that the NFκB network encodes memory of prior inflammatory stimuli which shapes the cell's response to subsequent stimuli. By combining microfluidic live cell imaging with small molecule inhibition, genetic knockout, cytokine inhibition, and gene expression measurements, this work identifies negative feedback motifs in fibroblasts and macrophages which encode tolerance (Figure 31). Furthermore, we characterize priming on the level of the intracellular NFκB network, showing that, in macrophages, polyI:C can induce priming through increasing the magnitude of NFκB activation dynamics, not just through paracrine secretion or chromatin remodeling. We show that memory can be distinguished on a single cell level through information-theoretic approaches, and that cellular subpopulations with different memory can be predicted by response to prior stimulus. This work connects NFκB dynamics to *in vivo* acute inflammation by showing that adult peritoneal macrophages undergo tolerogenic changes to NFκB dynamics as a result of endotoxemia. Finally, we connect memory encoding through NFκB dynamics to the larger body of literature on memory encoding in chromatin remodeling, showing that gene expression changes arise as a result of the interaction between altered NFκB dynamics and altered chromatin accessibility (Figure 29k). Through these approaches, this thesis proposes new models of memory encoding through changes in the dynamic processing of NFκB activation in two very different cell types and raises the possibility of targeting these memory-induced changes in activation dynamics in new therapeutic interventions.

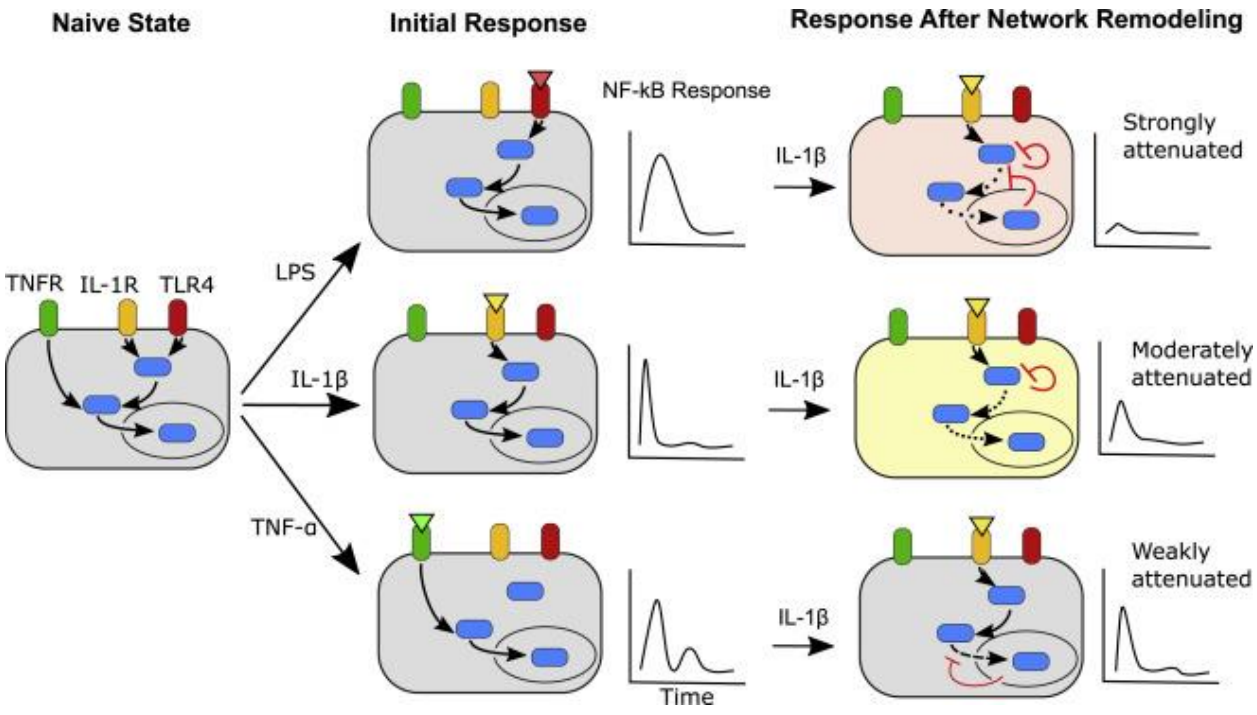

Figure 31. Exposure to inflammatory ligands triggers shared feedbacks to alter subsequent ligand responses

Naive cell (gray) activates in response to different inflammatory ligands, which each induce characteristic feedback responses. LPS (red cell) induces upstream and downstream negative feedback, IL-1β (yellow cell) primarily induces upstream negative feedback, and TNFα induces negative feedback, which primarily acts orthogonally to the other ligands. As a result, response to a subsequent IL-1β stimulus becomes attenuated in a ligand-specific manner and produces memory-informed NFκB responses.

Network-level changes as a model of innate immune memory

Previously, innate immune memory has primarily been studied on the level of cytokine output, gene expression changes, and the changes in epigenetic state which enable these changes[34,37,159]. Our work shows that changes at the level of signal transduction also take place as a result of inflammatory signal-induced memory in both fibroblasts and macrophages. In particular, we show that changes in the dynamics of activation in particular encode crucial information differentiating memory induced by different ligands. This observation adds increased depth to models of innate immune memory, especially at shorter timescales where network level changes are more likely to take place than global changes in chromatin structure[50,74]. Several negative feedbacks have been identified, largely through coarse-grained approaches like knockout, which play a role in tolerance, including IRAK-M, MyD88s, and A20[49]. However, a systems-level approach of how these feedbacks interact with the core NFκB network has been largely lacking. Here, we show that these feedbacks can operate on short timescales to tune the magnitude of tolerance depending on the memory-inducing stimulus. By showing how gene expression can be explained by a mixture of chromatin accessibility changes and dynamic changes in NFκB activity, we show that these changes in dynamics are relevant for gene expression changes as a result of memory and that solely transcription factor dynamics alone or chromatin accessibility alone are insufficient to explain these changes.

There has been great interest in therapeutically manipulating innate immune memory. Modulating tolerance can potentially prevent sepsis-induced immunosuppression[9] or reduce the inflammatory damage during acute infectious and immune crises[152]. Similarly, inducing primed states or trained immunity could increase general resistance to infection[191], while tuning down

facets of these states could also reduce autoimmune or inflammatory disease[52]. The findings from this work present new targets of modulating innate immune memory by showing that key nodes in signaling networks encode that memory. Furthermore, this work shows that a meaningful intermediary readout for innate immune memory can be found in transcription factor activation dynamics, which provide more nuanced information about memory state than total cytokine or gene expression output for a single gene. Targeting signaling network nodes and examining activation dynamics may therefore reveal previously unappreciated ability to manipulate innate immune memory.

Cell type specific encoding of NFκB dynamics and memory

By performing this work in two distinct cell types with different lineages, we are able to compare the extent of conservation in the NFκB regulatory network in different cell types. Our work with fibroblasts primarily finds induction of cross-tolerance for all ligands except TNFα, with the level of overlap explaining node-specific negative feedback effects, *e.g.,* autoinhibition of IRAK1 (Figure 31). In contrast, in macrophages we find that memory effects on LPS and TNFα stimulus are largely the same, with MyD88-dependent ligands inducing tolerance for both and polyI:C inducing priming for both. This suggests that memory encoding in macrophages may potentially operate at a more conserved level of the NFκB network shared by all stimuli, *e.g.,* at the highly conserved IKK or IκB nodes. Cell-type specific differences in regulation of signaling networks have not been profiled in great detail, particularly for cells in non-myeloid or lymphoid lineages[180,192,193]. Our work indicates that NFκB activation, and particularly NFκB-encoded memory, is differentially regulated by cell type, which may also be true in other signaling pathways. A number of negative feedbacks have been annotated which appear to act

primarily in myeloid lineages, but increased attention to signaling in fibroblasts and epithelial cells may be merited. These cell types are increasingly recognized to be active participants in innate immunity, involved in initial pathogen and injury sensing, anti-microbial defenses, recruitment of myeloid and lymphoid cells, and tissue repair[2]. It is unlikely that the signaling network features identified in macrophages are identical for these cells and thus more study of cell-type specific differences in NFκB dynamics is merited.

Furthermore, this work shows that NFκB dynamics, which have largely been reported *in vitro* in immortalized or primary cell culture, also can be changed by memory states *in vivo* through a model of endotoxemia. This finding emphasizes the importance of studying NFκB dynamics in other inflammatory contexts, including acute respiratory disease, colitis, cecal ligation, and *Staphylococcal* skin lesions. Already, researchers have shown that chronic conditions including Sjogren's syndrome[78] and age[179] can change NFκB dynamics in primary macrophages. It is likely that NFκB dynamics play a role in mediating the disease process in these examples of acute inflammation as well.

Particularly of note, however, our observations with peritoneal macrophages to not map perfectly on to our observations with bone-marrow-derived macrophages. While tolerance of subsequent TNFα restimulus was stronger that subsequent LPS restimulus in bone marrow-derived macrophages, peritoneal macrophages were entirely tolerized to subsequent LPS restimulus and only partially tolerized to subsequent TNFα restimulus. Similarly, peritoneal macrophages exhibit "plateau" like activation dynamics following TNFα stimulus, while bone-marrow derived macrophages display more pulse like activation dynamics. This observation raises the intriguing possibility that the NFκB network is wired and regulated differently in

different tissue-specific cell populations. Multiple lineages of both monocyte-derived and tissue-intrinsic macrophages derived from yolk-sac progenitors exist[194]. These different lineages of macrophages also can have different functions in the tissue, with tissue-intrinsic macrophages playing more of a homeostatic function and monocyte-derived populations being recruited in the event of an acute inflammation[3,195]. Furthermore, the level of microbial exposure in different tissue sites is oftentimes quite variable, which suggests that macrophages in those areas likely have different memory states from previous encounters with commensal or pathogenic bacteria[196]. A natural point of further development from this work is an exploration of NFκB dynamics in different tissue-specific macrophage contexts and consequent differences in memory encoding.

Determinism and stochasticity in single cell memory

One of the major advances introduced in this work is the integration of live cell microscopy and non-perturbative microfluidic culture to study memory encoding in individual cells. Previously, innate immune memory had been studied primarily using *in vivo* disease models and bulk measurements of chromatin state, transcriptional output, and cytokine secretion. These studies successfully identified the importance of prior exposure to particular ligands which increase clearance of subsequent infections (e.g. bacillus Calmette-Guerin and β-glucan)[36,39] and others which decreased clearance of subsequent infections (e.g. LPS)[182]. However, innate immune memory has been a topic largely untouched by the single cell revolution in immunology. Despite the recognition that pathogen clearance and immune response on a single cell level is highly heterogeneous and dependent on subpopulations of cells[95,111–113,115], it has been difficult to identify subpopulations of memory-conditioned innate immune cells. A major

challenge in this area has been the difficulty of using non-perturbative readouts to characterize both memory state and subsequent memory-conditioned response for the same cell. Cytokine secretion measurement does not offer the resolution and sequencing based approaches necessitate cell lysis which is incompatible with repeated measurement. As a result, it has been largely unknown what mediates single-cell heterogeneity in memory and whether memory-informed cellular responses could be predicted based on particular features of the cell state.

Live cell imaging of transcription factor dynamics tracks a key metric of cell state without requiring cell lysis and can potentially link cellular response to a memory-inducing stimulus and subsequent memory-conditioned response to restimulus. Microfluidics can provide multiple stimuli while continuously imaging cells. In this work, we show that single cell memory can be predicted by the cell's response to the memory-inducing stimulus. Both for priming and, more strongly, for tolerance, stronger NFκB response to the first stimulus induced greater memory. Information theoretic approaches showed that prior response magnitude encodes information about the memory-conditioned response to restimulus. Using mathematical modeling, we show that heterogeneity in response to the first stimulus can potentially be due to extrinsic noise in regulation of the NFκB| IκBα complex, and that an entirely deterministic model of memory induced by NFκB-specific positive and negative feedback loops can produce dramatically different memory effects with that input of extrinsic noise. While we observe that memory is quite deterministic, with a mutual information between groups reaching up to 0.44 bits, the lack of complete correlation between response to first and second stimulus implies other potential sources of noise. For example, extrinsic noise in other network components or chromatin state could buffer the deterministic relationship between NFκB input and feedback

output. Alternatively, if positive feedback, for example, which is only poorly deterministic, is mediated by a signaling process which is only loosely correlated with NFκB response, *e.g.* signaling through IRFs or MAPKs, NFκB might be a poor proxy for a more deterministic relationship with another signaling intermediary. Nonetheless, this work presents the first model for how innate immune memory can be encoded on a single cell level and predicted by prior response dynamics.

These findings may enable refinement of both approaches to manage inflammation and development of cell-based therapies. By observing that extrinsic noise governs cellular heterogeneity and is observable and predictable, we allow the possibility of targeting desired subpopulations of memory behavior. For example, sepsis-induced immunosuppression may be disadvantageous following resolution of acute septic shock and maintained by a subpopulation of cells with strongly tolerogenic conditioning[9]. Our results suggest that these cells can be identified by their strong induction of negative feedback, and thus may be successfully reprogrammed or eliminated to recover a more "naïve-like" immune response. Therapeutic avenues which are targeted at specific cellular subpopulations based on their memory state may enable increased therapeutic efficacy while reducing undesired or off-target effects. Similarly, deploying immune adjuvants which amplify single-cell memory states related to antigen uptake and presentation may enable effective amplification of vaccine responses without inducing overwhelming inflammation[197]. In these contexts, incorporating single-cell readouts of memory state could be used to identify key subpopulations of immune response to amplify or silence.

Cell-based therapies have also been an area of significant research due to the success of chimeric antigen receptor (CAR) T cell therapy for cancer[198]. Broadly, patient cells are extracted,

programmed to execute desired functions, and infused back into the patient. This research has included *ex vivo* programming of innate immune cells like macrophages and NK cells. However, an increasingly recognized problem with programmed cell therapies is the heterogeneity of cellular responses to programming, with a significant fraction of infused CAR-T cells becoming rapidly exhausted and anergic[199]. Fundamentally, programming of cell states can be considered a cell memory problem where the desired "program" is a memory state induced by prior stimulus[200]. Our work suggests that identification of key markers for priming and tolerance can enable enrichment for subpopulations which are primed for effective function and depletion of populations likely to rapidly exhaust. Thus, our work on encoding of exposure history and inflammatory memory likely can play a role in different approaches to improving therapeutic options and patient health.

Conclusion

Prior to this work, innate immune memory was largely thought to operate on longer timescales through epigenetic means. We used integrated live cell microscopy and microfluidics to profile memory in single cells, showing that durable memory-dependent changes in NFκB activation can take place as soon as two hours after stimulation. We show that single cell memory, although heterogeneous, is deterministic and can be predicted from prior stimulus response. We use a combination of small-molecule inhibition, genetic knockout, mathematical modeling, and transcriptomic profiling to identify NFκB-dependent feedback modules which give rise to deterministic memory. We show that fibroblasts and macrophages encode memory differently, with fibroblasts encoding overlap-dependent tolerance while macrophages can encode both tolerance and priming through a combination of positive and negative feedback. We

link the changes in NFκB dynamics to epigenetic changes and show how these two features combined can explain the ultimate transcriptional changes due to memory. Through this work, we introduce a new model of innate immune memory at short timescales which is primarily mediated through feedback-dependent changes in signaling networks and deterministic at the single cell level.

FUTURE ISSUES

How do single cell memory states identified using NFκB dynamics shape chromatin and transcriptional outputs?

Our work shows that subpopulations of memory responses can be identified based on NFκB activation dynamics to initial stimulus. However, our work linking these dynamics to chromatin and transcriptional changes is all in bulk. Characterization of how these subpopulations of memory-conditioned cells alter their chromatin and RNA states would enable greater insight into how these subpopulations are phenotypically different and reveal markers for potential label-free identification of cells with strong and weak memory states.

How does NFκB integrate with other key nodes of inflammatory signaling?

We focus on NFκB as a central node of inflammatory signaling, however several other key pathways are also active. In our transcriptomic and epigenetic analyses, we show that MAPK, STAT/IRF, and c/EBP signaling likely all play a role in the cellular reprograming due to stimulus memory. Live cell imaging of signaling dynamics across multiple families of signaling would give greater insight into how signaling is mediated through crosstalk and integration.

How do different acute inflammatory states encode inflammatory memory?

This work shows for the first time that pathological endotoxemia induces tolerance at the level of NFκB dynamics in adult macrophages. Other disease states may encode memory differently, including acute infection or autoimmune disease, and are still to be explored.

How does tissue specificity influence macrophage NFκB processing?

We observe distinct differences in dynamic processing between macrophages from the peritoneum and those generated from bone marrow. It is largely unappreciated how these and other tissue locations "train" macrophages according to their location and task. In particular, it may be possible that signaling networks are weighted differently depending on tissue location, which would challenge current conceptions of signal transduction.

REFERENCES

1. Ashley, N. T., Weil, Z. M. & Nelson, R. J. Inflammation: Mechanisms, Costs, and Natural Variation. *Annual Review of Ecology, Evolution, and Systematics* **43**, 385–406 (2012).

2. Nowarski, R., Jackson, R. & Flavell, R. A. The Stromal Intervention: Regulation of Immunity and Inflammation at the Epithelial-Mesenchymal Barrier. *Cell* **168**, 362–375 (2017).

3. Uderhardt, S., Martins, A. J., Tsang, J. S., Lämmermann, T. & Germain, R. N. Resident Macrophages Cloak Tissue Microlesions to Prevent Neutrophil-Driven Inflammatory Damage. *Cell* **177**, 541-555.e17 (2019).

4. Neupane, A. S. *et al.* Patrolling Alveolar Macrophages Conceal Bacteria from the Immune System to Maintain Homeostasis. *Cell* **183**, 110-125.e11 (2020).

5. Arango Duque, G. & Descoteaux, A. Macrophage Cytokines: Involvement in Immunity and Infectious Diseases. *Frontiers in Immunology* **5**, (2014).

6. Shi, C. & Pamer, E. G. Monocyte recruitment during infection and inflammation. *Nat Rev Immunol* **11**, 762–774 (2011).

7. Wong, P. & Pamer, E. G. CD8 T cell responses to infectious pathogens. *Annu Rev Immunol* **21**, 29–70 (2003).

8. Medzhitov, R., Schneider, D. S. & Soares, M. P. Disease Tolerance as a Defense Strategy. *Science* **335**, 936–941 (2012).

9. Delano, M. J. & Ward, P. A. The Immune System's Role in Sepsis Progression, Resolution and Long-Term Outcome. *Immunol Rev* **274**, 330–353 (2016).

10. Chen, L. *et al.* Inflammatory responses and inflammation-associated diseases in organs. *Oncotarget* **9**, 7204–7218 (2017).

11. Ramos-Casals, M., Brito-Zerón, P. & Mariette, X. Systemic and organ-specific immune-related manifestations of COVID-19. *Nat Rev Rheumatol* **17**, 315–332 (2021).

12. Fajgenbaum, D. C. & June, C. H. Cytokine Storm. *New England Journal of Medicine* **383**, 2255–2273 (2020).

13. Takeuchi, O. & Akira, S. Pattern Recognition Receptors and Inflammation. *Cell* **140**, 805–820 (2010).

14. Gong, T., Liu, L., Jiang, W. & Zhou, R. DAMP-sensing receptors in sterile inflammation and inflammatory diseases. *Nat Rev Immunol* **20**, 95–112 (2020).

15. Ozaki, K. & Leonard, W. J. Cytokine and Cytokine Receptor Pleiotropy and Redundancy*. *Journal of Biological Chemistry* **277**, 29355–29358 (2002).

16. Mendoza, J. L. *et al.* Structure of the IFNγ receptor complex guides design of biased agonists. *Nature* **567**, 56–60 (2019).

17. Ring, A. M. *et al.* Mechanistic and structural insight into the functional dichotomy between interleukin-2 and interleukin-15. *Nat Immunol* **13**, 1187–1195 (2012).

18. Fitzgerald, K. A. & Kagan, J. C. Toll-like Receptors and the Control of Immunity. *Cell* **180**, 1044–1066 (2020).

19. Tan, Y. & Kagan, J. C. Innate Immune Signaling Organelles Display Natural and Programmable Signaling Flexibility. *Cell* (2019) doi:10.1016/j.cell.2019.01.039.

20. Luecke, S., Sheu, K. M. & Hoffmann, A. Stimulus-specific responses in innate immunity: Multilayered regulatory circuits. *Immunity* **54**, 1915–1932 (2021).

21. Glass, C. K. & Natoli, G. Molecular control of activation and priming in macrophages. *Nat Immunol* **17**, 26–33 (2015).

22. Oeckinghaus, A. & Ghosh, S. The NF-κB Family of Transcription Factors and Its Regulation. *Cold Spring Harb Perspect Biol* **1**, a000034 (2009).

23. Hess, J., Angel, P. & Schorpp-Kistner, M. AP-1 subunits: quarrel and harmony among siblings. *Journal of Cell Science* **117**, 5965–5973 (2004).

24. Sego, T. J. *et al.* A modular framework for multiscale, multicellular, spatiotemporal modeling of acute primary viral infection and immune response in epithelial tissues and its application to drug therapy timing and effectiveness. *PLoS Comput Biol* **16**, e1008451 (2020).

25. Hackett, T.-L., Holloway, R., Holgate, S. T. & Warner, J. A. Dynamics of pro-inflammatory and anti-inflammatory cytokine release during zcute inflammation in chronic obstructive pulmonary disease: an ex vivo study. *Respir Res* **9**, 47 (2008).

26. Weavers, H. *et al.* Systems Analysis of the Dynamic Inflammatory Response to Tissue Damage Reveals Spatiotemporal Properties of the Wound Attractant Gradient. *Curr Biol* **26**, 1975–1989 (2016).

27. Kiers, D. *et al.* Characterization of a model of systemic inflammation in humans in vivo elicited by continuous infusion of endotoxin. *Sci Rep* **7**, 40149 (2017).

28. Mera, S. *et al.* Multiplex cytokine profiling in patients with sepsis. *APMIS* **119**, 155–163 (2011).

29. Rouhani, S. J. *et al. Severe COVID-19 infection is associated with aberrant cytokine production by infected lung epithelial cells rather than by systemic immune dysfunction*. 2021.12.09.21266492 https://www.medrxiv.org/content/10.1101/2021.12.09.21266492v1 (2021) doi:10.1101/2021.12.09.21266492.

30. Divangahi, M. *et al.* Trained immunity, tolerance, priming and differentiation: distinct immunological processes. *Nature Immunology* **22**, 2–6 (2021).

31. West, M. A. & Heagy, W. Endotoxin tolerance: A review. *Critical Care Medicine* **30**, S64 (2002).

32. López-Collazo, E. & del Fresno, C. Pathophysiology of endotoxin tolerance: mechanisms and clinical consequences. *Crit Care* **17**, 242 (2013).

33. Seeley, J. J. & Ghosh, S. Molecular mechanisms of innate memory and tolerance to LPS. *Journal of Leukocyte Biology* **101**, 107–119 (2017).

34. Foster, S. L., Hargreaves, D. C. & Medzhitov, R. Gene-specific control of inflammation by TLR-induced chromatin modifications. *Nature* **447**, 972–978 (2007).

35. Gourbal, B. *et al.* Innate immune memory: An evolutionary perspective. *Immunological Reviews* **283**, 21–40 (2018).

36. Quintin, J. *et al.* Candida albicans infection affords protection against reinfection via functional reprogramming of monocytes. *Cell Host Microbe* **12**, 223–232 (2012).

37. Saeed, S. *et al.* Epigenetic programming of monocyte-to-macrophage differentiation and trained innate immunity. *Science* **345**, 1251086 (2014).

38. Netea, M. G. *et al.* Defining trained immunity and its role in health and disease. *Nature Reviews Immunology* **20**, 375–388 (2020).

39. van 't Wout, J. W., Poell, R. & van Furth, R. The role of BCG/PPD-activated macrophages in resistance against systemic candidiasis in mice. *Scand J Immunol* **36**, 713–719 (1992).

40. Benn, C. S., Netea, M. G., Selin, L. K. & Aaby, P. A small jab - a big effect: nonspecific immunomodulation by vaccines. *Trends Immunol* **34**, 431–439 (2013).

41. Sun, S. & Barreiro, L. B. The epigenetic encoded memory of the innate immune system. *Curr Opin Immunol* **65**, 7–13 (2020).

42. Seeley, J. J. *et al.* Induction of innate immune memory via microRNA targeting of chromatin remodelling factors. *Nature* **559**, 114–119 (2018).

43. Novakovic, B. *et al.* β-Glucan Reverses the Epigenetic State of LPS-Induced Immunological Tolerance. *Cell* **167**, 1354-1368.e14 (2016).

44. Janssens, S., Burns, K., Vercammen, E., Tschopp, J. & Beyaert, R. MyD88S, a splice variant of MyD88, differentially modulates NF-κB- and AP-1-dependent gene expression. *FEBS Letters* **548**, 103–107 (2003).

45. Nahid, M. A., Satoh, M. & Chan, E. K. L. Interleukin 1β-Responsive MicroRNA-146a Is Critical for the Cytokine-Induced Tolerance and Cross-Tolerance to Toll-Like Receptor Ligands. *J Innate Immun* **7**, 428–440 (2015).

46. Sun, X. *et al.* Inhibition of microRNA-155 modulates endotoxin tolerance by upregulating suppressor of cytokine signaling 1 in microglia. *Exp Ther Med* **15**, 4709–4716 (2018).

47. O'Connell, R. M., Chaudhuri, A. A., Rao, D. S. & Baltimore, D. Inositol phosphatase SHIP1 is a primary target of miR-155. *Proc Natl Acad Sci U S A* **106**, 7113–7118 (2009).

48. Flores-Concha, M. & Oñate, Á. A. Long Non-coding RNAs in the Regulation of the Immune Response and Trained Immunity. *Front Genet* **11**, 718 (2020).

49. Renner, F. & Schmitz, M. L. Autoregulatory feedback loops terminating the NF-κB response. *Trends in Biochemical Sciences* **34**, 128–135 (2009).

50. Cheng, Q. J. *et al.* NF-κB dynamics determine the stimulus specificity of epigenomic reprogramming in macrophages. *Science* **372**, 1349–1353 (2021).

51. Mira, J. C. *et al.* Sepsis Pathophysiology, Chronic Critical Illness and PICS. *Crit Care Med* **45**, 253–262 (2017).

52. Arts, R. J. W., Joosten, L. A. B. & Netea, M. G. The Potential Role of Trained Immunity in Autoimmune and Autoinflammatory Disorders. *Front Immunol* **9**, 298 (2018).

53. Funes, S. C., Rios, M., Fernández-Fierro, A., Di Genaro, M. S. & Kalergis, A. M. Trained Immunity Contribution to Autoimmune and Inflammatory Disorders. *Front Immunol* **13**, 868343 (2022).

54. Brignall, R., Moody, A. T., Mathew, S. & Gaudet, S. Considering Abundance, Affinity, and Binding Site Availability in the NF-κB Target Selection Puzzle. *Front Immunol* **10**, 609 (2019).

55. Sun, S.-C. The non-canonical NF-κB pathway in immunity and inflammation. *Nat Rev Immunol* **17**, 545–558 (2017).

56. Chen, X. *et al.* RelB Sustains IκBα Expression during Endotoxin Tolerance. *Clin. Vaccine Immunol.* **16**, 104–110 (2009).

57. Wajant, H. & Scheurich, P. TNFR1-induced activation of the classical NF-κB pathway. *The FEBS Journal* **278**, 862–876 (2011).

58. Cohen, P. The TLR and IL-1 signalling network at a glance. *J Cell Sci* **127**, 2383–2390 (2014).

59. McGeachy, M. J., Cua, D. J. & Gaffen, S. L. The IL-17 family of cytokines in health and disease. *Immunity* **50**, 892–906 (2019).

60. Silke, J., Rickard, J. A. & Gerlic, M. The diverse role of RIP kinases in necroptosis and inflammation. *Nat Immunol* **16**, 689–697 (2015).

61. Ruland, J. & Hartjes, L. CARD–BCL-10–MALT1 signalling in protective and pathological immunity. *Nat Rev Immunol* **19**, 118–134 (2019).

62. Delhase, M., Hayakawa, M., Chen, Y. & Karin, M. Positive and negative regulation of IkappaB kinase activity through IKKbeta subunit phosphorylation. *Science* **284**, 309–313 (1999).

63. Behar, M. & Hoffmann, A. Tunable Signal Processing through a Kinase Control Cycle: the IKK Signaling Node. *Biophys J* **105**, 231–241 (2013).

64. Roff, M. *et al.* Role of IkBα Ubiquitination in Signal-induced Activation of NF-kB in Vivo(∗). *Journal of Biological Chemistry* **271**, 7844–7850 (1996).

65. Liu, T., Zhang, L., Joo, D. & Sun, S.-C. NF-κB signaling in inflammation. *Signal Transduct Target Ther* **2**, 17023 (2017).

66. Lenardo, M., Pierce, J. W. & Baltimore, D. Protein-Binding Sites in Ig Gene Enhancers Determine Transcriptional Activity and Inducibility. *Science* **236**, 1573–1577 (1987).

67. Sen, R. & Baltimore, D. Multiple nuclear factors interact with the immunoglobulin enhancer sequences. *Cell* **46**, 705–716 (1986).

68. Wong, D. *et al.* Extensive characterization of NF-κB binding uncovers non-canonical motifs and advances the interpretation of genetic functional traits. *Genome Biol* **12**, R70 (2011).

69. Siggers, T. *et al.* Principles of dimer-specific gene regulation revealed by a comprehensive characterization of NF-κB family DNA binding. *Nat Immunol* **13**, 95–102 (2011).

70. Nowak, D. E. *et al.* RelA Ser276 phosphorylation is required for activation of a subset of NF-kappaB-dependent genes by recruiting cyclin-dependent kinase 9/cyclin T1 complexes. *Mol Cell Biol* **28**, 3623–3638 (2008).

71. Yeung, F. *et al.* Modulation of NF-κB-dependent transcription and cell survival by the SIRT1 deacetylase. *EMBO J* **23**, 2369–2380 (2004).
72. Hoffmann, A., Levchenko, A., Scott, M. L. & Baltimore, D. The IkappaB-NF-kappaB signaling module: temporal control and selective gene activation. *Science* **298**, 1241–1245 (2002).

73. Nelson, D. E. *et al.* Oscillations in NF-kappaB signaling control the dynamics of gene expression. *Science* **306**, 704–708 (2004).

74. Sen, S., Cheng, Z., Sheu, K. M., Chen, Y. H. & Hoffmann, A. Gene Regulatory Strategies that Decode the Duration of NFκB Dynamics Contribute to LPS- versus TNF-Specific Gene Expression. *Cell Systems* **10**, 169-182.e5 (2020).

75. Purvis, J. E. *et al.* p53 dynamics control cell fate. *Science* **336**, 1440–1444 (2012).

76. Shankaran, H. *et al.* Rapid and sustained nuclear–cytoplasmic ERK oscillations induced by epidermal growth factor. *Mol Syst Biol* **5**, 332 (2009).

77. Shimojo, H., Ohtsuka, T. & Kageyama, R. Oscillations in Notch Signaling Regulate Maintenance of Neural Progenitors. *Neuron* **58**, 52–64 (2008).

78. Adelaja, A. *et al.* Six distinct NFκB signaling codons convey discrete information to distinguish stimuli and enable appropriate macrophage responses. *Immunity* **54**, 916-930.e7 (2021).

79. Yamamoto, M. *et al.* Role of adaptor TRIF in the MyD88-independent toll-like receptor signaling pathway. *Science* **301**, 640–643 (2003).

80. Zanoni, I. *et al.* CD14 controls the LPS-induced endocytosis of Toll-like Receptor 4. *Cell* **147**, 868–880 (2011).

81. Kondo, T., Kawai, T. & Akira, S. Dissecting negative regulation of Toll-like receptor signaling. *Trends in Immunology* **33**, 449–458 (2012).

82. Trompouki, E. *et al.* CYLD is a deubiquitinating enzyme that negatively regulates NF-κB activation by TNFR family members. *Nature* **424**, 793–796 (2003).

83. Shembade, N., Ma, A. & Harhaj, E. W. Inhibition of NF-κB Signaling by A20 Through Disruption of Ubiquitin Enzyme Complexes. *Science* **327**, 1135–1139 (2010).

84. DeFelice, M. M. *et al.* NF-κB signaling dynamics is controlled by a dose-sensing autoregulatory loop. *Sci. Signal.* **12**, eaau3568 (2019).

85. Witt, J. *et al.* Mechanism of PP2A-mediated IKKβ dephosphorylation: a systems biological approach. *BMC Syst Biol* **3**, 71 (2009).

86. Werner, S. L., Barken, D. & Hoffmann, A. Stimulus Specificity of Gene Expression Programs Determined by Temporal Control of IKK Activity. *Science* **309**, 1857–1861 (2005).

87. Kobayashi, K. *et al.* IRAK-M Is a Negative Regulator of Toll-like Receptor Signaling. *Cell* **110**, 191–202 (2002).

88. Wertz, I. E. *et al.* De-ubiquitination and ubiquitin ligase domains of A20 downregulate NF-κB signalling. *Nature* **430**, 694–699 (2004).

89. Kearns, J. D., Basak, S., Werner, S. L., Huang, C. S. & Hoffmann, A. IkappaBepsilon provides negative feedback to control NF-kappaB oscillations, signaling dynamics, and inflammatory gene expression. *J Cell Biol* **173**, 659–664 (2006).

90. Werner, S. L. *et al.* Encoding NF-κB temporal control in response to TNF: distinct roles for the negative regulators IκBα and A20. *Genes Dev* **22**, 2093–2101 (2008).

91. Shih, V. F.-S. *et al.* Kinetic control of negative feedback regulators of NF-κB/RelA determines their pathogen- and cytokine-receptor signaling specificity. *Proc Natl Acad Sci U S A* **106**, 9619–9624 (2009).

92. Wang, P., Wu, P., Siegel, M. I., Egan, R. W. & Billah, M. M. Interleukin (IL)-10 Inhibits Nuclear Factor κB (NFκB) Activation in Human Monocytes: IL-10 AND IL-4 SUPPRESS CYTOKINE SYNTHESIS BY DIFFERENT MECHANISMS (∗). *Journal of Biological Chemistry* **270**, 9558–9563 (1995).

93. Dorrington, M. G. & Fraser, I. D. C. NF-κB Signaling in Macrophages: Dynamics, Crosstalk, and Signal Integration. *Front Immunol* **10**, 705 (2019).

94. Lee, T. K. *et al.* A Noisy Paracrine Signal Determines the Cellular NF-κB Response to Lipopolysaccharide. *Sci Signal* **2**, ra65 (2009).

95. Xue, Q. *et al.* Analysis of single-cell cytokine secretion reveals a role for paracrine signaling in coordinating macrophage responses to TLR4 stimulation. *Sci Signal* **8**, ra59 (2015).

96. Sung, M.-H. *et al.* Switching of the Relative Dominance between Feedback Mechanisms in Lipopolysaccharide-Induced NF-κB Signaling. *Sci Signal* **7**, ra6 (2014).

97. Oh, K.-S. *et al.* Dual roles for Ikaros in regulation of macrophage chromatin state and inflammatory gene expression. *J Immunol* **201**, 757–771 (2018).

98. Litvak, V. *et al.* Role of the transcription factor C/EBPδ in a regulatory circuit that discriminates between transient and persistent Toll-like receptor 4-induced signals. *Nat Immunol* **10**, 437–443 (2009).

99. Adamson, A. *et al.* Signal transduction controls heterogeneous NF-κB dynamics and target gene expression through cytokine-specific refractory states. *Nat Commun* **7**, (2016).

100. Krishna, S., Jensen, M. H. & Sneppen, K. Minimal model of spiky oscillations in NF-κB signaling. *PNAS* **103**, 10840–10845 (2006).

101. Tay, S. *et al.* Single-cell NF-κB dynamics reveal digital activation and analog information processing in cells. *Nature* **466**, 267–271 (2010).

102. Son, M. *et al.* NF-κB responds to absolute differences in cytokine concentrations. *Sci. Signal.* **14**, (2021).

103. Alon, U. *An Introduction to Systems Biology: Design Principles of Biological Circuits*. (Chapman and Hall/CRC, 2006).

104. O'Dea, E. L. *et al.* A homeostatic model of IκB metabolism to control constitutive NF-κB activity. *Mol Syst Biol* **3**, 111 (2007).

105. Lipniacki, T., Paszek, P., Brasier, A. R. A. R., Luxon, B. & Kimmel, M. Mathematical model of NF-kappaB regulatory module. *J Theor Biol* **228**, 195–215 (2004).

106. Pękalski, J. *et al.* Spontaneous NF-κB activation by autocrine TNFα signaling: a computational analysis. *PLoS One* **8**, e78887 (2013).

107. Maity, A. & Wollman, R. Information transmission from NFkB signaling dynamics to gene expression. *PLOS Computational Biology* **16**, e1008011 (2020).

108. Longo, D. M. *et al.* Dual delayed feedback provides sensitivity and robustness to the NF-κB signaling module. *PLoS Comput Biol* **9**, e1003112 (2013).

109. Kellogg, R. A. & Tay, S. Noise Facilitates Transcriptional Control under Dynamic Inputs. *Cell* **160**, 381–392 (2015).

110. Schulte, M. B. & Andino, R. Single-Cell Analysis Uncovers Extensive Biological Noise in Poliovirus Replication. *J Virol* **88**, 6205–6212 (2014).

111. Drayman, N., Patel, P., Vistain, L. & Tay, S. HSV-1 single-cell analysis reveals the activation of anti-viral and developmental programs in distinct sub-populations. *eLife* **8**, e46339 (2019).

112. Avraham, R. *et al.* Pathogen Cell-to-Cell Variability Drives Heterogeneity in Host Immune Responses. *Cell* **162**, 1309–1321 (2015).

113. Avital, G. *et al.* The tempo and mode of gene regulatory programs during bacterial infection. *Cell Reports* **41**, 111477 (2022).

114. Lane, K., Andres-Terre, M., Kudo, T., Monack, D. M. & Covert, M. W. Escalating Threat Levels of Bacterial Infection Can Be Discriminated by Distinct MAPK and NF-κB Signaling Dynamics in Single Host Cells. *Cell Systems* **8**, 183-196.e4 (2019).

115. Shalek, A. K. *et al.* Single-cell RNA-seq reveals dynamic paracrine control of cellular variation. *Nature* **510**, 363–369 (2014).

116. Son, M. *et al.* Spatiotemporal NF-κB dynamics encodes the position, amplitude, and duration of local immune inputs. *Science Advances* **8**, (2022).

117. Son, M., Wang, A. G., Kenna, E. & Tay, S. High-throughput co-culture system for analysis of spatiotemporal cell-cell signaling. *Biosensors and Bioelectronics* **225**, 115089 (2023).

118. Laviron, M. *et al.* Tumor-associated macrophage heterogeneity is driven by tissue territories in breast cancer. *Cell Rep* **39**, 110865 (2022).

119. Li, S. *et al.* Metabolism drives macrophage heterogeneity in the tumor microenvironment. *Cell Rep* **39**, 110609 (2022).

120. Bagowski, C. P. & Ferrell, J. E. Bistability in the JNK cascade. *Curr Biol* **11**, 1176–1182 (2001).

121. Muzzey, D., Gómez-Uribe, C. A., Mettetal, J. T. & van Oudenaarden, A. A systems-level analysis of perfect adaptation in yeast osmoregulation. *Cell* **138**, 160–171 (2009).

122. Elowitz, M. B., Levine, A. J., Siggia, E. D. & Swain, P. S. Stochastic Gene Expression in a Single Cell. *Science* **297**, 1183–1186 (2002).

123. Patel, P., Drayman, N., Liu, P., Bilgic, M. & Tay, S. Computer vision reveals hidden variables underlying NF-κB activation in single cells. *Science Advances* **7**, eabg4135 (2021).

124. Kellogg, R. A., Gómez-Sjöberg, R., Leyrat, A. A. & Tay, S. High-throughput microfluidic single-cell analysis pipeline for studies of signaling dynamics. *Nat Protoc* **9**, 1713–1726 (2014).

125. Vistain, L. *et al.* Quantification of extracellular proteins, protein complexes and mRNAs in single cells by proximity sequencing. *Nat Methods* **19**, 1578–1589 (2022).

126. Picelli, S. *et al.* Full-length RNA-seq from single cells using Smart-seq2. *Nat Protoc* **9**, 171–181 (2014).

127. Kudo, T. *et al.* Live-cell measurements of kinase activity in single cells using translocation reporters. *Nature Protocols* **13**, 155–169 (2018).

128. Jetka, T., Nienałtowski, K., Winarski, T., Błoński, S. & Komorowski, M. Information-theoretic analysis of multivariate single-cell signaling responses. *PLOS Computational Biology* **15**, e1007132 (2019).

129. Selimkhanov, J. *et al.* Accurate information transmission through dynamic biochemical signaling networks. *Science* **346**, 1370–1373 (2014).

130. Shannon, C. E. A Mathematical Theory of Communication. *Bell System Technical Journal* **27**, 379–423 (1948).

131. Rice, N. R. & Ernst, M. K. In vivo control of NF-kappa B activation by I kappa B alpha. *EMBO J* **12**, 4685–4695 (1993).

132. Boone, D. L. *et al.* The ubiquitin-modifying enzyme A20 is required for termination of Toll-like receptor responses. *Nat Immunol* **5**, 1052–1060 (2004).

133. Swanson, J. A., Lee, M. & Knapp, P. E. Cellular dimensions affecting the nucleocytoplasmic volume ratio. *Journal of Cell Biology* **115**, 941–948 (1991).

134. Phelps, C. B., Sengchanthalangsy, L. L., Malek, S. & Ghosh, G. Mechanism of κB DNA binding by Rel/NF-κB dimers *. *Journal of Biological Chemistry* **275**, 24392–24399 (2000).

135. Schwanhäusser, B. *et al.* Global quantification of mammalian gene expression control. *Nature* **473**, 337–342 (2011).

136. Hayden, M. S. & Ghosh, S. NF-κB, the first quarter-century: remarkable progress and outstanding questions. *Genes Dev* **26**, 203–234 (2012).

137. Kawasaki, T. & Kawai, T. Toll-Like Receptor Signaling Pathways. *Front. Immunol.* **0**, (2014).

138. Dobin, A. *et al.* STAR: ultrafast universal RNA-seq aligner. *Bioinformatics* **29**, 15–21 (2013).

139. Liao, Y., Smyth, G. K. & Shi, W. featureCounts: an efficient general purpose program for assigning sequence reads to genomic features. *Bioinformatics* **30**, 923–930 (2014).

140. Robinson, M. D., McCarthy, D. J. & Smyth, G. K. edgeR: a Bioconductor package for differential expression analysis of digital gene expression data. *Bioinformatics* **26**, 139–140 (2010).

141. Ritchie, M. E. *et al.* limma powers differential expression analyses for RNA-sequencing and microarray studies. *Nucleic Acids Research* **43**, e47 (2015).

142. Luo, W. & Brouwer, C. Pathview: an R/Bioconductor package for pathway-based data integration and visualization. *Bioinformatics* **29**, 1830–1831 (2013).

143. Raudvere, U. *et al.* g:Profiler: a web server for functional enrichment analysis and conversions of gene lists (2019 update). *Nucleic Acids Research* **47**, W191–W198 (2019).

144. Keenan, A. B. *et al.* ChEA3: transcription factor enrichment analysis by orthogonal omics integration. *Nucleic Acids Res* **47**, W212–W224 (2019).

145. Zhang, Y. *et al.* Model-based Analysis of ChIP-Seq (MACS). *Genome Biology* **9**, R137 (2008).

146. Corces, M. R. *et al.* The chromatin accessibility landscape of primary human cancers. *Science* **362**, eaav1898 (2018).

147. Yu, G., Wang, L.-G. & He, Q.-Y. ChIPseeker: an R/Bioconductor package for ChIP peak annotation, comparison and visualization. *Bioinformatics* **31**, 2382–2383 (2015).

148. Castro-Mondragon, J. A. *et al.* JASPAR 2022: the 9th release of the open-access database of transcription factor binding profiles. *Nucleic Acids Research* **50**, D165–D173 (2022).

149. Machlab, D. *et al.* monaLisa: an R/Bioconductor package for identifying regulatory motifs. *Bioinformatics* **38**, 2624–2625 (2022).

150. Lawrence, M., Gentleman, R. & Carey, V. rtracklayer: an R package for interfacing with genome browsers. *Bioinformatics* **25**, 1841–1842 (2009).

151. Rao, P. *et al.* IkappaBbeta acts to inhibit and activate gene expression during the inflammatory response. *Nature* **466**, 1115–1119 (2010).

152. Luan, H. H. *et al.* GDF15 Is an Inflammation-Induced Central Mediator of Tissue Tolerance. *Cell* **178**, 1231-1244.e11 (2019).

153. Deng, H., Maitra, U., Morris, M. & Li, L. Molecular Mechanism Responsible for the Priming of Macrophage Activation. *J Biol Chem* **288**, 3897–3906 (2013).

154. Heremans, H., Van Damme, J., Dillen, C., Dijkmans, R. & Billiau, A. Interferon gamma, a mediator of lethal lipopolysaccharide-induced Shwartzman-like shock reactions in mice. *J Exp Med* **171**, 1853–1869 (1990).

155. Pulendran, B., S. Arunachalam, P. & O'Hagan, D. T. Emerging concepts in the science of vaccine adjuvants. *Nat Rev Drug Discov* **20**, 454–475 (2021).

156. Lérias, J. R. *et al.* Trained Immunity for Personalized Cancer Immunotherapy: Current Knowledge and Future Opportunities. *Front. Microbiol.* **0**, (2020).

157. Kellogg, R. A., Tian, C., Etzrodt, M. & Tay, S. Cellular Decision Making by Non-Integrative Processing of TLR Inputs. *Cell Reports* **19**, 125–135 (2017).

158. Ifrim, D. C. *et al.* Trained Immunity or Tolerance: Opposing Functional Programs Induced in Human Monocytes after Engagement of Various Pattern Recognition Receptors. *Clin. Vaccine Immunol.* **21**, 534–545 (2014).

159. Butcher, S. K., O'Carroll, C. E., Wells, C. A. & Carmody, R. J. Toll-Like Receptors Drive Specific Patterns of Tolerance and Training on Restimulation of Macrophages. *Front Immunol* **9**, (2018).

160. Lawrence, T. The Nuclear Factor NF-κB Pathway in Inflammation. *Cold Spring Harb Perspect Biol* **1**, a001651 (2009).

161. Ashall, L. *et al.* Pulsatile stimulation determines timing and specificity of NF-kappa B-dependent transcription. *Science* **324**, 242–246 (2009).

162. Newman, J. R. S. *et al.* Single-cell proteomic analysis of S. cerevisiae reveals the architecture of biological noise. *Nature* **441**, 840–846 (2006).

163. Taniguchi, Y. *et al.* Quantifying E. coli proteome and transcriptome with single-molecule sensitivity in single cells. *Science* **329**, 533–538 (2010).

164. Cheong, R., Rhee, A., Wang, C. J., Nemenman, I. & Levchenko, A. Information transduction capacity of noisy biochemical signaling networks. *Science* **334**, 354–358 (2011).

165. Tudelska, K. *et al.* Information processing in the NF-κB pathway. *Sci Rep* **7**, 15926 (2017).

166. Simpson, M. L. *et al.* Noise in biological circuits. *WIREs Nanomedicine and Nanobiotechnology* **1**, 214–225 (2009).

167. Fitzgerald, K. A. *et al.* LPS-TLR4 Signaling to IRF-3/7 and NF-κB Involves the Toll Adapters TRAM and TRIF. *J Exp Med* **198**, 1043–1055 (2003).

168. Yemelyanov, A. *et al.* Effects of IKK inhibitor PS1145 on NF-κB function, proliferation, apoptosis and invasion activity in prostate carcinoma cells. *Oncogene* **25**, 387–398 (2006).

169. Widmer, U., Manogue, K. R., Cerami, A. & Sherry, B. Genomic cloning and promoter analysis of macrophage inflammatory protein (MIP)-2, MIP-1 alpha, and MIP-1 beta, members of the chemokine superfamily of proinflammatory cytokines. *J Immunol* **150**, 4996–5012 (1993).

170. Nishizawa, M. & Nagata, S. Regulatory elements responsible for inducible expression of the granulocyte colony-stimulating factor gene in macrophages. *Mol Cell Biol* **10**, 2002–2011 (1990).

171. Bunting, K. *et al.* Genome-wide analysis of gene expression in T cells to identify targets of the NF-kappa B transcription factor c-Rel. *J Immunol* **178**, 7097–7109 (2007).

172. Kumar, R., Clermont, G., Vodovotz, Y. & Chow, C. C. The dynamics of acute inflammation. *Journal of Theoretical Biology* **230**, 145–155 (2004).

173. Zhang, Q. & Cao, X. Epigenetic Remodeling in Innate Immunity and Inflammation. *Annual Review of Immunology* **39**, 279–311 (2021).

174. Franken, L., Schiwon, M. & Kurts, C. Macrophages: sentinels and regulators of the immune system. *Cellular Microbiology* **18**, 475–487 (2016).

175. Hirohashi, N. & Morrison, D. C. Low-dose lipopolysaccharide (LPS) pretreatment of mouse macrophages modulates LPS-dependent interleukin-6 production in vitro. *Infect Immun* **64**, 1011–1015 (1996).

176. Maitra, U., Gan, L., Chang, S. & Li, L. Low-Dose Endotoxin Induces Inflammation by Selectively Removing Nuclear Receptors and Activating CCAAT/Enhancer-Binding Protein δ. *The Journal of Immunology* **186**, 4467–4473 (2011).

177. Fu, Y. *et al.* Network Topologies and Dynamics Leading to Endotoxin Tolerance and Priming in Innate Immune Cells. *PLOS Computational Biology* **8**, e1002526 (2012).

178. Kellogg, R. A., Tian, C., Lipniacki, T., Quake, S. R. & Tay, S. Digital signaling decouples activation probability and population heterogeneity. *eLife* **4**, e08931 (2015).

179. Rahman, S. M. T. *et al.* Double knockin mice show NF-κB trajectories in immune signaling and aging. *Cell Rep* **41**, 111682 (2022).

180. Kull, T. *et al.* NfκB signaling dynamics and their target genes differ between mouse blood cell types and induce distinct cell behavior. *Blood* **140**, 99–111 (2022).

181. Nakagawa, R. *et al.* SOCS-1 Participates in Negative Regulation of LPS Responses. *Immunity* **17**, 677–687 (2002).

182. Hotchkiss, R. S., Monneret, G. & Payen, D. Immunosuppression in sepsis: a novel understanding of the disorder and a new therapeutic approach. *Lancet Infect Dis* **13**, 260–268 (2013).

183. Shao, X. *et al.* CellTalkDB: a manually curated database of ligand–receptor interactions in humans and mice. *Briefings in Bioinformatics* **22**, bbaa269 (2021).

184. Junkin, M. *et al.* High-Content Quantification of Single-Cell Immune Dynamics. *Cell Rep* **15**, 411–422 (2016).

185. Savinova, O. V., Hoffmann, A. & Ghosh, G. The Nfkb1 and Nfkb2 Proteins p105 and p100 Function as the Core of High-Molecular-Weight Heterogeneous Complexes. *Mol Cell* **34**, 591–602 (2009).

186. van ‘t Veer, C. *et al.* Induction of IRAK-M Is Associated with Lipopolysaccharide Tolerance in a Human Endotoxemia Model. *The Journal of Immunology* **179**, 7110–7120 (2007).

187. Mahoney, D. J. *et al.* Both cIAP1 and cIAP2 regulate TNFα-mediated NF-κB activation. *Proc Natl Acad Sci U S A* **105**, 11778–11783 (2008).

188. Friedman, N., Cai, L. & Xie, X. S. Linking Stochastic Dynamics to Population Distribution: An Analytical Framework of Gene Expression. *Phys. Rev. Lett.* **97**, 168302 (2006).

189. Tong, A.-J. *et al.* A Stringent Systems Approach Uncovers Gene-Specific Mechanisms Regulating Inflammation. *Cell* **165**, 165–179 (2016).

190. Huber, R., Pietsch, D., Panterodt, T. & Brand, K. Regulation of C/EBPβ and resulting functions in cells of the monocytic lineage. *Cellular Signalling* **24**, 1287–1296 (2012).

191. Mulder, W. J. M., Ochando, J., Joosten, L. A. B., Fayad, Z. A. & Netea, M. G. Therapeutic targeting of trained immunity. *Nat Rev Drug Discov* **18**, 553–566 (2019).

192. Ajibade, A. A., Wang, H. Y. & Wang, R.-F. Cell type-specific function of TAK1 in innate immune signaling. *Trends in Immunology* **34**, 307–316 (2013).

193. Mussbacher, M. *et al.* Cell Type-Specific Roles of NF-κB Linking Inflammation and Thrombosis. *Frontiers in Immunology* **10**, (2019).

194. Epelman, S., Lavine, K. J. & Randolph, G. J. Origin and Functions of Tissue Macrophages. *Immunity* **41**, 21–35 (2014).

195. Guilliams, M. *et al.* Spatial proteogenomics reveals distinct and evolutionarily conserved hepatic macrophage niches. *Cell* **185**, 379-396.e38 (2022).

196. Abt, M. C. *et al.* Commensal Bacteria Calibrate the Activation Threshold of Innate Antiviral Immunity. *Immunity* **37**, 158–170 (2012).

197. Kim, J. Y. *et al.* Discovery of New States of Immunomodulation for Vaccine Adjuvants via High Throughput Screening: Expanding Innate Responses to PRRs. *ACS Cent. Sci.* (2023) doi:10.1021/acscentsci.2c01351.

198. Sterner, R. C. & Sterner, R. M. CAR-T cell therapy: current limitations and potential strategies. *Blood Cancer J* **11**, 69 (2021).

199. Gumber, D. & Wang, L. D. Improving CAR-T immunotherapy: Overcoming the challenges of T cell exhaustion. *eBioMedicine* **77**, (2022).

200. Kitada, T., DiAndreth, B., Teague, B. & Weiss, R. Programming gene and engineered-cell therapies with synthetic biology. *Science* **359**, eaad1067 (2018).